ENHANCED NEWMARK METHOD FOR SEISMIC ANALYSIS OF SUBMARINE SLOPES

NEDA ZANGENEH

Your file Votre référence
ISBN: 0-612-93073-4
Our file Notre référence
ISBN: 0-612-93073-4

ENHANCED NEWMARK METHOD FOR SEISMIC ANALYSIS OF SUBMARINE SLOPES

By

© Neda Zangeneh

A Thesis Submitted to the
School of Graduate Studies
In Partial Fulfillment of the Requirements
for the Degree of Master of Engineering

FACULTY OF ENGINEERING AND APPLIED SCIENCE

MEMORIAL UNIVERSITY OF NEWFOUNDLAND

June 2003

St. John's Newfoundland Canada

To my husband,

my parents ,

and my parents-in-law.

ABSTRACT

Newmark method of slope displacement analysis has been extensively applied in many slope stability analyses. However, there are some limitations in Newmark method that may lead to non-conservative predictions of slope displacements. To provide more realistic predictions of slope displacements, these limitations are considered throughout the study for enhancing Newmark method. The following additions to the original Newmark method have been included in this study: 1) accounting for seismically induced excess pore water pressure build-up, 2) accounting for excess pore water pressure dissipation after the end of shaking, and 3) accounting for possibility of multiple failure surfaces. Those enhancements are briefly discussed hereafter.

During an earthquake, non-cohesive soils may experience considerable pore water pressure build-up, which in the limit can lead to a state of zero effective stress and soil liquefaction. Therefore, in such a case, an effective stress approach should be used because a total stress analysis may give highly under-conservative results. In the present effective stress approach, the effects of excess pore water pressure and subsequent changes in soil shear strength are considered.

Also, after the end of the strong shaking period, pore water pressure starts dissipating. Dissipation of excess pore water pressure causes the soil to regain part of its original shear strength and consequently, the yield acceleration increases and becomes positive. Therefore, in such a case, considering the effects of excess pore water pressure dissipation gives better estimation of permanent slope displacements after the end of

shaking. In this study the effects of excess pore water pressure dissipation are also considered, based on the one-dimensional consolidation theory.

In homogeneous soil deposits the displacements are usually distributed with depth. For such situation, the rigid block assumption may induce significant differences between actual and predicted slope displacements. Therefore, two moving blocks have been considered to mitigate this limitation of Newmark method. The model is able to reproduce the gradual deformation of soil with depth and therefore provide a more realistic prediction for uniform sand deposits.

The proposed enhanced Newmark method has been implemented in a computer program.

ACKNOWLEDGMENTS

This study is part of COSTA-Canada, a Canadian contribution to the study of continental slope stability. The financial support provided by Natural Sciences and Engineering Research Council of Canada (NSERC) is acknowledged.

The author wishes to express her appreciation to Dr. Radu Popescu for his suggestions and guidance throughout this study.

In addition, the author would like to thank Dr. Leonard Lye for his guidance throughout the sensitivity analyses.

Finally, the author wishes to express her unending appreciation to her husband, Dr-to-be Alireza Azizian, for his invaluable encouragement and support throughout this research.

Above all, the author wishes to give her praise and thanks to a gracious and loving God, for the strength, hope, and mercy provided throughout her life.

TABLE OF CONTENTS

LIST OF TABLES

LIST OF FIGURES

LIST OF SYMBOLS

A: acceleration amplitude
A_f: Skempton's A pore pressure parameter at failure
B: Low-strain bulk modulus
B_0: Low-strain bulk modulus at reference mean stress
B_{av}: Average low-strain bulk modulus
CRR: cyclic resistance ratio
CSR: cyclic stress ratio
Dr: relative density
D_S: Static driving force
FS: pseudo-static factor of safety
G_s: soil specific gravity
M: earthquake magnitude
MSF: magnitude scaling factor
N: number of cycles of shear stress
N_{eq}: equivalent number of cycles
N_L: number of cycles to induce initial liquefaction
PGA: peak ground acceleration
R_S: available static resisting force
T_v: time factor
W: total weight of the sliding block
W': buoyant (or effective) weight of the sliding block
W_{sat}: saturated weight of the sliding block
$a_b^d(t)$: sliding block downslope acceleration
$a_b^u(t)$: sliding block upslope acceleration
a_h: horizontal acceleration
a_{max}: maximum acceleration of earthquake
a_y: yield acceleration
c: soil cohesion
c': soil effective cohesion
c_u: undrained shear strength
c_v: coefficient of consolidation
d: length of the longest drainage path
d_{rel}: relative displacement
f: true response function
g: gravitational acceleration
k: Hydraulic conductivity
$k(t)$: earthquake acceleration coefficient
$k_o(t)$: coefficient of earth pressure at rest
$k_h(t)$: horizontal earthquake acceleration coefficient
$k_y(t)$: yield acceleration coefficient
$k_y^d(t)$: downslope sliding yield acceleration coefficient at each time instant t
$k_y^d(t)$: upslope sliding yield acceleration coefficient at each time instant t

l: length along the base of the block
m_v : coefficient of volume compressibility
n^w : porosity of soil
p: vertical effective pressure
p' : effective confining pressure
p'_0 : Reference mean effective confining stress
r_d : depth reduction factor
r_u : excess pore water pressure ratio
u : total (hydrostatic + excess) pore water pressure
u_e : excess pore water pressure
$u_e(t,z)$: excess pore pressure at any time instant, t, and depth z
$u_i(z)$: initial excess pore pressure with depth
x_i : coded variables
y : true response of a system
Δt: duration of an acceleration pulse
α : pore pressure build-up parameter
β : slope angle
β_{ij} : regression coefficients
ε : source of variability not accounted for in true response function
ϕ, ϕ' : friction angle at failure
γ : total unit weight of soil
γ' : buoyant unit weight of soil
γ_{sat} : saturated unit weight of soil
γ_{water} : unit weight of water
ρ_w : density of water
σ : total stress
σ'_c : consolidation pressure
σ'_{v0} : initial effective vertical stress
σ_{v0} : initial total vertical stress
τ : shear stress developed on the failure plane
τ_c : cyclic shear stress
τ_f : available soil shear strength
ξ_i : controllable input variables (actual variables)

1 Research Purpose

1.1 Background

The serviceability of a slope after an earthquake is controlled by permanent deformations induced by the earthquake. As opposed to the pseudo-static method of slope stability analysis that provides only an index of stability (factor of safety), Newmark (1965) method of slope displacement analysis provides an estimate of seismic displacement associated with slope failure. The method considers the behaviour of a slope when the inertial forces acting on a potential failure mass become large enough so the total (static plus dynamic) driving forces exceed the available resisting forces and the pseudo-static factor of safety drops below 1.0. Slope displacements are then calculated by double integrating the soil block acceleration based on a stick-slip fashion of motion. That is, when the applied earthquake acceleration is more than a certain value, known as 'yield acceleration', the soil block movement initiates and accelerates; otherwise, it decelerates or does not move. Newmark method is a limit-equilibrium-based displacement analysis that predicts the displacement of an infinite slope during an earthquake based on a soil strength–dependent yield acceleration and purely kinematic criteria. In many applications of the Newmark method, the yield acceleration is assumed constant during the earthquake.

When applying the method to saturated granular soils, however, due to the build-up of excess pore water pressure, soil strength and consequently the yield acceleration will decrease. Therefore, for saturated soil such as encountered submarine slopes, the Newmark method should be integrated with the procedures of evaluating the build-up and dissipation of excess pore water pressure to account for the effects of dynamic loading on

strength of soil due to soil softening and also liquefaction. Also for homogeneous soils deposits, because of the fact that the displacements may be distributed in depth, the Newmark method should be integrated with a procedure to account for more than one failure surface.

The effect of excess pore water pressure build-up and, eventually, liquefaction is considered by including the simplified procedure of evaluating the build-up of excess pore water pressure (pioneered by Professor Seed). The effect of excess pore water pressure dissipation is considered by using one dimensional consolidation theory to estimate dissipation rate. In this way, the proposed model accounting for the fact that soil regains part of its original shear strength after the end of shaking. Also considering more than one rigid block accounts for possible gradual distribution of slope displacements in depth during seismic dynamic loading.

The above mentioned enhancements are applied to the original Newmark method to have a better estimation of slope displacements subjected to earthquake loading and provide more realistic results.

1.2 Specific Objectives

The enhanced Newmark method for seismic analysis of submarine slopes is developed based on well known state-of-practice methods. It also includes advanced soil dynamics principles that make the results comparable to results obtained by more advanced techniques (e.g. Finite Element method).

This study is part of COSTA-Canada, A Canadian Contribution to the Study of Continental Slope Stability contributes to the following short-term objectives of the project (see COSTA – Canada web site, short-term objectives No. 5 & 6), i.e.:

- Modeling of forces and mechanical processes that control the initiation of slope instabilities (release mechanisms), flow dynamics and initiation of tsunamis (objective No. 5).

- Assessment of risk-fields related to slope stability (objective No. 6).

1.3 Outline

A literature review on seismic analysis of submarine slopes, with specific concentration on Newmark analysis and various improvements to Newmark method is presented in Chapter 2.

A methodology for calculating the excess pore water pressure build-up for a specific soil deposit subjected to a given seismic motion and its implementation in the classical Newmark model is presented in Chapter 3.

In order to identify the factors that have more effects on the predicted permanent displacements of a slope, a sensitivity analysis based on Response Surface Methodology is presented in Chapter 4. The sensitivity analysis shows that the analysis method considering only effects of excess pore water pressure build-up is very sensitive to the maximum earthquake acceleration which leads us to the importance of accounting for the effect of excess pore water pressure dissipation.

The model is further upgraded in Chapter 5 to include the effects of dissipation of excess pore water pressure after the earthquake and the fact that during the dissipation phase soil regains part of its shear strength and the yield acceleration increases. That yields a more realistic prediction of permanent displacement of the slope. The proposed model is validated based on centrifuge test results.

However, because of the fact that the recorded values in the centrifuge model show the gradual deformation in the soil and because by using a single rigid block, the model is not able to reproduce gradual soil deformation, it is important to account for more than one rigid block to achieve the distribution of displacement with depth. This limitation can be mitigated by considering a stack of rigid blocks. In Chapter 6, two moving blocks have been considered to investigate the importance of accounting for more than one block on the predicted slope displacements. The results show that by considering more than one rigid block, the model is able to reproduce the gradual deformation of soil with depth and therefore provide more realistic prediction for uniform sand deposit.

Throughout the thesis, all of the new features are verified based on centrifuge experimental results.

The proposed methodology was implemented in the computer program ENEDAS. A user's manual is included in appendix C.

1.4 Original contributions

- Original method and algorithm for including effects of pore water pressure build-up and dissipation into Newmark method for seismic analysis of slope displacements.

- Two-block analysis of saturated soil slopes using Newmark method.
- Program ENEDAS (Enhanced NEwmark Displacement Analysis of Slopes) for calculating seismically induced displacements of submarine slopes.

2 Literature Review

2.1 Introduction

In his Rankine Lecture in 1965, Professor Newmark introduced a methodology to enhance the classical pseudo-static method of slope stability analysis to calculate permanent slope displacement due to earthquake shaking. The methodology was so simple and clear, yet original, that has had numerous applications in the analysis of natural slopes as well as earth structures such as embankment dams. Since then, many modifications have been proposed to reduce the inaccuracies inherent in the method; however, none of them has been as simple as the method itself, and indeed many enhancements have added more complexity to the approach.

Displacement analysis of submarine slopes can also be performed using the Newmark method, but a few considerations should be made in the pseudo-static phase of the approach. For a very long and wide submarine slope where assumptions of plane strain is appropriate the infinite slope stability analysis can be applied.

In the following sections, fundamentals of the Newmark sliding block analysis are first explained in case of on-shore dry slopes. Then, different approaches to the calculation of yield (threshold) acceleration are described, specifically for the application of the method to submarine slope analysis. In particular, the regional method of submarine slope stability (Lee and Edwards, 1986) is discussed. Finally, limitations of the methodology that arise from the nature of submarine sediments are discussed, mainly because, 1) submarine sediments are in general fully saturated and some of them (e.g., sand or silty sand) are highly susceptible to cyclic liquefaction and the assumption of constant yield

acceleration is not valid, and 2) soft sediments can be found in recent layers of shallow sea depth and the Newmark assumption of the rigidity of the deposit is not completely appropriate. Some other limitations are discussed as well.

2.2 Fundamentals of Newmark Sliding Block Analysis

2.2.1 Sliding Block Analogy

The serviceability of a slope after an earthquake is controlled by permanent deformations induced by earthquake. As opposed to the pseudo-static method of slope stability analysis, which provides a factor of safety with respect to the peak ground acceleration but no information on displacement associated with slope failure, the Newmark method can provide a prediction of slope performance based on the total displacement at the end of shaking. Newmark (1965) considered the behavior of a slope when the inertial forces acting on a potential failure mass become large enough that the total (static plus dynamic) driving forces exceed the available resisting forces and the factor of safety will drop below 1.0. When the factor of safety is less than 1.0, the potential failure mass is no longer in equilibrium and then it will be accelerated by the unbalanced force. Newmark assumed this situation is analogues to that of a block resting on an inclined plane (Figure2.1). He used this analogy to develop a method for prediction of the permanent displacement of a slope subjected to seismic ground motion.

In the following sections, the procedure is illustrated first for a dry soil in order to show the basics of the method clearly. Then, extension of the method to the analysis of submarine (submerged) slopes is presented.

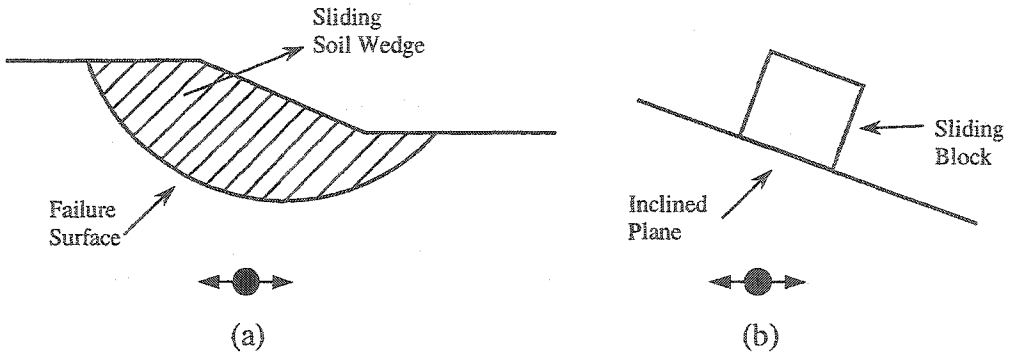

Figure 2-1. Analogy between potential landslide and block resting on inclined plane.

2.2.2 Pseudo-Static Factor of Safety

Under static conditions, equilibrium of a block of dry soil (in the direction parallel to the plane) requires that the available static resisting force, R_S, exceeds the static driving force, D_S (Figure 2.2.a.). Assuming that the block's resistance to sliding is purely frictional (c = 0), the factor of safety can be computed as:

$$FS = \frac{R_S}{D_S} = \frac{W\cos\beta\tan\phi}{W\sin\beta} = \frac{\tan\phi}{\tan\beta} \tag{2.1}$$

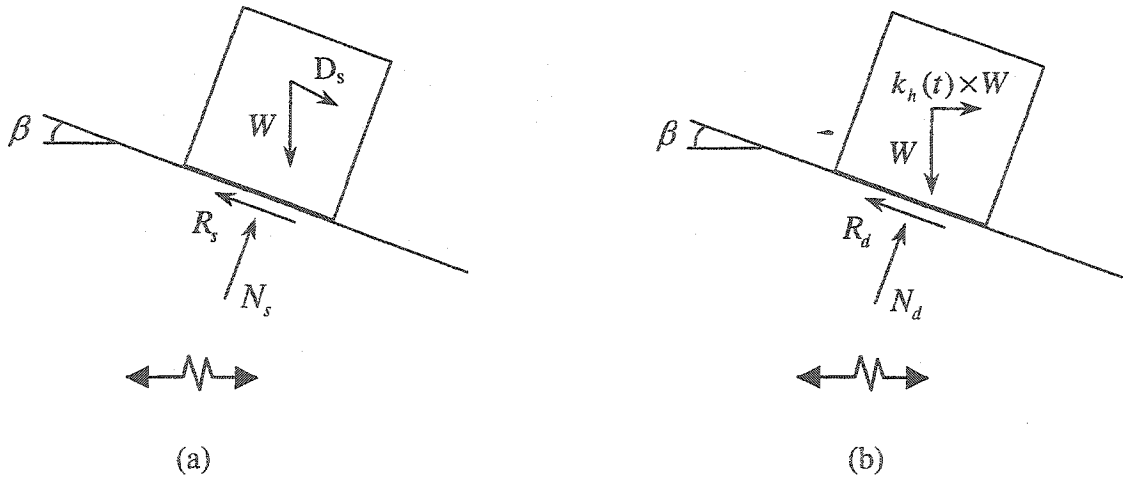

Figure 2-2. Forces acting on a block resting on an inclined plane: (a) static conditions; (b) dynamic (pseudo-static) conditions.

However, considering horizontal vibration of the inclined plane with horizontal acceleration $a_h(t) = k_h(t) \times g$ at a particular instant of time, the horizontal acceleration of the block will induce a horizontal inertial force, $k_h \times W$ (Figure 2.2.b.). The pseudo-static factor of safety will be as follows:

$$FS(t) = \frac{R_d(t)}{D_d(t)} = \frac{[\cos\beta - k_h(t)\sin\beta]\tan\phi}{\sin\beta + k_h(t)\cos\beta} \tag{2.2}$$

The pseudo-static factor of safety decreases as k_h and β increase, also, the factor of safety decreases when the friction angle at failure decreases (Figure 2.3).

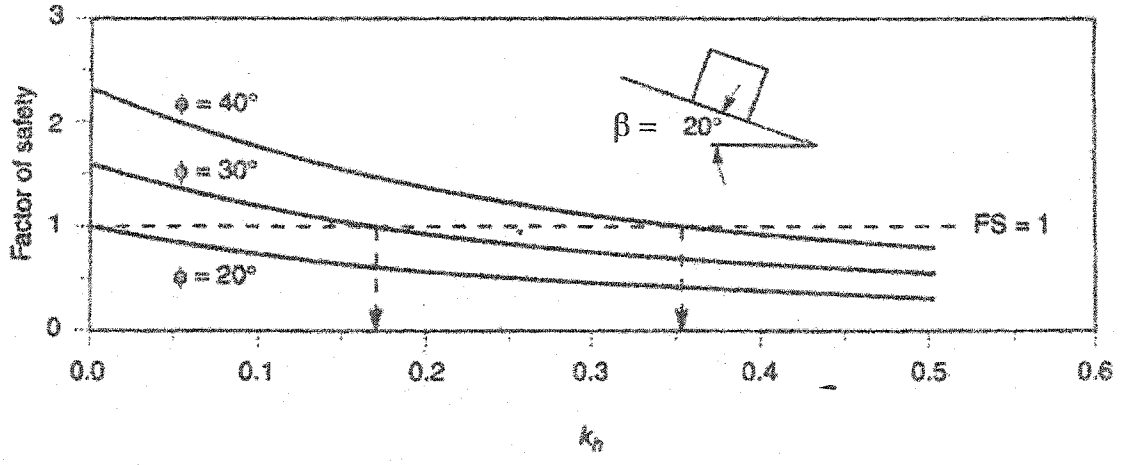

Figure 2-3. Variation of pseudo-static factor of safety with horizontal psedustatic coefficient for block on plane inclined at 20° for soils with different friction angle. (after Kramer, 1996)

2.2.3 Yield Acceleration

A value of k_h leading to a factor of safety equal to 1.0 is termed as the yield coefficient, k_y, that corresponds to the yield acceleration, $a_y = k_y \times g$. The yield acceleration is the

minimum horizontal acceleration required to produce instability of the block. For the block of Figure 2.2, sliding in the downslope direction, this value is:

$$k_y = \tan(\phi - \beta) \tag{2.3}$$

For sliding in the upslope direction, which can occur when β and ϕ are small, the yield acceleration is:

$$k_y = \tan(\phi + \beta) \tag{2.4}$$

Figure 2.3 shows the variation of the factor of safety with friction angle and seismic coefficient for a block on a plane inclined at 20°. A horizontal dashed line corresponding to FS = 1 is drawn to graphically demonstrate the threshold values of seismic coefficient, i.e. yield coefficient.

2.2.4 Calculation of Permanent Displacement

When a block on an inclined plane is subjected to a pulse of acceleration that exceeds the yield acceleration, the block will move relative to the plane. Consider a case in which an inclined plane is subjected to a single rectangular acceleration pulse in the direction of increasing slope, of amplitude, A, and duration Δt. The relative movement of the block during this period can be obtained by integrating the relative acceleration twice, as shown in Figure 2.4.

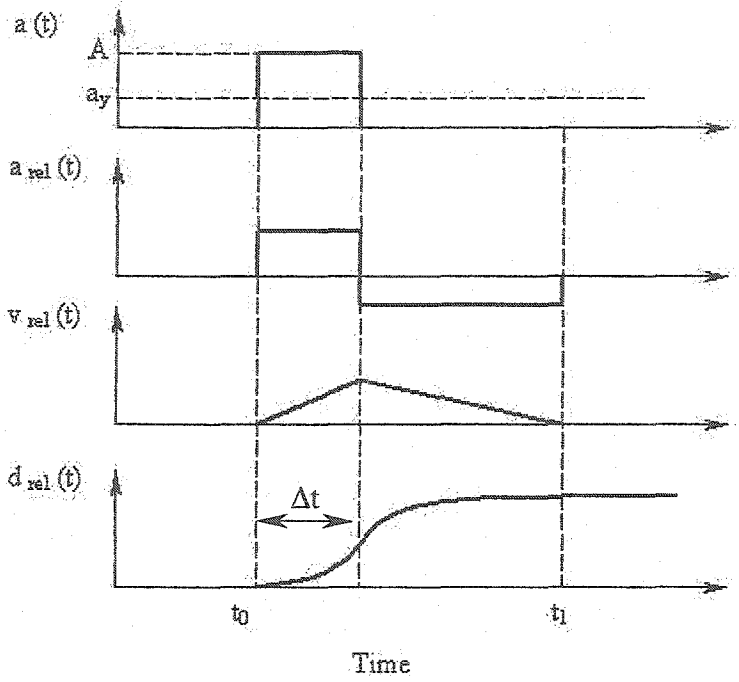

Figure 2-4. Variation of relative velocity and relative displacement between sliding block and inclined plane (modified after Kramer, 1996).

The total relative displacement is as follows (Kramer, 1996):

$$d_{rel}(t) = \frac{1}{2}(A - a_y)\Delta t^2 \frac{A}{a_y} \qquad (2.5)$$

Thus, the total relative displacement depends on both:

1. The amount by which the yield acceleration is exceeded, i.e. A- a_y, and

2. The length of time during which the yield acceleration is exceeded, i.e. Δt.

Therefore, the relative displacement caused by a single pulse of strong ground motion should be related to both the amplitude and duration of that pulse. Increments of displacement can occur a number of times during an earthquake motion, thus the total

displacement calculated by Newmark method will be influenced by strong-motion duration and amplitude.

2.3 Application of Newmark Method to Submarine Slopes

In the previous part, fundamentals of the Newmark method of seismic analysis of slopes were discussed. Since it was intended to show only the basics of the method in the simplest form, it was assumed that a dry, purely frictional soil is subjected to a single pulse of earthquake inertial acceleration. However, extension of the method so that it can be applied to the analysis of submarine slopes requires some modifications that are discussed below.

2.3.1 Buoyant Weight

A simple, yet important, point that should be mentioned before proceeding to any further discussion is related to the careful consideration of the soil weight into the analysis. Submarine slopes are submerged and presumably fully saturated. Therefore, the buoyant (or effective) weight of the sliding block, W', should replace the total weight used in the previous equations. However, because during a seismic event soil behavior is almost undrained, it is often assumed that the pseudo-static inertial force of the earthquake is applied to both soil particles and pore water. Thus, as depicted in Figure 2.5, the pseudo-static inertial force is equal to $k_h \times W_{sat}$, where as the effective weight of the block is computed from its buoyant unit weight:

$$\gamma' = \gamma_{sat} - \gamma_{water} \tag{2.6}$$

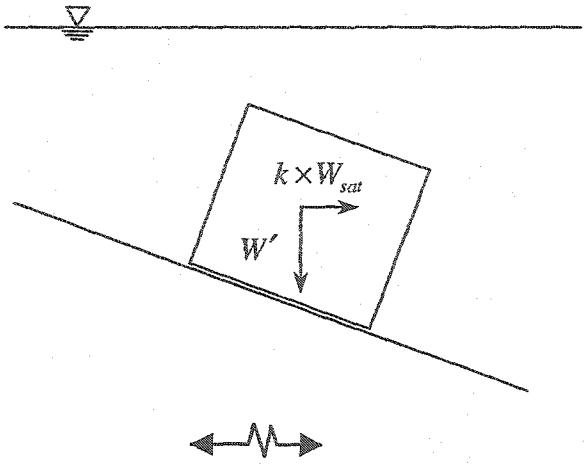

Figure 2-5. Applied forces on submerged sliding block.

One should note that this type of analysis neglects the hydrodynamic forces that are beneficial for the slope stability in this situation. Therefore this analysis is on the conservative side.

2.3.2 Total Stress Analysis

According to Morgenstern (1967), when a fully saturated soil is sheared under undrained conditions and the results are interpreted in terms of total stresses, the material behaves as if it is purely cohesive. This behavior holds for *saturated sands and clays* (Bishop and Eldin, 1950). The undrained shear strength (c_u) for a *normally consolidated clay or a sand* is related to the stresses under which the soil has been consolidated, the effective angle of shearing resistance, and the pore pressure at failure (Morgenstern 1967):

$$\frac{c_u}{p} = \frac{\sin\phi'\left[1-\sin\phi'+A_f\sin\phi'\right]}{1+(2A_f-1)\sin\phi'} \tag{2.7}$$

where p is the vertical effective pressure, and A_f is the appropriate pore pressure parameter at failure (Skempton, 1954). Thus, for any particular normally consolidated

soil, the ratio c_u / p is a constant and indicates that the undrained strength increases with depth linearly.

As was mentioned previously, the influence of an earthquake in the analysis of undrained sliding may be incorporated by a horizontal body force, k, as some percentage of gravity and considering the equilibrium of a block in the infinite slope.

Considering the equilibrium of the block shown in Figure 2.6, and resolving forces parallel to the slope, the pseudo-static factor of safety will be as follows (Morgenstern 1967):

$$FS_d(t) = \frac{R_d(t)}{D_d(t)} = \frac{c_u l}{W' \sin\beta + k(t) W \cos\beta} \tag{2.8}$$

where, c_u is the undrained strength mobilized at failure, W' is the submerged weight of the block ($\gamma' b.h$), W is the bulk (saturated) weight of the block ($\gamma_{sat} b.h$), l is the length along the base of the block, and k is the seismic coefficient.

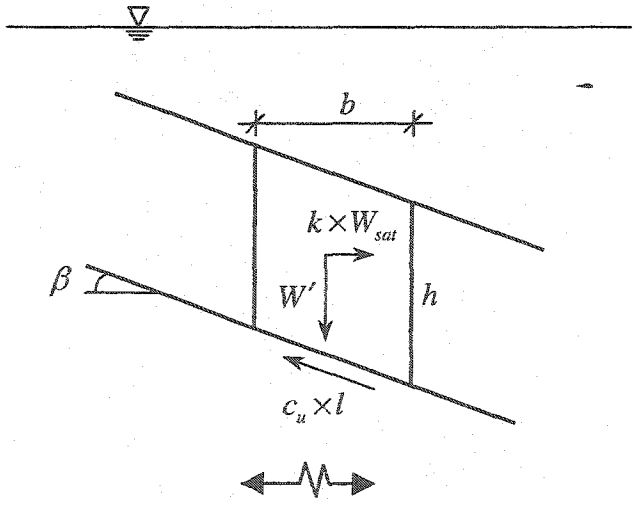

Figure 2-6. Applied forces in total stress approach.

Equation (2.8) now becomes (Morgenstern 1967):

$$FS_d(t) = \frac{R_d(t)}{D_d(t)} = \frac{\frac{c_u}{\gamma' h}}{\frac{1}{2}\sin 2\beta + k(t)\frac{\gamma}{\gamma'}\cos^2\beta} \tag{2.9}$$

$\frac{c_u}{\gamma' h} = \frac{c_u}{p}$ is constant with depth for NC clays. Therefore, by denoting this ratio as N and setting the above factor of safety equal to one, the yield coefficient corresponding to total stress analysis can be obtained as follows (Morgenstern 1967):

$$k_y = \frac{\gamma'}{\gamma \cos^2\beta} N - \frac{\gamma'}{\gamma}\tan\beta \tag{2.10}$$

This value of the yield coefficient can then be used in the Newmark analysis to calculate the permanent displacement of a clay deposit subjected to earthquake.

2.3.2.1 Regional Method

The Regional Method introduced by Lee and Edwards (1986) is based on the total stress analysis method presented in the previous section and can be used for regional evaluation of submarine slope stability. They measured the cyclic shear-strength properties of marine-sediment core samples, and expressed the results in a normalized manner that allowed approximate extrapolation of test results below the limited depth of sampling. By assuming a simplified infinite slope, Lee et al. (1999) calculated the peak seismic acceleration (a_y) that would be required to cause failure. This value is a direct measure of ground failure susceptibility. Because Lee and Edwards (1986) considered only relatively small offshore areas, they assumed that ground failure opportunity did not vary. That is,

the anticipated level of seismic shaking would be the same, independent of where the core was taken. Accordingly, the relative value of k_y becomes a direct measure of ground failure potential, with the lowest values corresponding to the highest potential. To develop a relationship for the yield acceleration the following procedure is applied.

First, a modified version of the equation introduced by Morgenstern (1967), Equations 2.9 and 2.10, for seismic loading on a gentle infinite slope is considered:

$$\frac{\tau_f}{\gamma' h} = k\left(\frac{\gamma}{\gamma'}\right) + \sin\beta \qquad (2.11)$$

where, τ_f is available soil shear strength (denoted as c_u in Eq. 2.9), γ' and γ are the submerged (buoyant) and total unit weight of the sediment, h is the depth of the failure plane in the sediment, k is the horizontal earthquake acceleration coefficient (as a fraction of the acceleration of gravity), and β is the slope angle. This relationship is simplified slightly from the original form and is applicable only to small ($<10^{o}$) slope angles.

Then, a series of cyclic tests are performed on samples obtained from 10 different failed offshore areas such as California, Alaska, New Zealand, Spain, etc., in order to determine the cyclic stress ratio (CSR) at failure as a function of the number of load cycles applied (Figure 2.7). CSR is defined as the cyclic shear stress, τ_c, divided by the consolidation stress, σ_c'. It should be noted that in the recent years, the value of CSR at failure is usually referred to as the cyclic resistance ratio, CRR, and is recommended by Youd and Idriss (2001). On a semi-log diagram, the cyclic stress ratio is plotted versus the number

of cycles to failure (Figure 2.7). If a number of samples with the same lithology are tested at different levels of CSR, such a plot typically generates a nearly linear relationship.

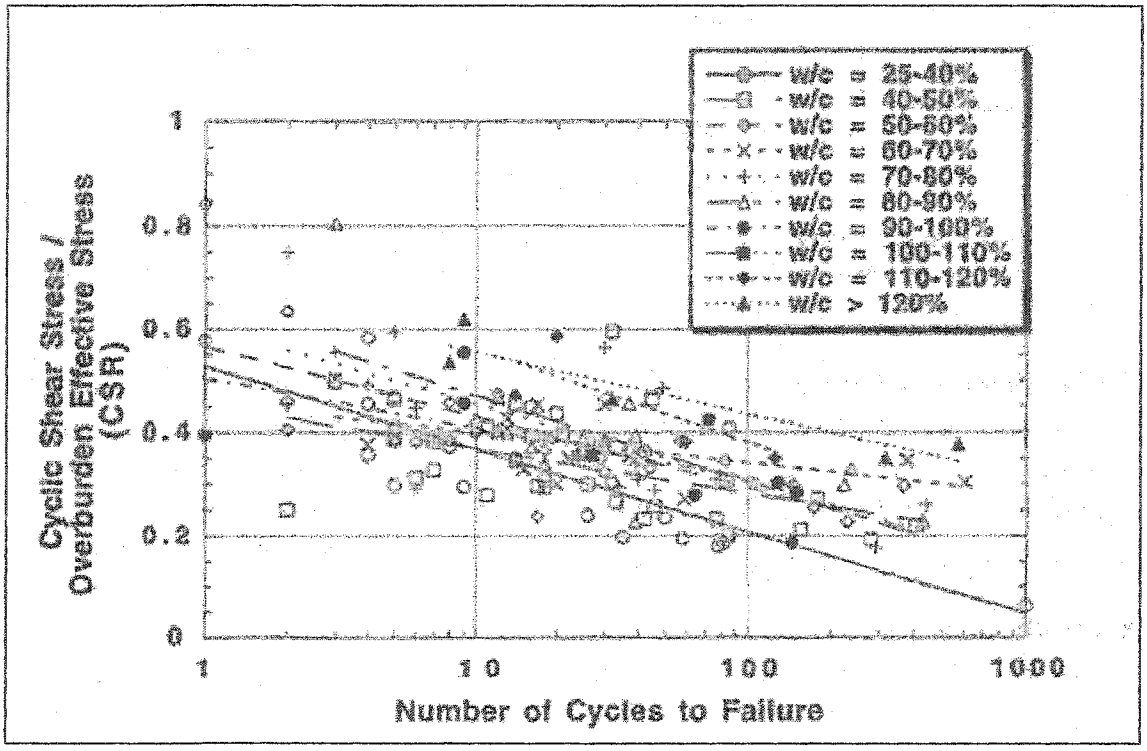

Figure 2-7. Cyclic shear stress normalized by consolidation stress (CSR) versus number of cycles to failure (15% strain) from 144 cyclic triaxial tests performed on sediment from ten marine study areas distributed worldwide. Data points are identified according to initial water content (w/c) of the sediment tested (Lee et al., 1999).

Finally, an empirical relationship is proposed by Lee et al. (1999), following the procedure introduced by Lee and Edwards (1986), to calculate the yield acceleration coefficient based on CSR_{10} as a substitute for normalized shear strength of the sediment ($\tau_f / \gamma' h$):

$$k_y = (\frac{\gamma'}{\gamma})[CSR_{10} - \sin\beta] \qquad (2.12)$$

Selection of CSR_{10} is because a representative number of applied cycles by a typical strong earthquake is approximately ten for the particular region they applied the method

for. It is worth mentioning that in this research the yield acceleration coefficient was calculated based on the residual undrained strength, accounting for the effects of seismically induced pore water pressure build-up.

One of the recent applications of the regional method is the spatial slope stability hazard analysis of the Saguenay Fjord, Quebec, Canada (Urgeles et al., 2001). Geotechnical and geophysical data are integrated to evaluate the stability of the region in terms of Newmark displacements (Figure 2.8) obtained from calculated yield acceleration (Figure 2.9). The main advantage of the Newmark method, based on yield accelerations obtained from the regional method, is obviously illustrated in Figure 2.8. According to this plot, during an earthquake with M_w = 6.75, most of the region is not stable, however, the displacement is somewhere between 0 to 1 cm that is very low for practical purposes. If the pseudo-static approach were selected alone, the result would be a factor of safety less than one for most of the areas, but according to the Newmark methodology the region is almost stable and safe.

It should be emphasized that in Urgeles et al. (2001) analysis, a constant value of yield acceleration with time corresponding to undrained residual strength is considered for the entire duration of the earthquake. Figure 2.9 only shows the spatial variability of k_y, assuming a constant value during shaking. See limitations of Newmark method for further discussion.

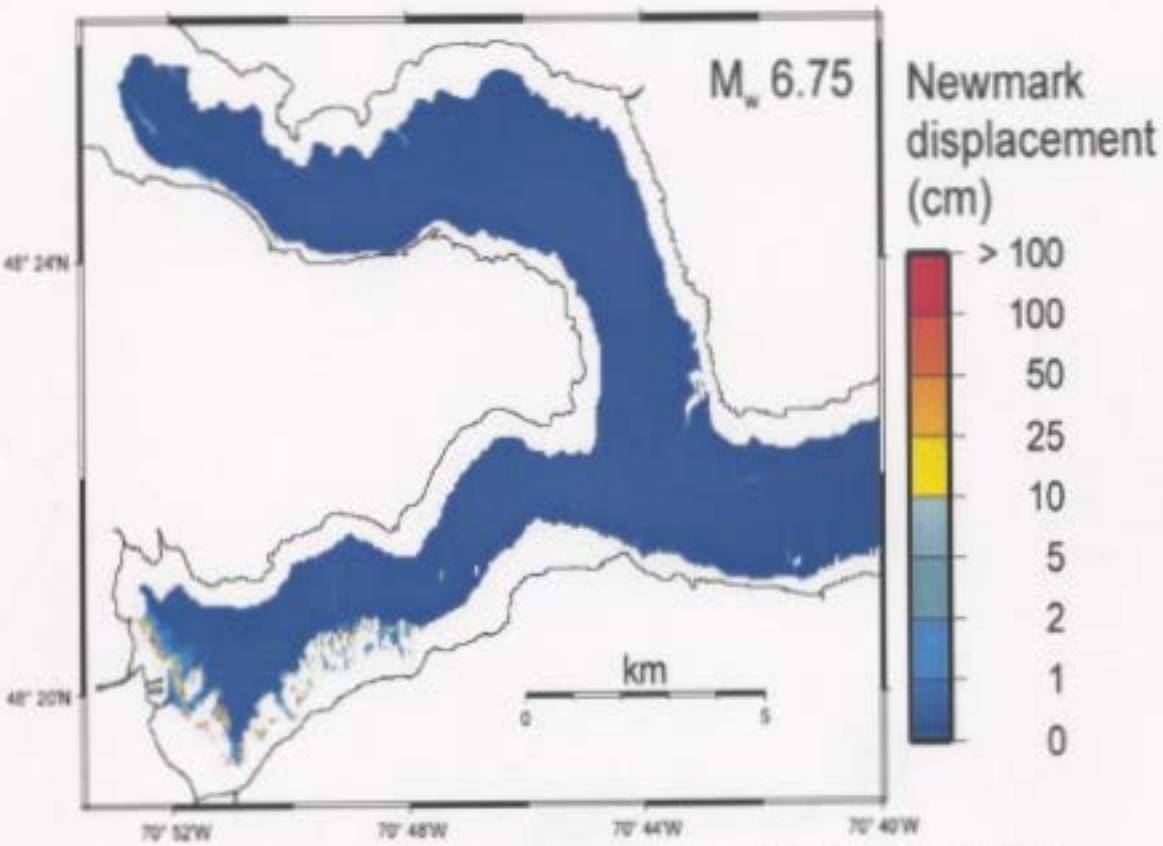

Figure 2-8. Application of Newmark method to spatial slope stability hazard analysis of Saguenay Fjord (Urgeles et al., 2001), calculated Newmark displacements.

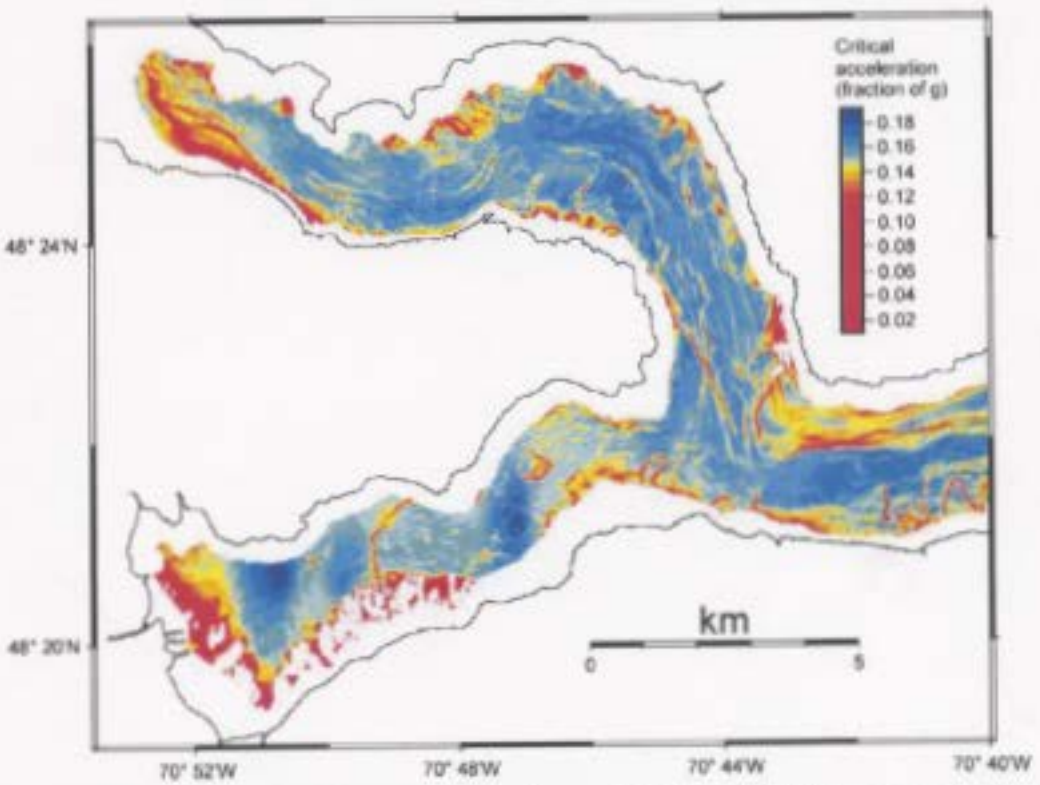

Figure 2-9. Application of Newmark method to spatial slope stability hazard analysis of Saguenay Fjord (Urgeles et al., 2001), spatial variability of yield acceleration calculated from regional method.

2.3.3 Effective Stress Analysis

In the previous section, the yield acceleration of a cohesive material was presented in order to perform a total stress analysis. Non-cohesive materials, usually experience a significant increase in the pore water pressure due to cyclic or earthquake loading, leading to reduction of effective confining stresses and consequently of the shear strength.

Zeng (1996), among others, mentioned that for dry soils, Newmark method has been widely used to estimate sliding displacement and this method is also straightforward to apply. However, for saturated soils, since the magnitude of excess pore water pressure is difficult to predict, threshold acceleration cannot be derived directly. Under such circumstances, it is necessary to use a more comprehensive numerical procedure.

Effective stress analysis is indicated for such partially drained conditions. The following discussion describes the main steps of doing such an analysis in a simplified fashion rather than using advanced methods that are based on the mechanics of porous media .

Approximate prediction of the excess pore water pressure can be performed using the procedure presented in the following section. The effects of pore water pressure on the yield acceleration coefficient can then be included in a Newmark-type analysis, as described by, e.g., Biondi and Cascone (2000) and Azizian and Popescu (2001).

2.3.4 Simplified Procedure for Estimating Excess Pore Water Pressure Build-up

Seed and Idriss (1982) measured the rate of excess pore water pressure increase using cyclic simple shear tests. As it is shown in Figure 2.10, the range of the variation of the

ratio of excess pore water pressure to initial effective stress during cyclic loading is assumed to range between 0 and 1.0. The average value of the variation of $r_u = u_e / \sigma'_{v0}$ with respect to the number of equivalent cycles can be expressed in a non-dimensional form as follows (Seed et al. 1975b)

$$r_u = \frac{u_e}{\sigma'_{v0}} = \left(\frac{2}{\pi}\right) \arcsin\left(\frac{N_{eq}}{N_L}\right)^{\frac{1}{2\alpha}} \tag{2.13}$$

where, u_e is the excess pore water pressure generated, σ'_{v0} is the initial effective vertical stress, N is the number of cycles of shear stress applied until a certain time instant, N_L is the number of cycles of shear stress needed for initial liquefaction, and α is a constant with a value of about 0.7 for the average curve shown in Figure 2.10.

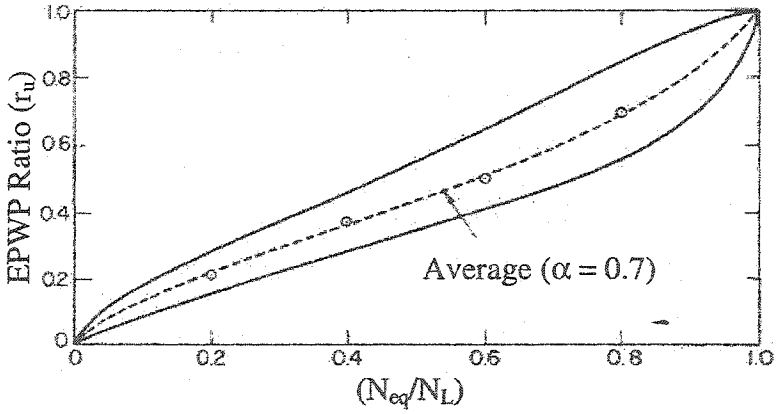

Figure 2-10. Rate of pore water pressure buildup in cyclic simple shear test (Seed et al. 1975b).

Unlike in the case of cyclic laboratory tests, during an earthquake event an irregular loading is applied to the soil deposit. Therefore, it is necessary to determine an equivalent number of uniform stress cycles for an earthquake that has irregular stress-time history. Seed et al. (1975), proposed a method for estimating the equivalent number of uniform

cycles at $0.65\tau_{max}$ induced by an irregular seismic acceleration. The method is described in Appendix A.

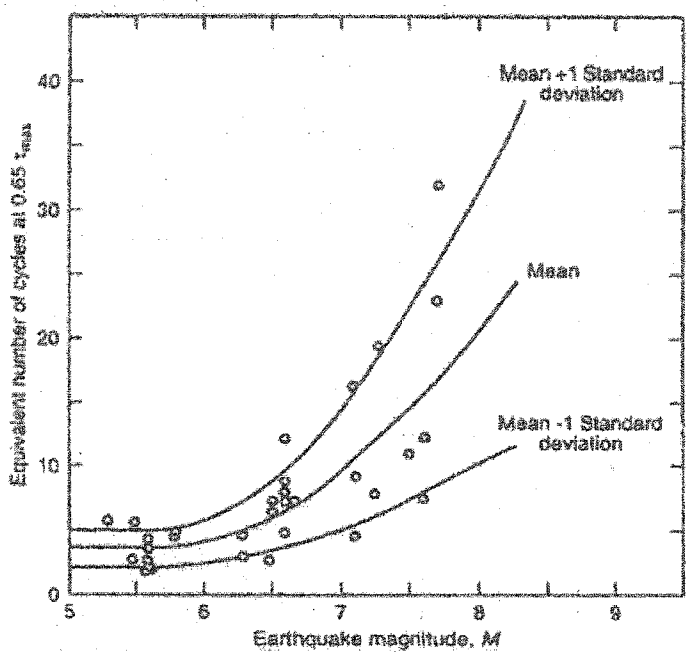

Figure 2-11. Number of equivalent stress cycles Neq, for earthquakes of different magnitude (after Seed et al. 1975).

The equivalent number of cycles , N_{eq}, can be related to the earthquake magnitude, M, as shown in Figure 2.11 (after Seed et al. 1975). More recent guidelines are also available (Youd et al. 2001) (see Appendix B).

2.4 Limitations of Newmark Method

In the previous sections, fundamentals of the Newmark method as well as different approaches that can be applied for the evaluation of yield acceleration necessary to perform a Newmark analysis were discussed. Both parts, i.e. calculation of the yield acceleration and that of the permanent displacements, suffer from some limitations that

are discussed below. It should be noted, however, that some of these limitations are more related to method used for calculating the yield acceleration.

2.4.1 Softening and Hardening of Soils

The Newmark method assumes rigid-perfectly plastic stress-strain behavior (Figure 2.12) for a planar failure surface. However, this assumption may not be valid as soil behavior is not perfectly plastic. It usually exhibits strain-hardening or strain-softening behavior after yielding (Figure 2.12).

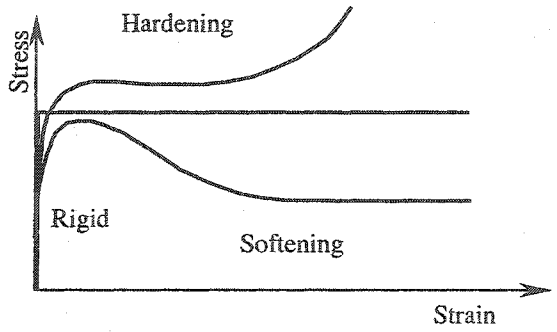

Figure 2-12. Idealized stress-strain behavior of soil materials.

A particular case of strain softening is due to pore pressure build-up that can be estimated as discussed earlier and included in the Newmark analysis. However, it should be noted that such an approach adopted by some researchers has a major limitation. It has been shown (e.g. Seed and Idriss, 1982) that in some soils after build-up of pore pressure due to strong shaking, excess pore pressure dissipates after the earthquake with a rate depending upon soil properties such as hydraulic conductivity. Dissipation can even start during the earthquake after the strong shaking portion of the event. Such a behavior leads to an increase in the yield acceleration after its decrease due to excess pressure. If dissipation is not taken into account, the final value of yield acceleration remains unchanged (Figure 2.13). Considering the sensitivity of the Newmark method to the value

of the yield acceleration, it can be concluded that ignoring excess pore pressure dissipation may result in overly- conservative predictions of slope displacement.

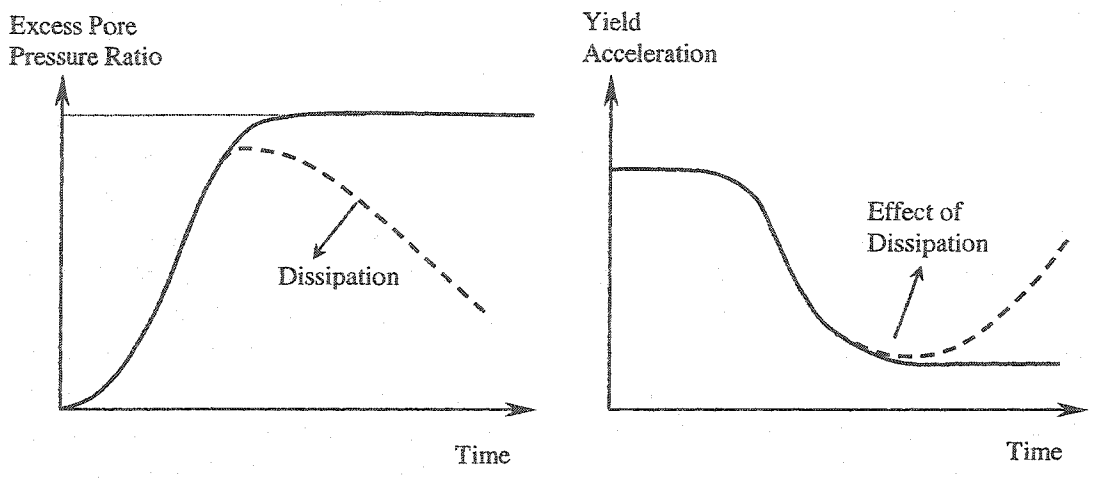

Figure 2-13.Effect of excess pore water pressure dissipation on yield acceleration.

2.4.2 Soil Deformability

The original method introduced by Newmark (1965) is based on assuming the soil as a rigid block with rigid-perfectly plastic behavior at the sliding surface (Figure 2.12). This results in a stick-slip fashion of block displacement with the same input motion at all depths in the soil deposit. Therefore, in most Newmark analyses, it is assumed that the base motion at the level of underlying stiff material is identically transmitted to the sliding block at the level of failure surface (Figure 2.1).

Adapting the original Newmark rigid sliding block analogy to the more realistic case of deformable potential sliding mass was first studied by Makdisi and Seed (1978). According to this method, dynamic response analysis of earth structure (or soil deposit) is first performed, ignoring the potential for sliding. Then, instead of applying the same base motion to the potential sliding mass, a seismic coefficient time-history (i.e.,

$k = \tau_h / \sigma_v$) calculated from dynamic analysis is applied to the rigid sliding block and displacement is computed consequently. This method was further developed by several researchers and led to the conclusion that it can result in displacements higher than those predicted by original Newmark method, therefore, giving conservative predictions. Rathje and Bray (1999, 2000b), however, showed that this conclusion is not always true. They termed Makdisi-Seed approach as "decoupled" analysis and performed a series of "coupled" analyses by modelling soil as: a) linear elastic, and b) nonlinear lumped mass material (Figure 2.14).

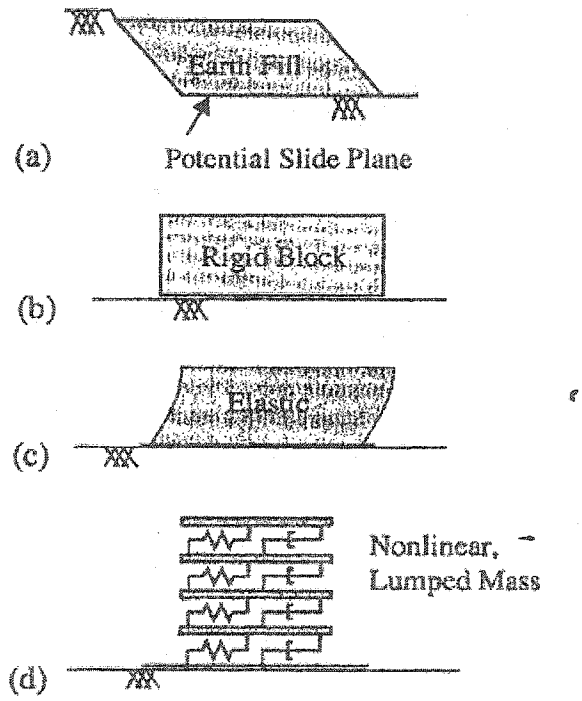

Figure 2-14. Coupled analysis illustration: a) Problem analyzed, b) Newmark's original rigid block model, c) linear elastic, modal, coupled sliding model, d) non-linear lumped mass, coupled sliding model (Rathje and Bray 2000b).

Comparing the results of so called decoupled and coupled deformable sliding block analyses using several earthquake ground motions and sinusoidal input motions indicate

that a decoupled analysis does not always provide a conservative estimate of sliding displacement if it is compared to the fully coupled analysis results (Rathje and Bray 1999).

In summary, according to Rathje and Bray (2000a), Newmark's original rigid sliding block can be non-conservative and should not be used when the period of sliding mass is near that of input ground motion. Decoupled analysis provides a reasonable and conservative estimate in many cases, except for intense ground motions with low values of k_y. Rathje and Bray (2000b) conclude that since such a calculated displacement is merely an index of seismic performance, the decoupled approach is judged to be a useful engineering approximation for most projects.

Byrne and Hendra (1992) presented an analysis procedure for predicting the earthquake induced displacements of earth dams. The procedure extends the Newmark method from a single-degree-of-freedom rigid plastic to a multi-degree-of-freedom flexible system using energy concepts. Byrne (1990) and Byrne et al. (1991) extended Newmark approach to a multi-degree-of-freedom system. Byrne and Hendra (1992) concluded that the predicted and observed displacements were in good agreement in terms of both the magnitude of displacements as well as their pattern.

2.5 VELACS tests results

For a numerical analysis of soil liquefaction induced by earthquake it is necessary to have a verification and validation by comparison of the numerical analysis results with observed performance.

The VELACS (VErification of Liquefaction Analysis by Centrifuge Studies) Project was sponsored by the National Science Foundation and involved the cooperative efforts of seven universities. Nine centrifuge models were selected to supply experimental data with well-defined boundary conditions and soil properties for 'before the event' predictions using a wide variety of numerical codes (Arulandan and Scott (1994)).

In a centrifuge test, the in-situ stresses in soil deposits are simulated at reduced the geometrical scale through centrifuge loading. In the test, the confining environment in the model soil is increased, so that the confining stress is identical in both model and prototype at homologous points. Therefore, to calibrate and verify the proposed numerical analysis, the results of VELACS centrifuge test for model 2 (Figure 3.7) have been used. The model 2 consist of a 20 cm high, 46 cm horizontal loose Nevada sand layer with uniform density in a laminar box which is inclined 2 degree. The system is shaken at the base while spinning at 50g. The test corresponds in the prototype scale to a semi infinite slope of 10 m thick water-saturated layer of gravel having the dynamic properties and compressibility of the Nevada sand which is 50 times more permeable.

3 Accounting for excess pore water pressure build-up

3.1 Introduction

Displacement analysis is a more rational alternative to pseudo-static seismic analysis of slope stability. Newmark (1965) introduced a limit-equilibrium-based displacement analysis method that predicts the displacements of an infinite slope during an earthquake based on a soil strength–dependent yield acceleration and purely kinematic criteria (a detailed description of the original Newmark method is presented in section 2.2). As opposed to the pseudo-static method of slope stability analysis, which provides a factor of safety applying to very short time instants during an earthquake, the Newmark method characterizes the slope performance by predicting the total displacement at the end of shaking. In many applications of the Newmark method, the yield acceleration is assumed constant during the earthquake. When applying the method to saturated granular soils, however, due to the build-up of excess pore water pressure (EPWP), soil strength and consequently the yield acceleration will decrease. In this chapter, the effects of excess pore water pressure build-up are investigated, and a procedure for calculating permanent displacements of submarine slopes subjected to seismic loads is introduced. The method is based on the algorithm proposed by Newmark, and it uses state-of-practice methods for estimating excess pore water pressure build-up. The proposed method is verified based on centrifuge test results.

The original Newmark method considers the behaviour of a slope when the inertial forces acting on a potential failure mass become large enough that the total (static plus dynamic) driving forces exceed the available resisting forces and the factor of safety drops below 1.0. When the factor of safety is less than 1.0, the failing soil mass is no longer in

equilibrium and then it will be accelerated by the unbalanced forces. Newmark assumed this situation is analogous to that of a block resting on an inclined plane, and calculated the total (permanent) displacement of the block by integrating twice the relative acceleration, as shown in Figure 2.4. for the case of an inclined plane subjected to a single rectangular acceleration pulse of amplitude, A, and duration, Δt. The yield acceleration, a_y, depends on shear strength of soil on the failure surface.

3.2 Analysis Procedure

Non-cohesive soils may experience significant pore water pressure build-up due to cyclic or earthquake loading. In the limit, it can lead to a state of zero effective stress and soil liquefaction. Therefore, in case of non-cohesive deposits, a total stress analysis is not appropriate and may give highly under-conservative results. Instead, an effective stress approach should be used to consider the effects of excess pore water pressure and changes in soil shear strength.

3.2.1 Yield Acceleration

The following procedure is applicable for a very long and wide submarine slope where the plane strain assumption is appropriate. The failure surface is assumed a plane parallel to the slope (Figure 3.1).

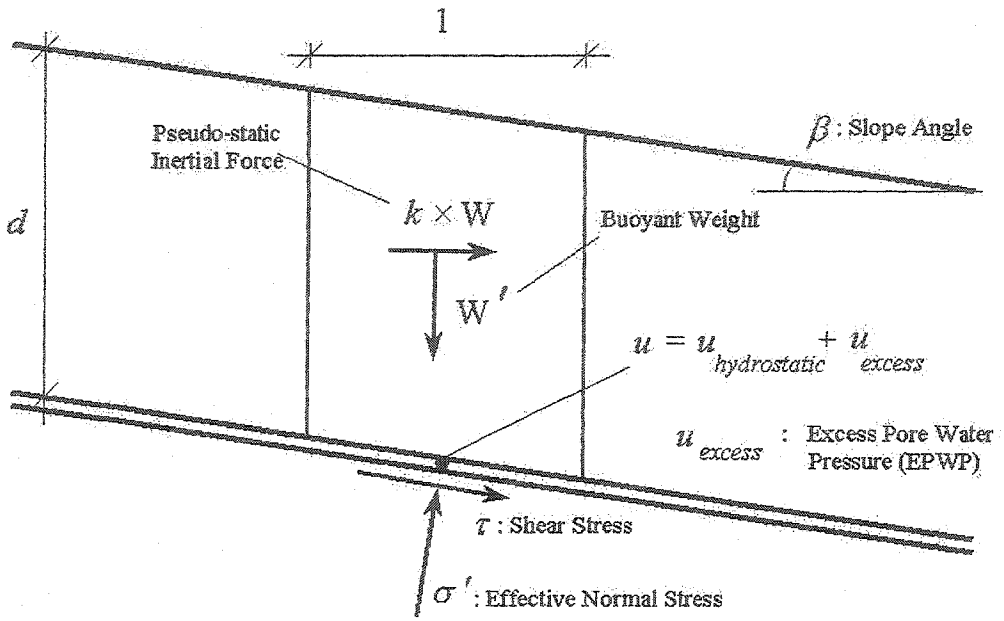

Figure 3-1. Pseudo-static analysis of an infinite submarine slope.

The factor of safety (FS) is expressed by the ratio of available soil shear strength (τ_f) to the shear stress developed on the failure plane (τ):

$$FS = \frac{\tau_f}{\tau} \tag{3.1}$$

in which, soil shear strength at failure is expressed in terms of effective parameters according to the Mohr-Coulomb failure criterion:

$$\tau_f = c' + (\sigma - u)\tan\phi' \tag{3.2}$$

where c' is the soil effective cohesion, ϕ' is the effective internal friction angle, σ is the total stress (normal to the failure surface), and u is the total (hydrostatic + excess) pore water pressure. Therefore, the factor of safety can be written as follows:

$$FS = \frac{c' + (\gamma' d \cos^2 \beta - u_e - k\gamma d \sin\beta \cos\beta)\tan\phi'}{\gamma' d \sin\beta\cos\beta + k\gamma d \cos^2\beta} \tag{3.3}$$

where with reference to Figure 3.1, γ' is the effective (or buoyant) unit weight of soil, d the depth of failure plane, β is the slope angle, u_e is the excess pore water pressure (in excess of hydrostatic) generated during the shaking, and k is the seismic coefficient defined as the ratio between the horizontal earthquake acceleration and the gravitational acceleration (g).

In this study, only fully saturated soils are taken into account. The buoyant (or effective) weight of the sliding block, W', is used in Equation (3.3) to calculate the normal effective stress. However, because it is assumed that during a seismic event, the soil behaviour is mostly undrained, the inertial force of the earthquake is applied to both soil particles and pore water. Thus, the inertial force is equal to $k \times W_{sat}$, and the saturated unit weight, γ, is used in equation (3.3).

By setting the factor of safety equal to 1, the yield acceleration coefficient at each time instant t for downslope sliding can be obtained as follows:

$$k_y^d(t) = \frac{c' + [\gamma' d \cos^2\beta - u_e(t)]\tan\phi' - \gamma' d \sin\beta\cos\beta}{\gamma d \cos^2\beta + \gamma d \sin\beta\cos\beta\tan\phi'} \tag{3.4}$$

or, with $r_u = u_e / \sigma'_{v0}$ (the ratio between excess pore water pressure and initial effective vertical stress) and $\sigma'_{v0} = \gamma' d \cos^2\beta$:

$$k_y^d(t) = \frac{c' + \gamma' d \cos^2\beta[1 - r_u(t)]\tan\phi' - \gamma' d \sin\beta\cos\beta}{\gamma d \cos^2\beta + \gamma d \sin\beta\cos\beta\tan\phi'} \tag{3.5}$$

The yield acceleration coefficient is defined here as $k_y = a_y / g$, where a_y is the yield acceleration and g is the acceleration of gravity.

Equation 3.4 clearly shows that due to the excess pore-water pressure build-up (u_e) the yield coefficient will decrease, with resulting increasing slope displacement (Figure 3.2). In other words, the earthquake-induced displacements in a saturated cohesionless slope are strongly affected by reduction in effective stress and slope deformations may bring the slope to a limit state of serviceability. Therefore, slope displacement may occur even for seismic acceleration lower than initial yield acceleration, because of increase in pore pressure.

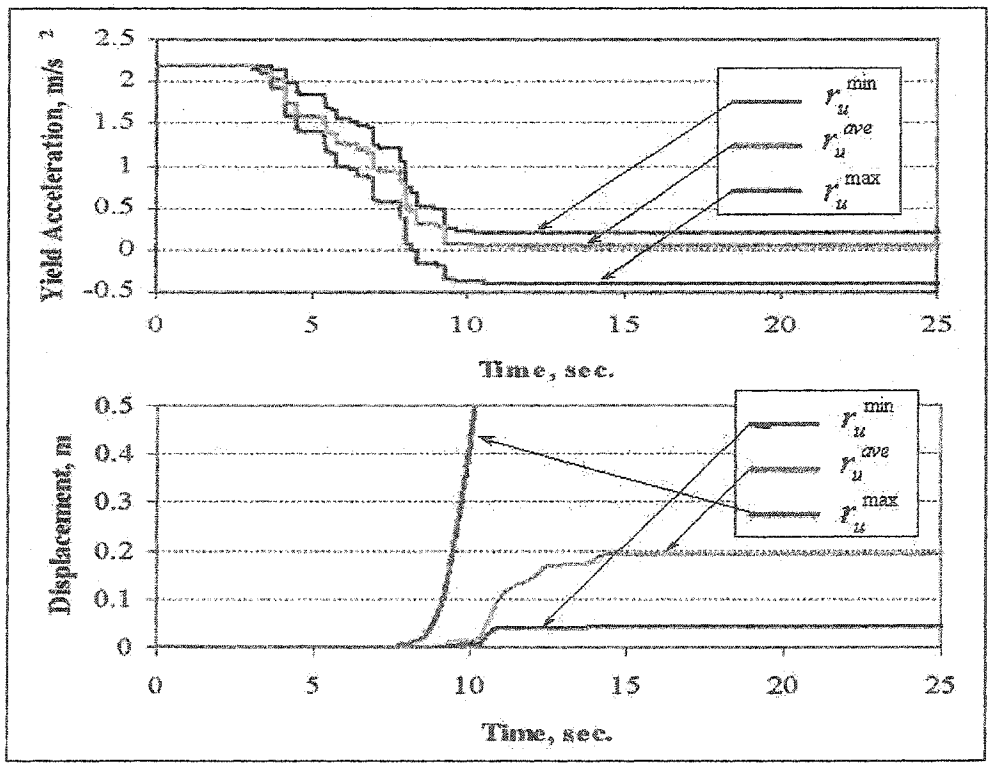

Figure 3-2. Influence of excess pore water pressure build-up on the yield acceleration and slope displacement.

For the case of very mild slopes, it may be worth considering also the possibility of seismically induced upslope sliding. The yield acceleration coefficient for upslope sliding is:

$$k_y^u(t) = \frac{-c' - \gamma' d\cos^2\beta[1 - r_u(t)]\tan\phi' - \gamma' d\sin\beta\cos\beta}{\gamma d\cos^2\beta - \gamma d\sin\beta\cos\beta\tan\phi'} \tag{3.6}$$

The sliding block downslope $a_b^d(t)$ and upslope $a_b^u(t)$ accelerations can be calculated using the following equations:

$$a_b^d(t) = \left(k(t) - k_y^d(t)\right)g\frac{\cos(\phi' - \beta)}{\cos(\phi')} \tag{3.7}$$

$$a_b^u(t) = \left(k(t) - k_y^u(t)\right)g\frac{\cos(\phi' + \beta)}{\cos(\phi')} \tag{3.8}$$

where $k(t)\cdot g$ represents the horizontal seismic acceleration of the ground (below failure surface). Finally, the slope displacement can be computed by integrating twice the block acceleration based on the direction of motion.

It is worth noting that when $r_u = 1$, i.e. when the soil is liquefied, the downslope and upslope yield accelerations are:

$$k_y^d(t) = -\frac{\gamma'}{\gamma}\sin(\beta)\frac{\cos(\phi')}{\cos(\phi' - \beta)} \tag{3.9}$$

$$k_y^u(t) = -\frac{\gamma'}{\gamma}\sin(\beta)\frac{\cos(\phi')}{\cos(\phi' + \beta)} \tag{3.10}$$

3.2.2 Estimation of Excess Pore Pressure Build-up

According to Seed and Idriss (1982), the rate of pore pressure development in undrained cyclic simple shear tests on most granular soils, falls within a fairly narrow range when plotted in the normalized form shown in Figure 3.3.

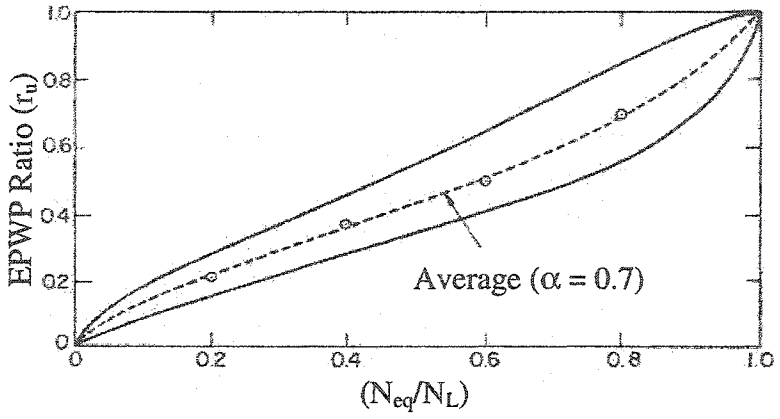

Figure 3-3. Rate of pore water pressure build-up in cyclic simple shear tests (Seed et al. 1975b).

Curves such as those shown in Figure 3.3 can be expressed by the following relation (Seed et al. 1975b):

$$r_u = \frac{u_e}{\sigma'_{v0}} = \left(\frac{2}{\pi}\right)\arcsin\left(\frac{N_{eq}}{N_L}\right)^{\frac{1}{2\alpha}} \tag{3.11}$$

where r_u is the ratio between excess pore water pressure and initial vertical effective stress, u_e is excess pore water pressure, σ'_{v0} is initial vertical effective stress, N_{eq} is the number of equivalent stress cycles applied to the sample up to a certain moment, N_L is the number of stress cycles required to produce a excess pore pressure ratio of 100% or liquefaction, and α is called the pore pressure build-up parameter. For a real acceleration time history, the number of equivalent stress cycles, N_{eq}, can be calculated based on a procedure introduced by Seed (1975a) and explained in details in Appendix A. By

varying the value of α, Equation (3.11) can fit a large palette of undrained pore water pressure generation curves, as shown in Figure 3.4.

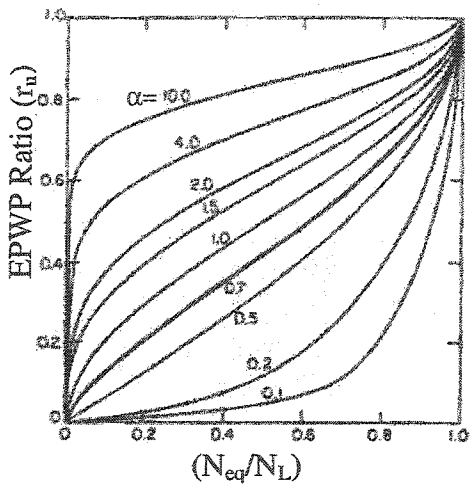

Figure 3-4. Rate of pore pressure generation for different values of α (Seed and Idriss 1982).

The results of a typical Newmark analysis, as described before, which accounts for the decrease of yield acceleration due to excess pore water pressure build-up are shown in Figure 3.5. As the earthquake induces a gradual increase in pore pressure, the yield accelerations decrease gradually. In this particular example, one should note that if no reduction in the yield acceleration were considered, the permanent displacement would be much smaller, and therefore, the results may have been on the under-conservative side. Also note that in Figure 3.6, two different permanent displacements are calculated, one of which considers the possibility of upslope sliding that is reasonable for nearly flat submarine slopes.

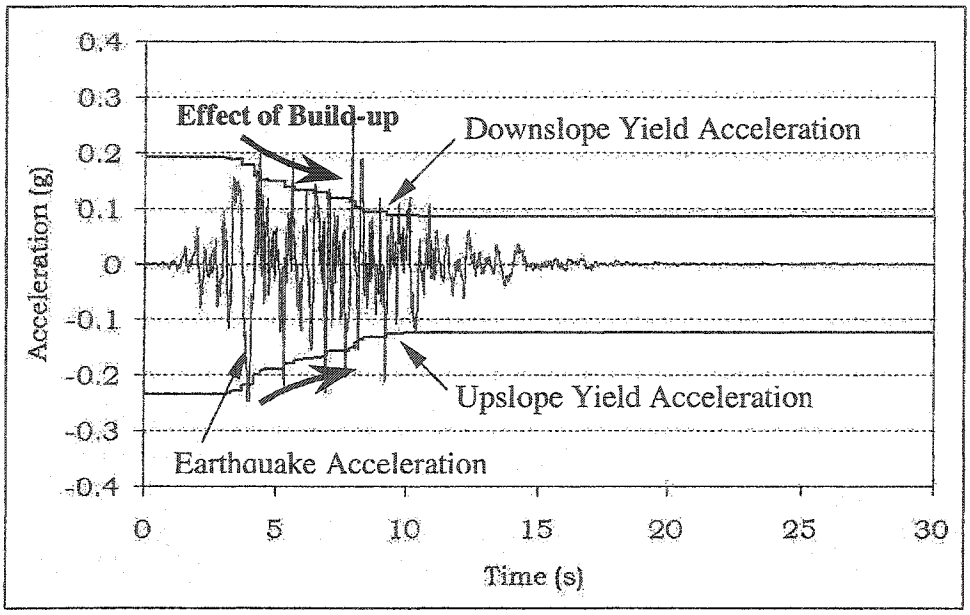

Figure 3-5. Yield accelerations considering the effect of pore water pressure build-up.

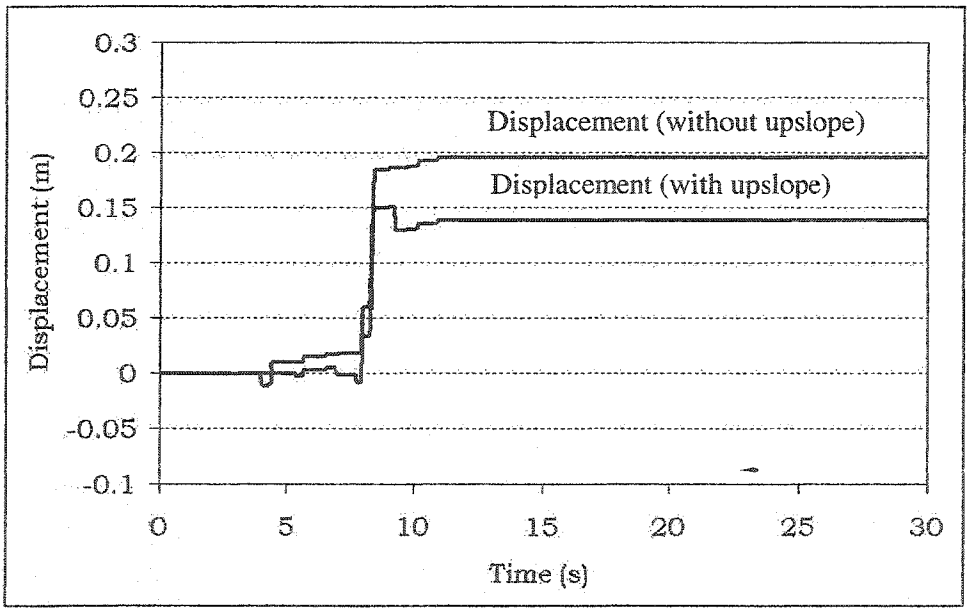

Figure 3-6. Slope displacements considering the effect of pore water pressure build-up.

3.3 Calibration and Validation Using Centrifuge Test Results

To calibrate and verify the analysis procedure described in the previous section, the results of VELACS (VErification of Liquefaction Analysis by Centrifuge Studies, Arulandan and Scott, 19943) centrifuge test for model 2 performed by RPI (Figure 3.7)

have been used (http://geoinfo.usc.edu/gees/velacs/). The VELACS tests were aimed at better understanding the mechanisms of soil liquefaction and at acquiring data for the verification of various analysis procedures. Nine centrifuge models (horizontal and sloping, homogeneous and non-homogeneous soil deposits, embankments, and structures on liquefiable soil) subjected to seismic motion were tested and duplicated at several centrifuge centers in US and UK. The numerical predictions were based on the results of conventional laboratory soil tests performed on the soil materials to be used in the centrifuge models. A detailed comparison, showing all recorded and predicted pore pressure, displacement and acceleration time histories, has been posted on the web at: http://geoinfo.usc.edu/gees/velacs/.

The model 2 consists of a 20 cm high, 46 cm horizontal loose Nevada sand layer with uniform density in a laminar box which is tilted 2° (Figure 3.7). After the deposition together with the laminar box and the shaker, the system is shaken at the base while spinning at 50g. The container is formed by aluminium alloy rectangular rings. All geometrical dimensions, mechanical properties of the rings and some technical specifications for the shaker are given by Taboada and Dobry (1993).

Through use of a laminar box, the test for model 2 simulates an infinite submarine slope with an angle of 2° and a depth of 10 m subject to an earthquake with maximum acceleration of about 0.2g. The soil is a uniform sand with relative density Dr = 40%.

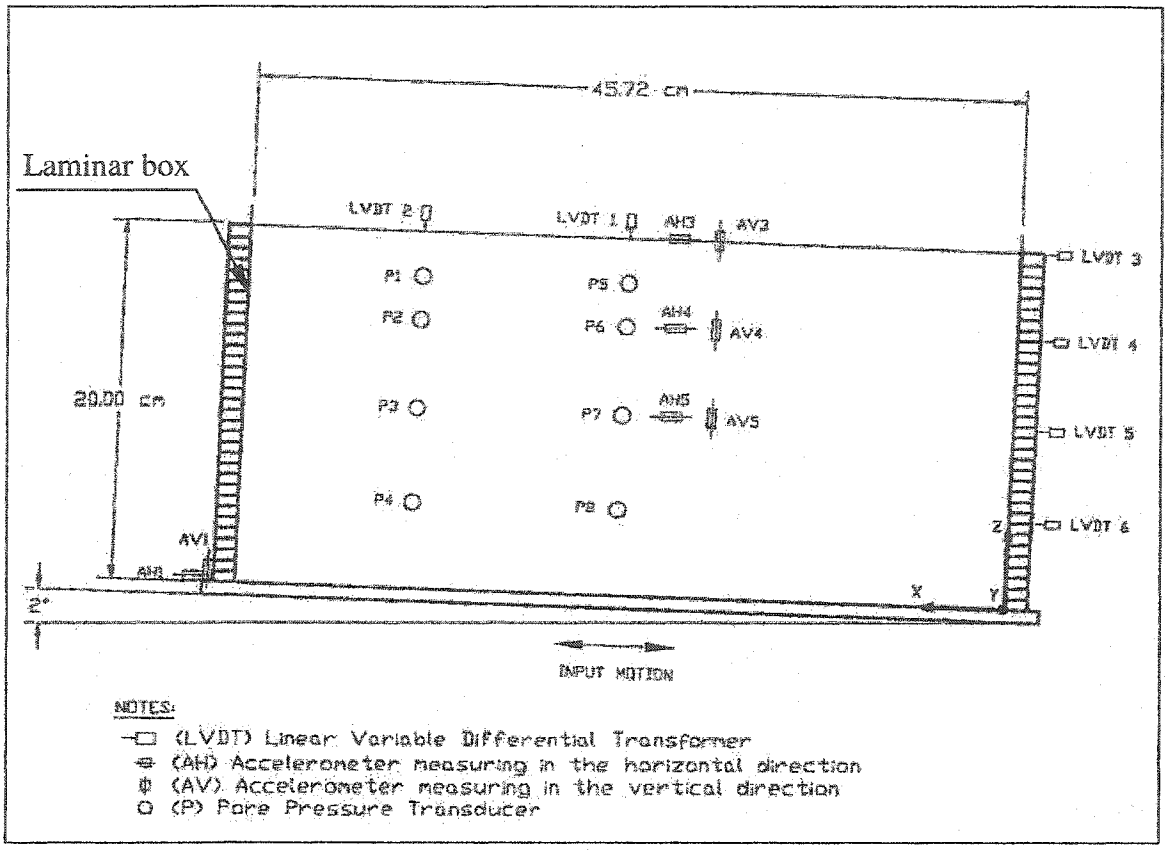

Figure 3-7. VELACS Model #2 Configuration (VELACS, http://geoinfo.usc.edu/gees/velacs/).

The geomechanical soil properties were inferred by Popescu and Prevost (1993), based on results of laboratory soil tests.

3.3.1 Pore pressure build-up parameter (α)

3.3.1.1 Using the acceleration at levels of each pore pressure transducer

In this section, α is back calculated for two intermediate elevations where both excess pore water pressure and accelerations were recorded, namely (P6,AH4) and (P7,AH5) as shown in Figure 3.7. Pore water pressure build-up curves (Eq. 3.11) corresponding to values of α equal to 0.5, 0.7, 2, and 4 are plotted in Figures 3.8 and 3.9. The equivalent number of cycles, N_{eq}, are calculated at each time instant based on the accelerations

recorded at each level (P6 and P7) in the centrifuge experiment. The recorded values of pore water pressure are also plotted for locations P6 and P7, respectively.

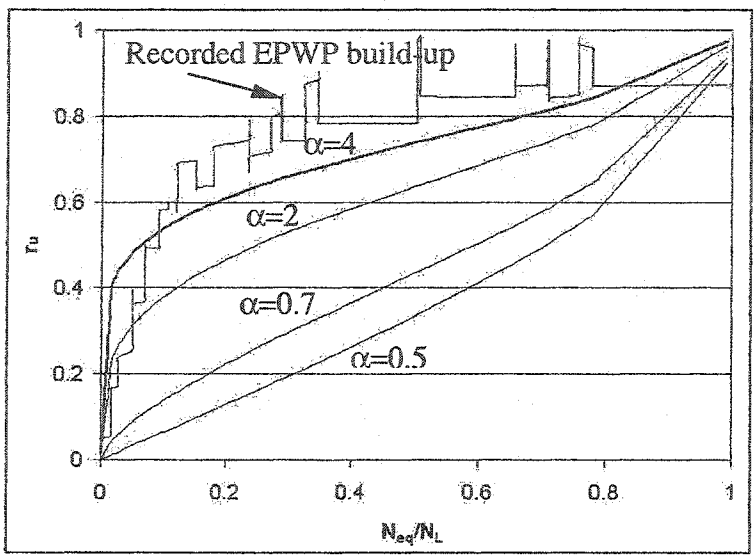

Figure 3-8. Calibration of a using the acceleration at level P6.

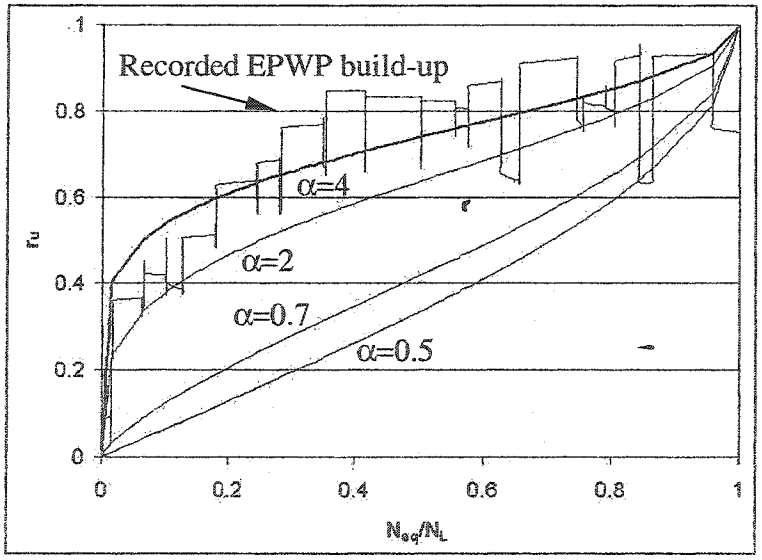

Figure 3-9. Calibration of a using the acceleration at level P7.

The excess pore water pressure parameter α corresponding to the best curve fit is α = 4 for both locations. The value of the number of cycles to liquefaction, N_L, is directly obtained from the pore pressure records and the equivalent number of cycles of the input motion.

3.3.1.2 Using the acceleration of the box (measured at the base of the model)

The curve-fit procedure has been repeated for the same points at the same levels but using the centrifuge box acceleration to calculate N_{eq} . In this case the best curve fit can be obtained for $\alpha = 2$ to 4 (Figures 3.10 and 3.11), which is close to the values obtained in section 3.3.1.1. It can be concluded that one could use the base (bedrock) seismic acceleration and still obtain acceptable prediction.

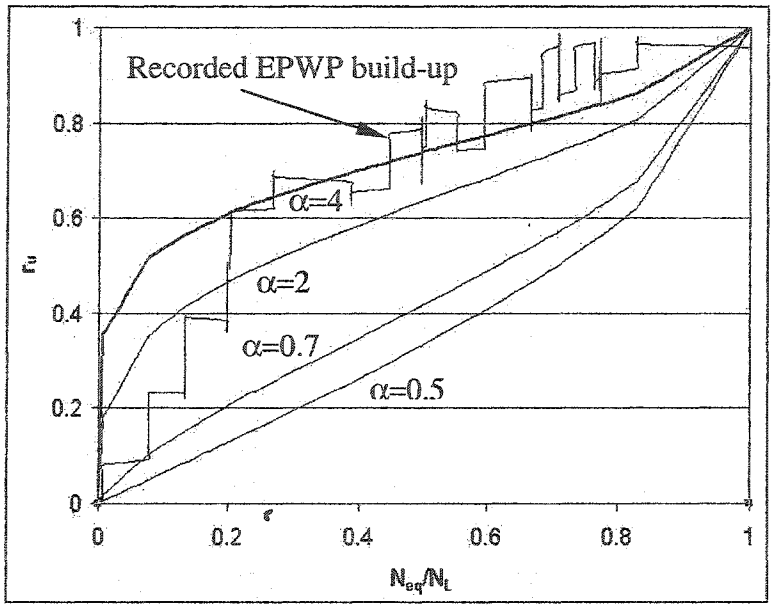

Figure 3-10. Calibration of a using the acceleration of the box for level P6.

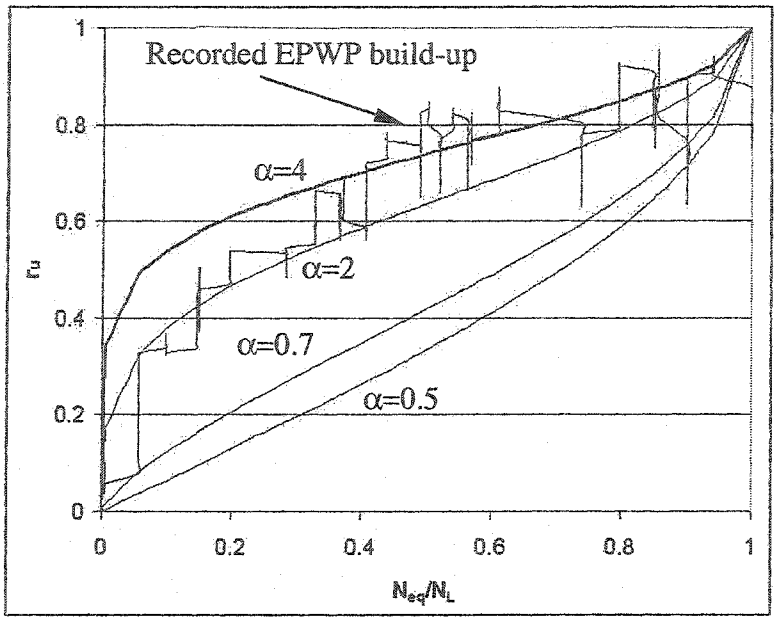

Figure 3-11. Calibration of a using the acceleration of the box for level P7.

3.4 Slope displacements considering build-up

By applying the previously described procedures the yield accelerations (using Eq. 3.5 and Eq. 36) for level P6 and level P7 are calculated and shown in Figures 3.12 and 3.13, respectively .By double integrating the yield acceleration, the displacements for level P6 and P7 are calculated and shown in Figure 3.14 and 3.15, respectively. The values of excess pore water pressure ratio, $r_u(t)$, in equation 3.5 are calculated as shown in equation 2.13 using α=4 (Figures 3.8, 3.9, 3.10, and 3.11). The equivalent number of cycles (N_{eq} in Eq. 3.5) is equal to 13.62 and the number of cycles to induce liquefaction (N_L in Eq. 3.5) is equal to 13.47. All the other parameters in Eq. 3.5 are given in Table C-1, in Appendix C.

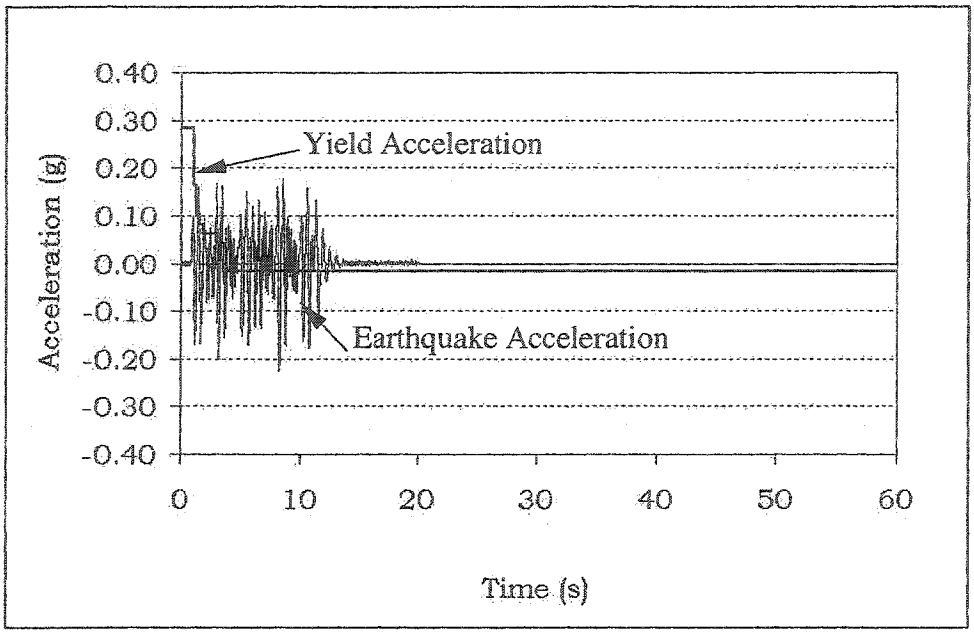

Figure 3-12. Yield Acceleration considering excess pore water pressure build-up effects (for P6 – see Figure 3.7).

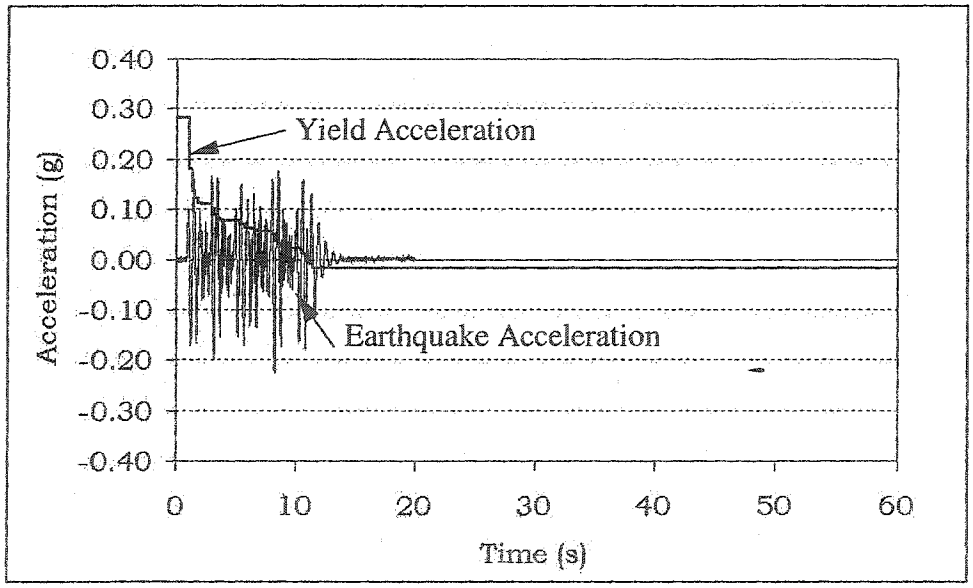

Figure 3-13. Yield Acceleration considering excess pore water pressure build-up effects (for P7 – see Figure 3.7).

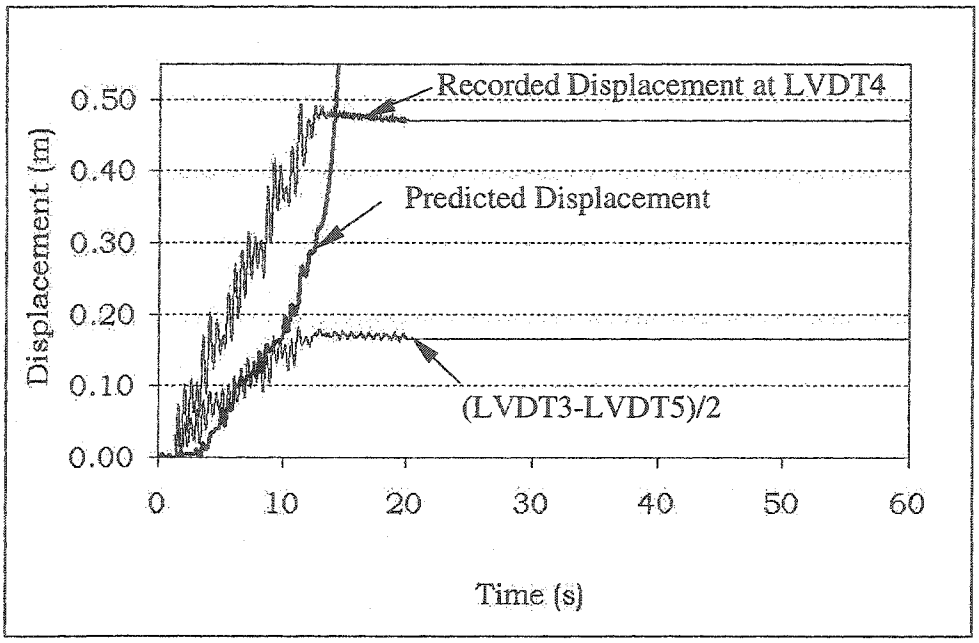

Figure 3-14. The predicted and measured permanent displacements considering excess pore water pressure build-up effects (for P6 – see Figure 3.7).

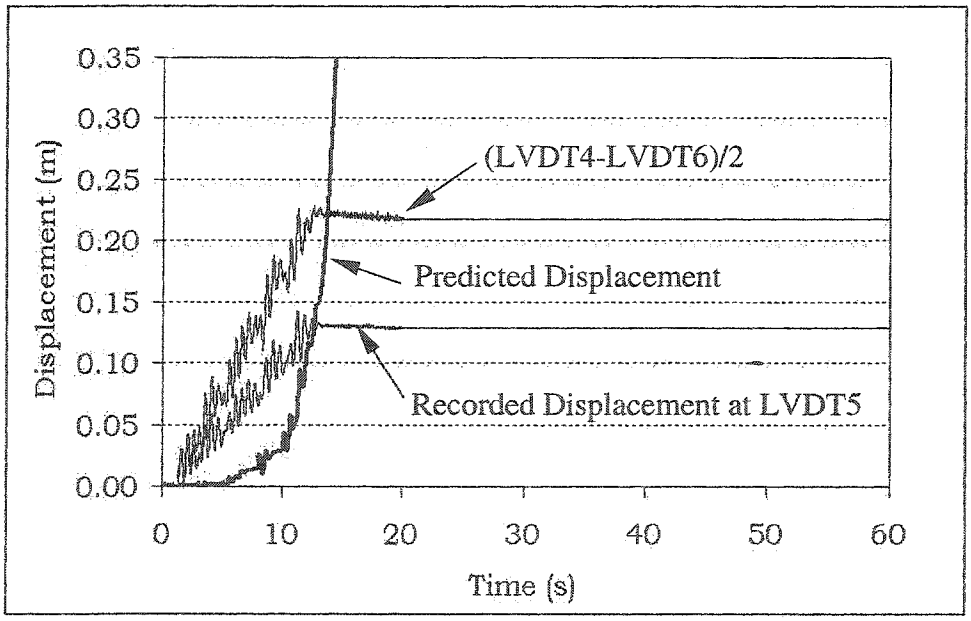

Figure 3-15. The predicted and measured permanent displacements considering excess pore water pressure build-up effects (for P7 – see Figure 3.7).

The predicted values are compared with a range of recorded displacements:

1) total displacements recorded at the level of assumed failure surface (LVDT4 for level P6 and LVDT5 for level P7), and

2) displacements resulting from shearing of a 2.5m thick soil layer centered at the level of assumed failure surface: (LVDT5-LVDT3)/2 for level P6 and (LVDT4-LVDT6)/2 for level P7.

It can be observed from the results presented in Figures 3.14 and 3.15 that the predicted displacements at the end of shaking are in fair agreement with the values recorded in the centrifuge experiment. For both locations analyzed, it was recorded in the centrifuge experiments and predicted by the numerical model that the soil was liquefied at the end of earthquake (time = 12sec.). Therefore, the yield accelerations at the end of earthquake are negative, this leading to predicting infinite post earthquake displacements. In the centrifuge model, on the other hand, due to relative rapid dissipation of excess pore water pressure, the displacements stop short time after the end of earthquake (Figure 3.14, Figure 3.15). It is therefore important to investigate the effects of excess pore water pressure dissipation after the shaking. Those effects are accounted for in Chapter 5, and more realistic predictions of slope displacements are obtained.

4 Sensitivity analysis

4.1 Introduction

In order to identify the factors and model parameters that have more effects on the predicted permanent displacements of a slope, a sensitivity analysis based on a design of experiment approach known as Response Surface Methodology (RSM). This was done on the model described in Chapter 3.

Response Surface Methodology (RSM) is a set of techniques used in the empirical study of relationships between one or more responses and a group of variables (Cornell, 1990). Although it is usually referred to as the process of identifying and fitting an appropriate response surface model from experimental data, it can be applied to numerical modeling studies, where each run can be regarded as an experiment. RSM comprises of three techniques or methods (Myers and Montgomery, 1995): (1) Statistical experimental design, in particular, two-level factorial or fractional factorial design, (2) Regression modelling techniques, and (3) Optimization methods.

RSM can be viewed from three major standpoints (Cornell, 1990):

- If the system response is rather well-studied, RSM techniques are used to find the best (optimum) value of the response.
- If obtaining the best value is beyond the available resources of the experiment, then RSM techniques are used to at least gain a better understanding of the overall response of the system.

- If obtaining the system response necessitates a very complicated analysis that requires hours of run-time and advanced computational resources then a simplified equivalent response surface may be obtained by a few numbers of runs to replace the complicated analysis.

In this chapter, advantages of RSM are discussed with regard to three aspects that are all related to the relatively complex and time-consuming nature of dynamic geotechnical analysis (even though the selected geotechnical example is one of the simplest dynamic analyses compared to recent state-of-the-art methods based on complicated constitutive relationships):

- Two-level factorial design methods, in particular fractional factorial design method, reduce the number of runs required for studying the significance of different factors that may affect the response of interest.

- The response surface model is a simplified relationship that can be used for practical engineering purposes, where spending the high costs of performing advanced numerical analysis is not desirable.

The response surface developed can replace the original model in an uncertainty analysis using Monte Carlo Simulation, and therefore, with the same number of iterations, it can reduce analysis time significantly.

In the following sections, first, a general overview of the RSM is given. Then, the method is applied to two practical examples. The first example, which studies the effects

of only three factors, is selected so that the advantages of RSM can be explained and illustrated more clearly.

The second example, which studies the effects of six factors, identifies the most important factors that have more effects on the values of the response. Finally, a comparison is made between the results of direct and indirect simulations, i.e. replicating the Newmark analysis procedure itself versus replicating the replacement model obtained by RSM.

4.2 Response Surface Methodology (General Overview)

Box and Wilson (1951) introduced the Response Surface Methodology (RSM) and others developed it for designing experiments and subsequent analysis of experimental data. The method uses Design of Experiments techniques or DOE (e.g. Montgomery, 1997), such as Two-level Full and Fractional Factorial Designs, as well as regression analysis methods (e.g. Montgomery et al., 2000), where DOE techniques are employed before, during, and after the regression analysis to evaluate the accuracy of the model.

The main idea is to replace a complicated response function with an approximate function by studying the relative significance of the effects of several factors supposed to have influence on the response of interest. Assume that the true response, y, of a system depends on k controllable input variables (or factors) $\xi_1,\xi_2,...,\xi_k$ as (Myers and Montgomery, 1995):

$$y = f(\xi_1, \xi_2, ..., \xi_k) + \varepsilon \tag{4.1}$$

The function f is called the true response function, form of which is unknown and usually complicated, and ε is a term representing sources of variability not accounted for in f. The term ε is treated as a statistical error. For two factors, (i.e. $k = 2$), a second-order polynomial approximation of the true response function is:

$$\hat{y} = \beta_0 + \beta_1 x_1 + \beta_2 x_2 + \beta_{12} x_1 x_2 + \beta_{11} x_1^2 + \beta_{22} x_2^2 \qquad (4.2)$$

where x_i are called "coded variables", which are transformed values of the "actual variables", ξ_i, to the domain of [-1,1]; and β_{ij} are called regression coefficients. In some cases, the first four terms of the above equation can satisfactorily predict the response, i.e. quadratic terms are not necessary. In most cases, the second-order model is adequate for well-behaved responses. This empirical model is called a "response surface model".

It should be noted, however, that the main limitation of the method is that RSM is a "black box" approach (Cox and Baybutt, 1981). That is, estimating the accuracy of approximation, or in other words the magnitude of the approximation errors, is difficult. The other limitation of the method is that it is a local analysis. The developed response surface is invalid for regions outside the studied ranges of factors.

In the context of Two-level Factorial Design of experiments (TFD), where low- and high-level values of each factor (i.e. minimum and maximum values of input parameters) are used to evaluate relative significance of the effects of several factors, a special notation is used that can be described briefly as follows:

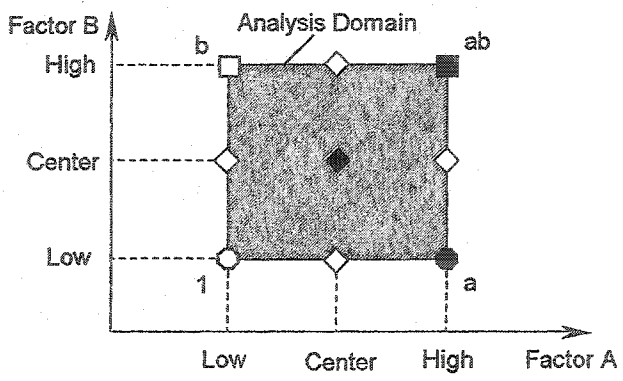

Figure 4-1. Levels of factors and analysis domain.

- Upper case letters denote factors.

- Lower case letters denote the observed response when a certain combination of factor values is used. These combinations are called "treatments". For example, for a 2-factor experiment, as shown in Figure 4.1, '1' (open circle) denotes the response obtained using low-level values of both factors, 'b' (open square) denotes the response obtained using low-level value of A and high-level value of B, and so forth.

- Upper case letters enclosed in brackets denote effects of factors. For example, [A] the main effect of factor A, has the mathematical meaning of the mean gradient of the response in direction of increasing factor A. [AB], interaction effect of factors A and B, is the joint effect of factors A and B on the response. It is the estimate of the effect of B on the effect of A, or the difference in the response that occurs when both factors are changed simultaneously from what was expected to occur based on the effect of changing the factors individually. For example, if only two factors A and B are involved in a problem, [A] and [AB] can be calculated as follows:

$$[A] = (-1 + a - b + ab)/2 \tag{4.3}$$

$$[AB] = (1 - a - b + ab)/2 \tag{4.4}$$

4.3 Application of RSM to Newmark displacement analysis of submarine slopes

In the following section the typical Newmark displacement analysis that accounts for the effect of excess pore water pressure build-up by reduction of the yield acceleration with time is considered. In this analysis, the upslope yield acceleration is considered because in nearly flat submarine slopes, upslope displacement during shaking is possible.

4.3.1 Three-Factor Analysis

To illustrate basic steps of RSM analysis, only three parameters are selected as variables; therefore, in this example only three factors are involved. Other influencing parameters are regarded as constants. Techniques of two-level factorial design of experiments (TFD) are manipulated to study the important factors affecting slope displacement due to seismic loading using Newmark analysis. Then, a response surface is obtained by using regression techniques.

4.3.1.1 Factors and Response

As mentioned in the previous section, three parameters are selected in this example: slope angle, β, friction angle, ϕ', and the earthquake type (in which only the frequency content of earthquake varies). As Newmark method is pseudo-static type method unable to capture dynamic effects, consideration of factor C (earthquake type) is to show the capability of the RSM to identify insignificant factors. Low- and high-level values of factors are shown in Table 4.1. The ranges of variable parameters are selected based on slope angles typically involved in a submarine (near- and off-shore) slope stability analysis of loose to medium dense sands. Earthquake acceleration time-histories are compatible with UBC (1994) response spectra of soil types II and III, i.e. deep

cohesionless or stiff clay soils, and soft to medium clays and sands, respectively. Earthquake records have approximately the same number of equivalent cycles (11.5) and only differ in frequency content. The details of simulating the response spectrum compatible acceleration time-histories used in this study are presented by Popescu (2002). Values of other parameters (such as porosity or number of cycles to initial liquefaction, N_L) are assumed constant. In this simplified example, N_L is selected such that no reduction in yield acceleration occurs (i.e., N_L is set to a value large enough that no build-up of excess pore water pressure occurs) and thus the lines representing the yield accelerations in Figure 3.6 are horizontal. A full consideration of the effect of pore pressure build-up is discussed in the next example.

Table 4-1. Selected Factors, Low- and High-Level Values

Factor	Notation	DOE Notation	Low	High
Slope Angle (°)	β	A	5	20
Friction Angle (°)	ϕ'	B	25	35
Earthquake Type	Type	C	II	III

The response is the slope displacement (in m) at the end of the earthquake, i.e. t = 20 sec. The constants are as follows: Gravitational acceleration, $g = 9.81\,\text{m/s}^2$; density of water, $\rho_w = 1000\,\text{kg/m}^3$; soil specific gravity, $G_s = 2.67$; porosity of soil, $n^w = 0.4$; soil cohesion, $c' = 0$; peak ground acceleration, $PGA = 0.2$. Because in this case c' is zero, yield acceleration is independent of the depth of failure plane. Further, N_L is set to a large constant value.

4.3.1.2 Factorial Design Method and Significant Effects

To study effects of three factors, $2^3 = 8$ runs are required. Table 4.2 shows the treatments, factor values and the corresponding responses obtained.

Table 4-2. Treatments, Factor Values, and Responses.

Treatment	A	B	C	Response
1	5	25	II	5.600E-05
a	20	25	II	1.096E-01
b	5	35	II	0.000E+00
ab	20	35	II	1.538E-03
c	5	25	III	3.301E-05
ac	20	25	III	1.911E-01
bc	5	35	III	0.000E+00
abc	20	35	III	1.382E-03

Analysis of variance method (ANOVA) is used to select significant factors. Effects A and B (slope angle and soil friction angle) are found to be significant. Effect C (earthquake type) is found not significant. Additionally, interaction of effects of AB is found to be significant. The interaction between A and B is negative, i.e. the increase in response due to increase in A is more pronounced when B is low (Figure 4.2).

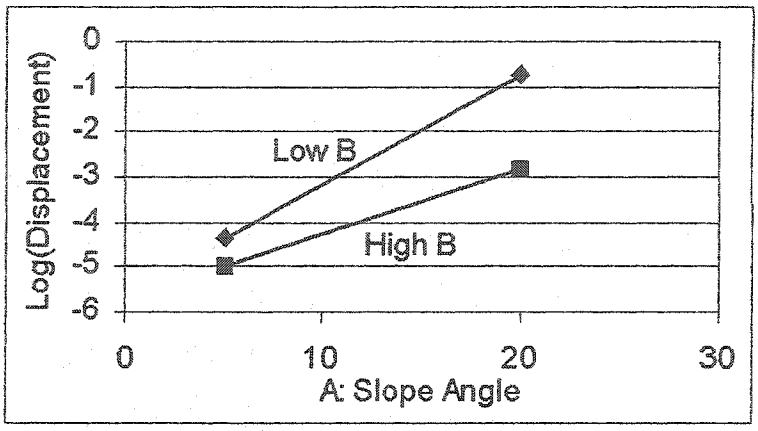

Figure 4-2. Interaction graph.

Alternatively, the above results can be obtained visually from the Normal probability plot of effects method shown in Figure 4.3. Non-significant effects tend to be normally distributed and will fall along a straight line on the normal probability plot, while significant effects fall off the line.

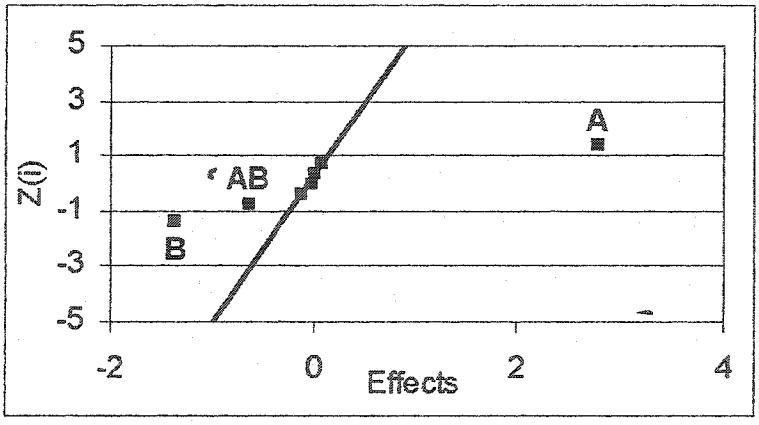

Figure 4-3. Selecting significant effects from the Normal probability plot.

From a geotechnical point of view, slope angle and soil friction angle (factors A and B) have not only significant main effects but also significant interaction effect. The negative interaction shows that an increase in slope displacement due to increase in slope angle is more pronounced when friction angle is lower (Figure 4.2). For the ranges selected in this study, it resulted that the effect of slope angle on slope permanent displacement is greater

than that of soil friction angle. Further, it is shown that earthquake type (factor C) is not significant, which is in fact because of the limitations of the Newmark method. In this respect, it has been shown by several researchers, e.g. Madabhushi and Schofield (1993) by centrifuge experiments, Popescu et al. (1997) and Popescu (2002) by numerical analysis, that the seismic loading rate, or frequency content of the seismic acceleration, has significant effects on the dynamic response of soil and soil-structure systems, especially when pore water pressure build-up is involved. To overcome this limitation, one may include in a Newmark type analysis the flexibility of soil as suggested by Rathje and Bray (2000b).

4.3.1.3 Regression Analysis

Based on the results obtained from the TFD, the following regression models are developed in terms of the coded and actual values of the significant factors, respectively:

$$\log(Disp.) = -3.236 + 1.400A - 0.6801B - 0.3168AB \tag{4.5}$$

$$\log(Disp.) = -4.657 + 0.4401\beta - 0.03042\phi' - 0.008448\beta\phi' \tag{4.6}$$

Note that a very small constant value (10^{-5}) is added to the displacements before log-transformation. The residuals of the model are approximately normally distributed and the variance of the residuals is homoscedastic i.e. in a plot of residual versus predicted values, data points lie between two parallel lines, which indicates that variance of residuals is constant and the log transformation is appropriate. The R^2 of the regression model is 0.9976. The predicted R^2 is 0.96.

The aforementioned regression model is based on two levels of factors. Significance of curvature of the response surface is checked by including additional levels (diamonds in Figure 4.1). In this study, a face-centered central composite design (CCD) was used. Again, significance is determined using ANOVA. According to this method, it is found that the curvature of the surface is significant. Therefore, there is need to consider second-order terms. The regression model, in terms of the coded and actual factors, is as follows:

$$\log(Disp.) = -3.515 + 1.901A - 1.335B + 0.4211A^2 - 0.1454B^2 - 0.3169AB + 0.6548A^2B - 0.5014AB^2 \quad (4.7)$$

$$\log(Disp.) = 13.26 - 0.3407\beta - 1.454\phi' - 0.06236\beta^2 + 0.02761\phi'^2 + 0.09379\beta\phi' + 0.002328\beta^2\phi' - 0.002674\beta\phi'^2 \quad (4.8)$$

The plot of the predicted versus actual values, shown in Figure 4.4, indicates the very good agreement between the response surface model and the actual values. Equation 4.8 is depicted in Figure 4.5.

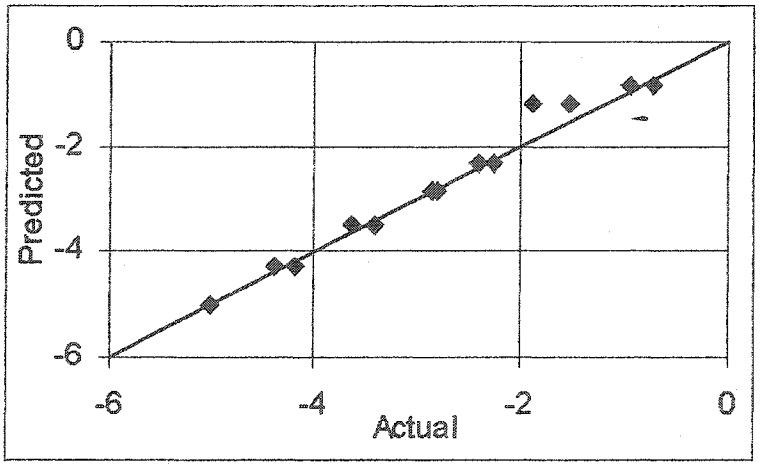

Figure 4-4. Graph of predicted versus actual values.

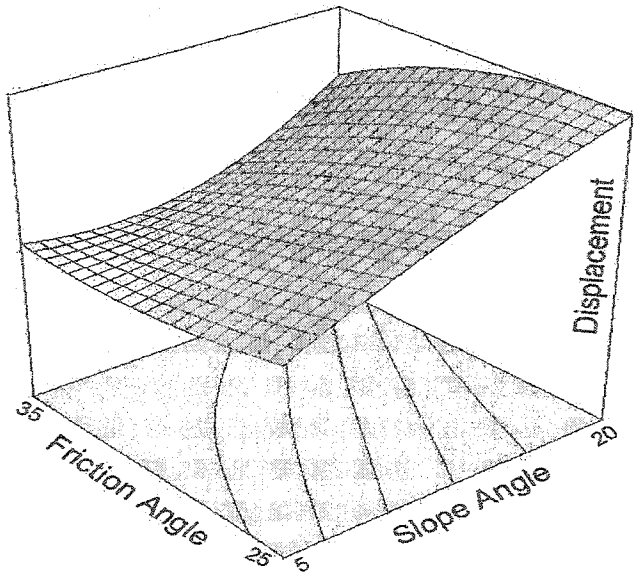

Figure 4-5. Three-dimensional presentation of the developed response surface model.

4.3.2 Six-Factor Analysis

In this next example, six parameters are selected: slope angle, β, friction angle, ϕ', a parameter defining the rate of excess pore water pressure (EPWP) generation, α (see Eq. 3.11), earthquake peak ground acceleration, PGA, and equation parameters a and b relating N_L to cyclic stress ratio (CSR) as follows:

$$CSR = a[Log(N_L)]^b \tag{4.9}$$

where CSR is defined as (Seed and Idriss, 1971):

$$CSR = \frac{\tau_{av.}}{\sigma'_{v0}} = 0.65\frac{a_{\max}}{g}\frac{\sigma_{v0}}{\sigma'_{v0}}r_d \tag{4.10}$$

in which σ_{v0} and σ'_{v0} are initial total and effective stresses, respectively, $a_{\max}$ maximum acceleration of earthquake at ground level, and r_d is a depth reduction factor. Note that $PGA = a_{\max}/g$, and for a submarine slope, the ratio between σ_{v0} and σ'_{v0} in the above

equation is taken equal to the ratio between saturated and buoyant unit weights of the soil.

As in the first example, techniques of two-level factorial design of experiments (TFD) are used to identify the significant factors. Results of the full factorial design are then compared to the results of two-level fractional factorial design (TFFD), in which much lower number of runs are required to identify the significant factors. Specifically, the half-fraction design requires only half the number of runs compared to a full TFD.

4.3.2.1 Factors and Response

Low- and high-level values of factors noted in the previous section are selected as shown in Table 4.3.

Table 4-3. Selected Factors, Low- and High-Level Values.

Factor	Notation	DOE Notation	Low	High
Slope Angle (°)	β	A	5	10
Friction Angle (°)	ϕ'	B	30	35
EPWP Rate	α	C	0.5	0.9
Peak Horizontal Acceleration (m/s^2)	PGA	D	0.15	0.25
N_L Parameter	a	E	0.35	0.45
N_L Parameter	b	F	-0.7	-0.5

The response is the slope displacement (in m) at the end of the earthquake (t = 20 sec.) using Newmark method. The other parameters are assumed constant and are as follows: Gravitational acceleration, $g = 9.81\,\text{m/s}^2$; density of water, $\rho_w = 1000\,\text{kg/m}^3$; soil specific

gravity, $G_s = 2.67$; porosity of soil, $n = 0.4$; and soil cohesion, $c' = 0$. Because c' is zero, yield acceleration is independent of the depth of failure plane.

4.3.2.2 Full Factorial Method

To study the effects of six factors, $2^6 = 64$ runs are required. Analysis of variance method (ANOVA) is used to find factors with significant effects. Effects A, B, C, D, E, F, AD, BD, CD, DE, and DF are found to be significant. Effect D (peak ground acceleration, PGA) that is the most significant effect, has significant interactions with all other factors. Alternatively, these results can be obtained visually from the Normal probability plot of effects method shown in Figure 4.6.

From a geotechnical point of view, the above results are interesting. It is shown that, in spite of the relatively narrow range considered for this study, PGA (factor D) is the most significant main effect that has significant interactions with all other factors (such as slope angle, friction angle, etc.); therefore, the slope displacement, obtained by the method presented in Chapter 3 (Newmark analysis accounting for effects of pore water pressure build-up), is highly sensitive to the earthquake maximum acceleration (PGA). A slight increase in the maximum acceleration results in a sharp increase in the displacement, especially when the soil liquefaction potential is significant, i.e. when N_L is smaller than (or close to) the equivalent number of cycles induced by the earthquake.

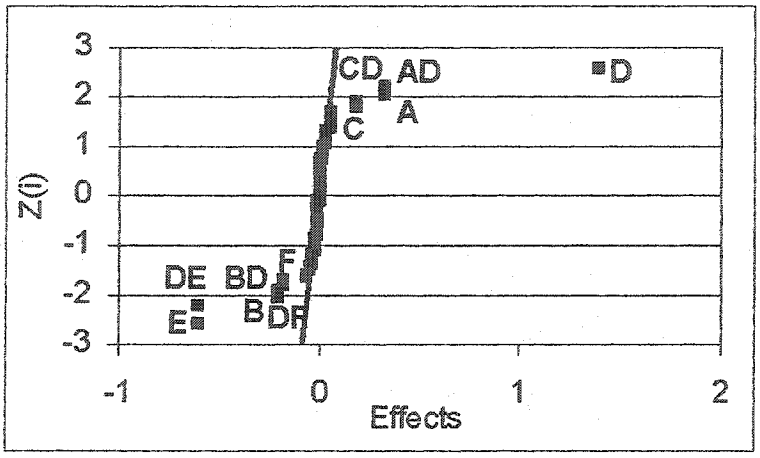

Figure 4-6. Selecting significant effects from the Normal probability plot.

In addition, it is shown that there is no significant interaction between other factors because the interaction between PGA and factors A to F are dominant. The negative interaction between soil friction angle and PGA (effect BD), for example, shows that the increase in slope displacement due to increase in PGA is sharper when friction angle is lower. In general, sensitivity of the slope displacement to PGA is larger when friction angle, and N_L parameters are lower, or slope angle and EPWP rate are higher.

4.3.2.3 Regression Analysis

Based on the results obtained from TFD, the following regression models, in terms of coded and actual factors, are obtained:

$$\log(\textit{Disp}.) = -3.607 + 0.3239\,A - 0.1979\,B + 0.1888\,C + 1.3925\,D - 0.5994\,E - 0.1738\,F + 0.3240\,AD - 0.1979\,BD + 0.1888\,CD - 0.5994\,DE - 0.1738\,DF \quad (4.11)$$

$$\log(Disp.) = -23.26 - 0.3888\beta + 0.2375\phi' - 2.832\alpha + 121.7\,PGA + 35.96a + 5.215b + 2.592\beta \times PGA - 1.584\phi' \times PGA + 18.88\alpha \times PGA - 239.77a \times PGA - 34.77b \times PGA \quad (4.12)$$

The residuals of the model are approximately normally distributed and the variance of the residuals is homoscedastic. The R^2 of the regression model is 0.9833. The predicted R^2 is 0.95. The response surface curvature is checked by including additional levels of factors

and it is found that it is not significant. The plot of the predicted versus actual values of log Displacement (Figure 4.7) shows the very good agreement between the response surface model and the actual values.

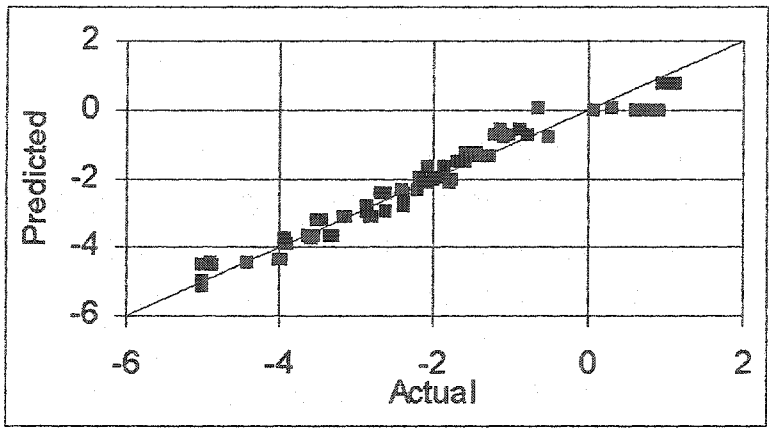

Figure 4-7. Graph of predicted versus actual values of log Displacement.

4.3.2.4 Fractional Factorial Method

In problems involving large number of factors, two-level fractional factorial design (TFFD) can be used to reduce the number of runs required to estimate main and interaction effects. The idea is based on neglecting high-order interaction effects. Normally, interactions of three and more factors can be neglected.

In this example, a half-fractional factorial analysis is carried out by selecting the defining contrast as ABCDEF. Therefore, only half of 64 runs (= 32) are enough to estimate the main and two-factor interaction effect with high accuracy.

Analysis of variance method (ANOVA) is used to find factors with significant effects. In this case, effects A, B, C, D, E, F, AD, BD, CD, DE, and DF are found to be significant model terms. This qualitative result is identical to the result obtained from the full factorial method.

Based on the results obtained from TFFD, the following regression models, in terms of coded and actual factors, are obtained:

$$\log(Disp.) = -4.146 + 0.3704A - 0.2544B + 0.2173C + 1.854D - 0.6563E - 0.1842F + 0.3704AD - 0.2544BD + 0.2173CD - 0.6563DE - 0.1842DF \quad (4.13)$$

$$\log(Disp.) = -28.30 - 0.4445\beta + 0.3053\phi' - 3.259\alpha + 148.7PGA + 39.38a + 5.527b + 2.963\beta \times PGA - 2.0352\phi' \times PGA + 21.73\alpha \times PGA - 262.51a \times PGA - 36.85b \times PGA \quad (4.14)$$

Comparing Eqs. 4.14 and 4.12 (or 4.13 and 4.11) shows that the estimates of the effects (or equivalently, regression coefficients) are slightly different; however, the R^2 of the model is 0.9740, which is very close to the value of R^2 obtained from full factorial method. This indicates that since both model predictions obtained from the full and fractional factorial methods are satisfactorily accurate and approximately similar (see also Figure 4.8), for future studies on other ranges of the selected factors the fractional method may be used with sufficient accuracy, leading to significant reduction in the number of runs and analysis time.

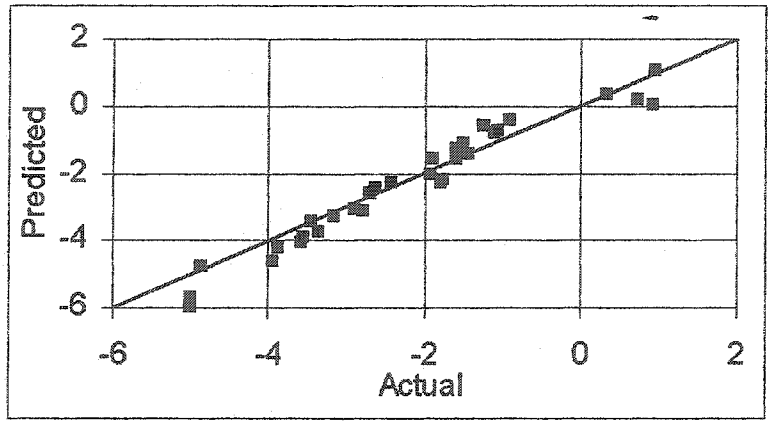

Figure 4-8. Graph of predicted versus actual values.

4.3.3 Monte Carlo Simulation

According to Cox and Baybutt (1981), response surface methods of uncertainty analysis were developed to overcome the disadvantages of the Monte Carlo approach, related to computational effort.

Figure 4.9 shows a comparison between cumulative distribution functions (CDF) of slope displacement obtained from Monte Carlo simulations of the actual model (i.e., Newmark analysis procedure) and RSM replacement model (Eq. 4.8). In this example, the three-factor analysis is selected to show the advantage of using the RSM replacement model with regard to analysis time.

For this analysis, it is assumed that slope and soil friction angles are normally distributed, with mean values of 10^{o} and 28^{o}, respectively, and standard deviation of 1^{o}.

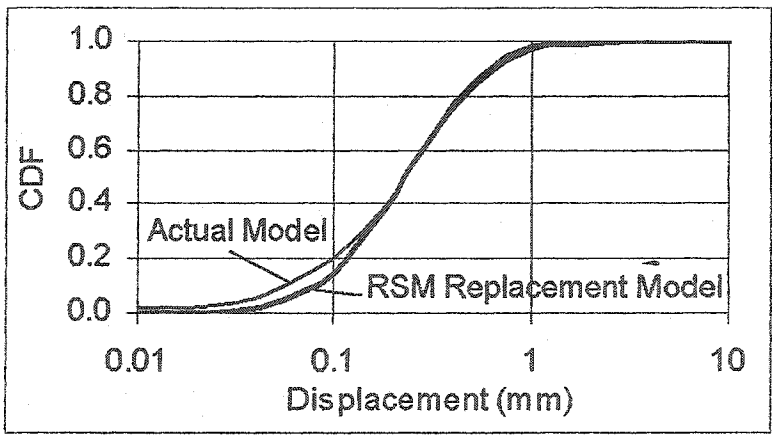

Figure 4-9. Comparison between CDF's of displacement obtained from Monte Carlo simulations of the actual and RSM replacement models.

It is obvious that the result of Monte Carlo simulation integrated with RSM is very close to that obtained from simulating the actual model; especially, when displacement is larger

than 0.1 mm the two results are almost identical. In fact, this portion of the curve is of more importance for risk evaluation purposes.

Even though the Newmark analysis does not require a very long computational time, the time benefit of using RSM replacement model is significant owing to the number of replications required for Monte Carlo simulation. Obviously, replicating the Newmark analysis procedure 1000 times takes more time than replicating a simple formula.

4.4 Summary

General and specific advantages of the Response Surface Methodology (RSM) applied to Newmark displacement analysis of submarine slopes subject to earthquakes were discussed. It is shown that:

- By using RSM techniques, specifically two-level factorial design method, one can efficiently identify the significant factors. Most importantly, it is shown that Newmark displacement (obtained from an analysis that accounts for the effect of excess pore water pressure build-up) is highly sensitive to maximum acceleration of the earthquake (or peak ground acceleration, PGA). Newmark analysis assumption cannot take into account the effects of frequency content of the seismic motion. All other factors considered here, including slope angle, soil friction angle, excess pore water pressure rate, etc. are not only significant but also have significant interaction effects with the PGA.

- Simple relationships between slope displacement and the significant influencing factors considered in this study are obtained using regression analysis. Within the assumptions of the Newmark method, predictions provided by these relationships are

satisfactorily accurate in the selected ranges of factors. These relationships, or response surfaces, can be used as replacements of the actual model, in which several analysis procedures should be followed in order to calculate the slope displacements.

- The replacement model obtained by the RSM can be used in an uncertainty analysis by Monte Carlo simulation method. It is shown that the result obtained from Monte Carlo integrated with the RSM is very close to that obtained from replicating the actual model. The analysis time, however, is significantly different, which indicates the advantage of using the RSM replacement model in uncertainty analyses.

One should note, however, that the response surface models obtained are valid only in the selected ranges of the parameters.

One of the most important results of this study is that RSM techniques show that the analysis method presented in Chapter 3 is very sensitive to the maximum earthquake acceleration which leads us to the importance of accounting for the effects of excess pore water pressure dissipation. In case where soil liquefies, the yield acceleration at the end of earthquake is less than zero, which results in infinite displacement of the slope. However, considering the dissipation of excess pore water pressure after the earthquake and the fact that during the dissipation phase soil regains part of its shear strength and the yield acceleration increases yields a more realistic prediction of permanent displacement of the slope.

5 Accounting for excess pore water pressure dissipation

5.1 Introduction

After the end of shaking the generated pore pressures start to dissipate with time, which results in increasing soil strength and yield acceleration. In this chapter, the effects of excess pore water pressure dissipation are investigated, and a procedure for calculating permanent displacements of submarine slopes subjected to seismic loads is introduced. The model presented in chapter 3 is upgraded to include upward dissipation of excess pore water pressure after the end of shaking. The proposed model is validated based on centrifuge test results.

5.2 Analysis Procedure

When using the model presented in chapter 3 for analyzing slopes where soil liquefies, the yield acceleration at the end of shaking is less than zero, which results in infinite post earthquake displacements (Figure 5.1).

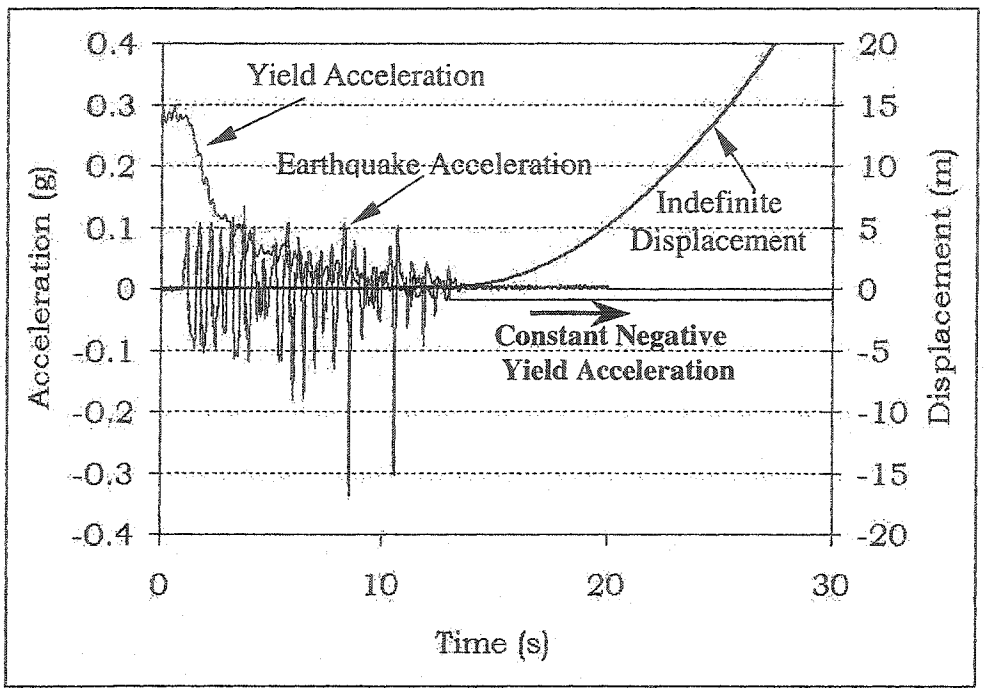

Figure 5-1. Slope displacement ignoring the effect of excess pore water pressure dissipation.

In reality, however, due to dissipation of pore pressure the soil regains part of its original shear strength and the yield acceleration increases and becomes positive (Figure 5.2). This results in limiting the displacements. Therefore, accounting for excess pore water pressure dissipation after the earthquake may provide a more realistic prediction of post-seismic displacements. It is assumed that dissipation phase starts at the end of strong shaking period when the equivalent number of cycles remains constant.

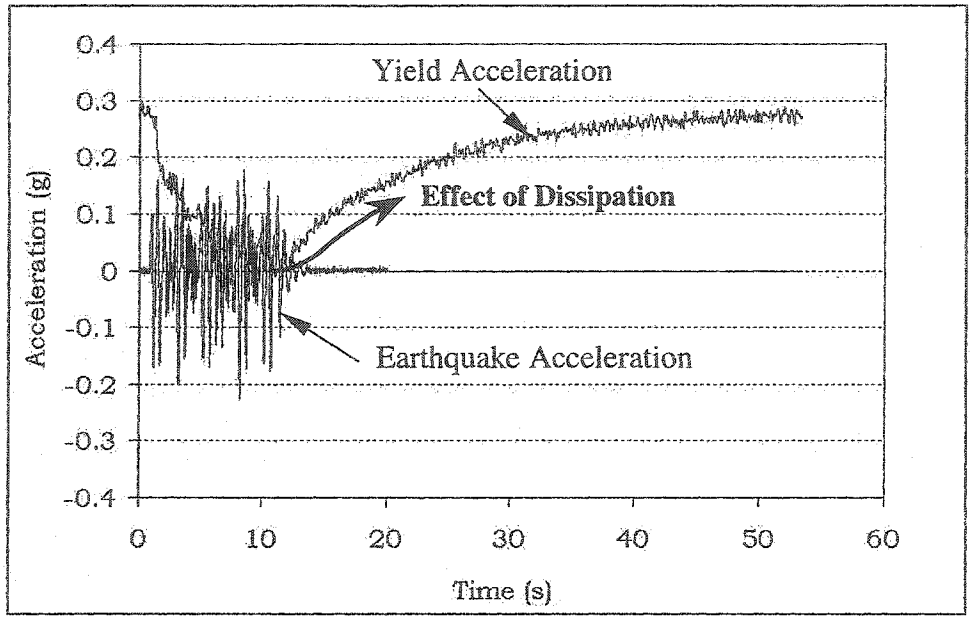

Figure 5-2. The variation yield acceleration during and after the earthquake based on recorded values of pore water pressure for level P7, VELACS Model #2 (Figure 3.7).

The one-dimensional consolidation theory can be applied to estimate the excess pore water pressure dissipation rate. In this study it is assumed that dissipation occurs only upward and excess pore water pressure is linearly increasing with depth.

In a soil layer with an arbitrary distribution of the initial excess pore pressure with depth $[u_i(z)]$, the excess pore pressure, $u_e(t,z)$ at any time instant, t, and depth z is (e.g. Craig 1992):

$$u_e(t,z) = \sum_{n=1}^{n=\infty}[(\frac{1}{d}\int_0^{2d} u_i(z)\sin\frac{n\pi z}{2d}dz)(\sin\frac{n\pi z}{2d})\exp(-\frac{n^2\pi^2 c_v t}{4d^2})] \qquad (5.1)$$

where $[u_i(z)]$is initial excess pore water pressure, in general a function of depth z, and $c_v = k/(m_v\gamma_w)$ is the coefficient of consolidation with k being the hydraulic conductivity , m_v the coefficient of volume compressibility and γ_w the unit weight of water. Assuming

that the soil layer liquefies during the earthquake to a depth d below soil surface, and considering upward dissipation only, d in Equation (5.1) represents the length of the longest drainage path. Under the previous assumptions, the initial excess pore water pressure (at the beginning of dissipation phase) is equal to the initial vertical effective stress; therefore, u_i is a linear function of z and can be expressed by the following relation:

$$u_i = \sigma'_{vo} = \gamma' z \cos^2 \beta \qquad \text{for } 0 \le z \le d \tag{5.2}$$

where γ' is the soil buoyant unit weight and β is slope angle. By substituting u_i in Equation 5.2 , the first term of Equation 5.1 becomes:

$$(\frac{1}{d}\int_0^{2d} cz \sin\frac{n\pi z}{2d} dz) = (\frac{c}{d}\int_0^{2d} z \sin\frac{n\pi z}{2d} dz) \tag{5.3}$$

For simplicity parameter c is substituted for $\gamma' \cos^2 \beta$, which is constant. Using integration-by-parts as follows, Equation 5.4 can be obtained for calculating the excess pore water pressure during the dissipation.

Let $u = z$, $\alpha = \frac{n\pi}{2d}$, $dv = \sin(\alpha z)dz$ $\therefore v = -\frac{1}{\alpha}\cos\alpha z$ and $du = dz$.

We know that $\int udv = uv - \int vdu$, therefore:

$$\int_0^{2d} z \sin\frac{n\pi z}{2d} dz = -\frac{1}{\alpha} z \cos\alpha z \Big]_0^{2d} - \int_0^{2d} -\frac{1}{\alpha}\cos\alpha z dz$$

$$= -\frac{1}{\alpha} z \cos\alpha z \Big]_0^{2d} + \frac{1}{\alpha^2}\sin\alpha z \Big]_0^{2d}$$

$$= -\frac{4d^2}{n\pi}\cos n\pi + \frac{4d^2}{n^2\pi^2}\sin n\pi$$

$$\therefore \frac{1}{d}\int_0^{2d} cz \sin\frac{n\pi z}{2d}dz = c(-\frac{4d}{n\pi}\cos n\pi + \frac{4d}{n^2\pi^2}\sin n\pi)$$

$$\therefore u_e(t,z) = \sum_{n=1}^{n=\infty}[\gamma' \cos^2\beta(-\frac{4d}{n\pi}\cos n\pi)(\sin\frac{n\pi z}{2d})\exp(-\frac{n^2\pi^2 T_v}{4})] \qquad (5.4)$$

where T_v is the time factor:

$$T_v = \frac{c_v t}{d^2} \qquad (5.5)$$

When using Equation (5.4) to calculate $u_e(t,z)$, one has to decide on a finite number of terms n_{max} after which the infinite summation is truncated. Different values of n_{max} are considered to find an optimum value combining sufficient numerical accuracy and limited computational effort. The values of excess pore water pressure ratio for n_{max} equal to 5, 10, 15 and 20 are considered (Figure 5.3). It is shown that for t<1 second, the values of excess pore water pressure ratio for different values of n_{max} are different and after that the values of excess pore water pressure ratio for all n_{max}'s will be the same (Figure 5.4). By increasing the value of n_{max} to 20, the value of excess pore water pressure ratio at the beginning of the dissipation phase goes close to the corrected value. Therefore the value $n_{max} = 20$ is used in Equation (5.4).

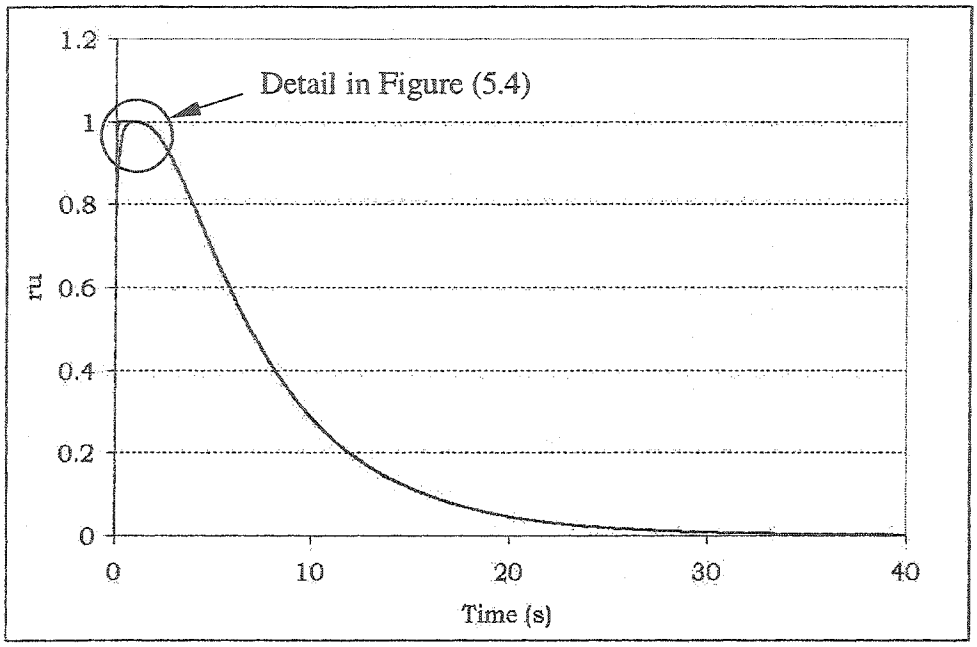

Figure 5-3. Excess pore water pressure ratio for different values of n $_{max}$.

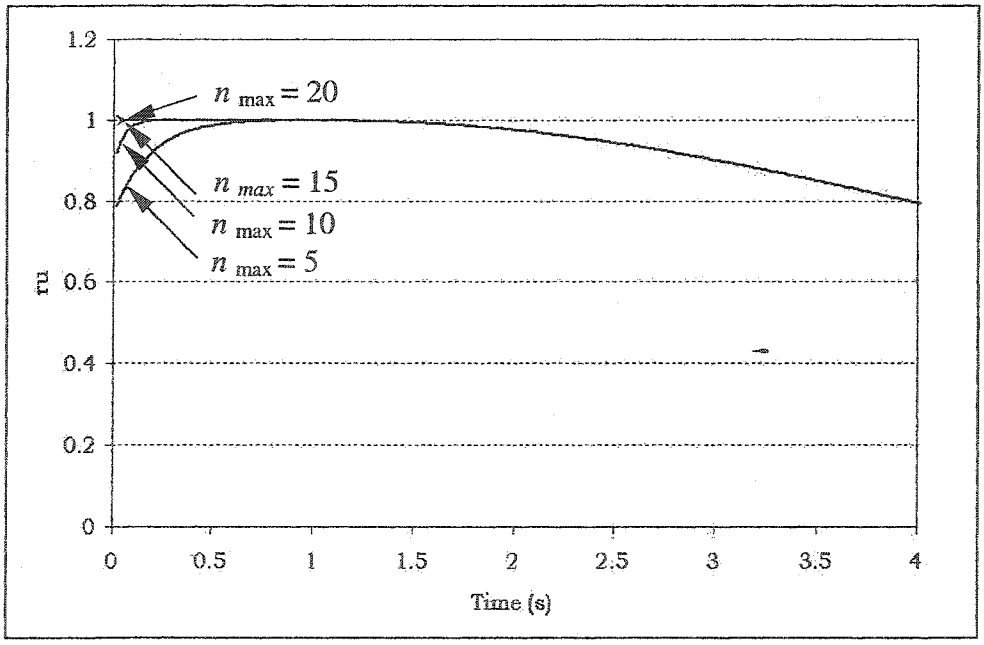

Figure 5-4. Excess pore water pressure ratio for different values of n $_{max}$ (Detail).

5.3 Calibration and Validation Using Centrifuge Test Results

To calibrate and verify the analysis procedure described in the previous section, the results of centrifuge test for model 2 (described in section 3.3) for both level P6 and P7

have been used. The geomechanical soil properties were inferred by Popescu and Prevost (1993), based on results of laboratory soil tests.

5.3.1 Estimating the coefficient of consolidation

The values of excess pore water pressure after dissipation calculated using Equation (5.4) as well as the values recorded in the centrifuge test at point P6 and P7 are shown in Figure 5.5 and 5.6 respectively. All other parameters are described in Section 3.4.

For this comparison, since the base of the centrifuge box is impervious, the boundary condition at the base is considered as impervious, and it is assumed that the soil deposit is liquefied over the entire depth at the end of shaking. Therefore, the length of the longest drainage path, d in Equation (5.1), is set equal to 10m.

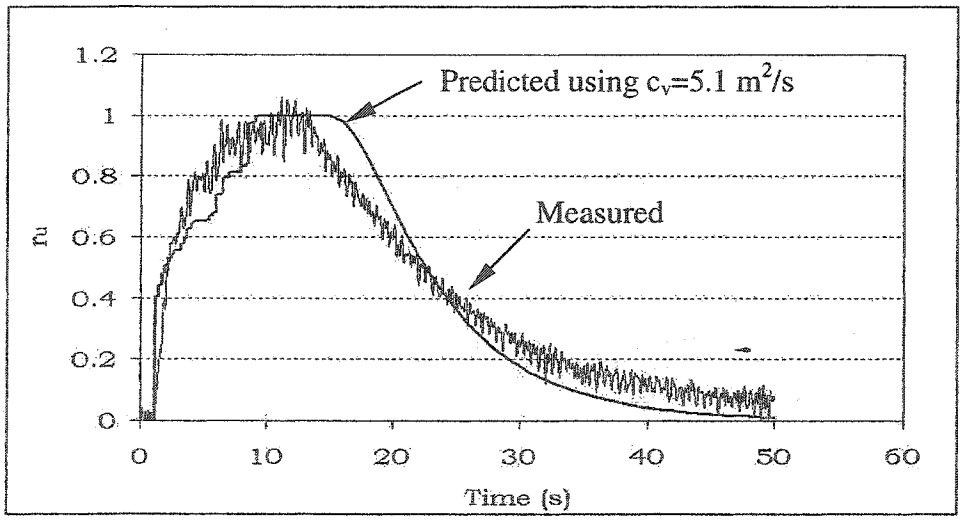

Figure 5-5. Predicted and measured excess pore water pressures at transducer P6 (see Figure 3.7).

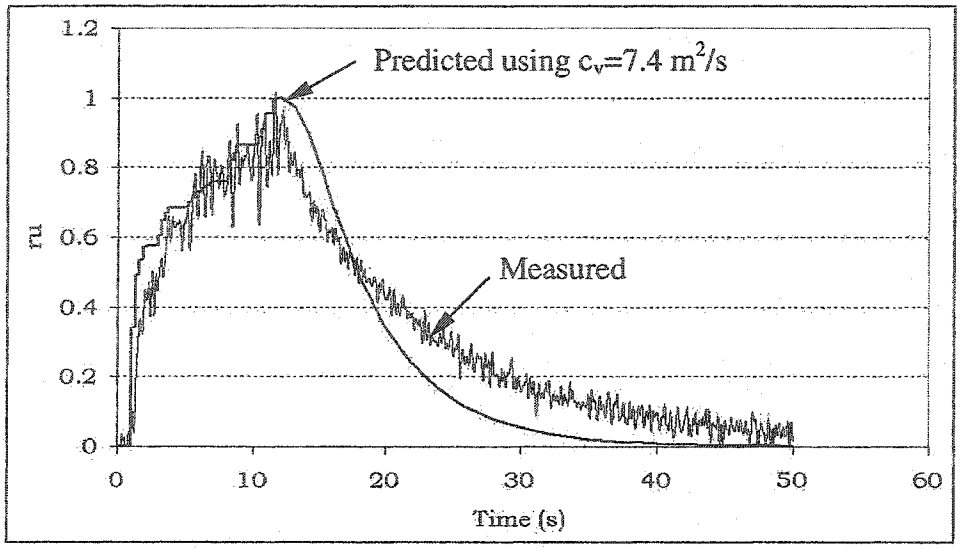

Figure 5-6. Predicted and measured excess pore water pressures at transducer P7 (see Figure 7).

During the dissipation phase, the effective confining stress may vary between values as low as zero to the initial values before the earthquake. Therefore, the coefficient of consolidation, c_v, may vary over a wide range. In this study, an average value of c_v is considered, corresponding to the average bulk modulus of soil during the dissipation phase. Values of c_v = 5.1 m/s^2 and c_v = 7.4 m/s^2 were calculated for the two locations (P6 and P7) using a value $k = 3.3\times10^{-3} m/s$ for hydraulic conductivity (Popescu & Prevost 1993) and computing the coefficient of volume compressibility as $m_v = 1/B_{av}$. B_{av} is the average low strain bulk modulus of the soil that is a function of the average effective confining stress during the dissipation phase. At any effective confining pressure, p':

$$B = B_0\left(\frac{p'}{p'_0}\right)^n \tag{5.6}$$

with $n \approx 0.5$ for sands. According to Popescu and Prevost (1993), the low strain bulk modulus for Nevada sand at 40% relative density used in VELACS project is $B_0 = 54.2$ MPa at confining pressure $p'_0 = 100$ kPa. For the point under question, since it is assumed

that the soil goes from a state of liquefaction (zero effective stress) to a state of complete dissipation of excess pore pressures, we can assume that the average confining pressure is:

$$p' = 0.5\sigma'_{v0}\frac{1+2k_0}{3} \tag{5.7}$$

where $k_0 = 0.47$ is the coefficient of earth pressure at rest.

Back analyzed values of c_v from the centrifuge test results at the two locations resulted as $c_v = 5.7$ m/s^2 and 7.6 m/s^2, which are satisfactorily close to the calculated values.

According to Martin and Seed (1979), the values of coefficient of compressibility is influenced by the excess pore water pressure ratio for relative density larger than 60% (Figure 5.7). This figure also shows the variation of m_v with r_u for relative density equal to 40% used in this study which is between D_r=30% and D_r=50%.

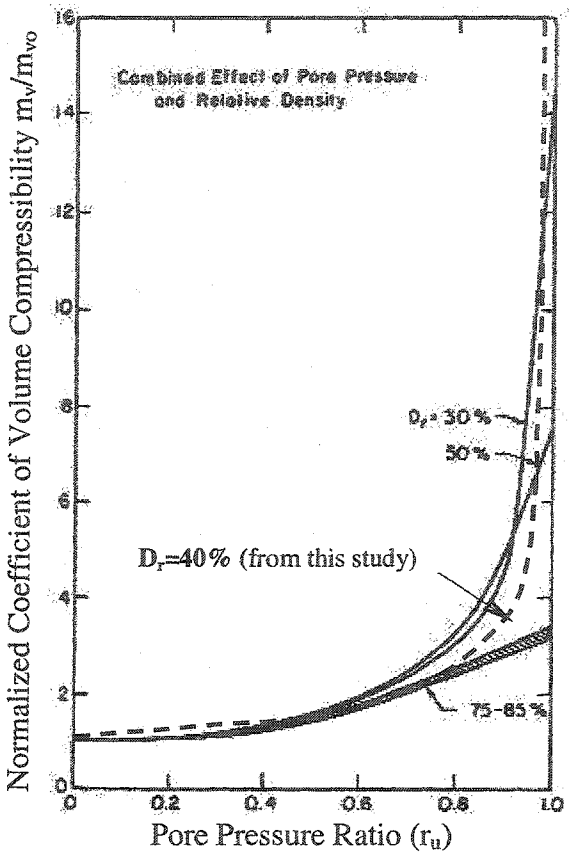

Figure 5-7. Compressibility of saturated sands following pore pressure build-up(Martin and Seed, 1979).

Figure 5-8 shows the variation of c_v with r_u changing from zero to one for level P7.The average value used above is also shown in Figure 5-8.

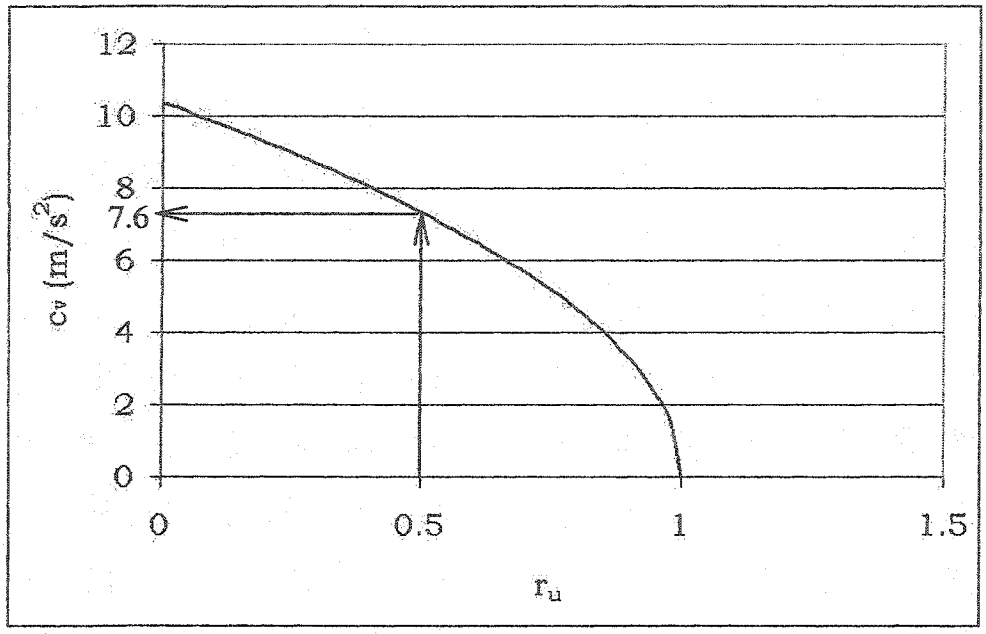

Figure 5-8. Variation of coefficient of consolidation (c_v) with excess pore water pressure ratio (r_u).

5.4 Slope displacements considering build-up and dissipation

Finally, by applying all the previously described procedures the yield accelerations for level P6 and level P7 are calculated and shown in Figures 5.9 and 5.10 respectively. Also the permanent displacements for levels P6 and P7 are calculated and shown in Figures 5.11 and 5.12 respectively. The recorded displacement for level P6 is assumed equal to (LVDT3-LVDT5)/2 and the recorded displacement for level P7 is assumed equal to (LVDT4-LVDT6)/2, where LVDTi represents the horizontal displacements reported by the device LVDTi (see Figure 3.7). The predicted values are satisfactorily close to the recorded values.

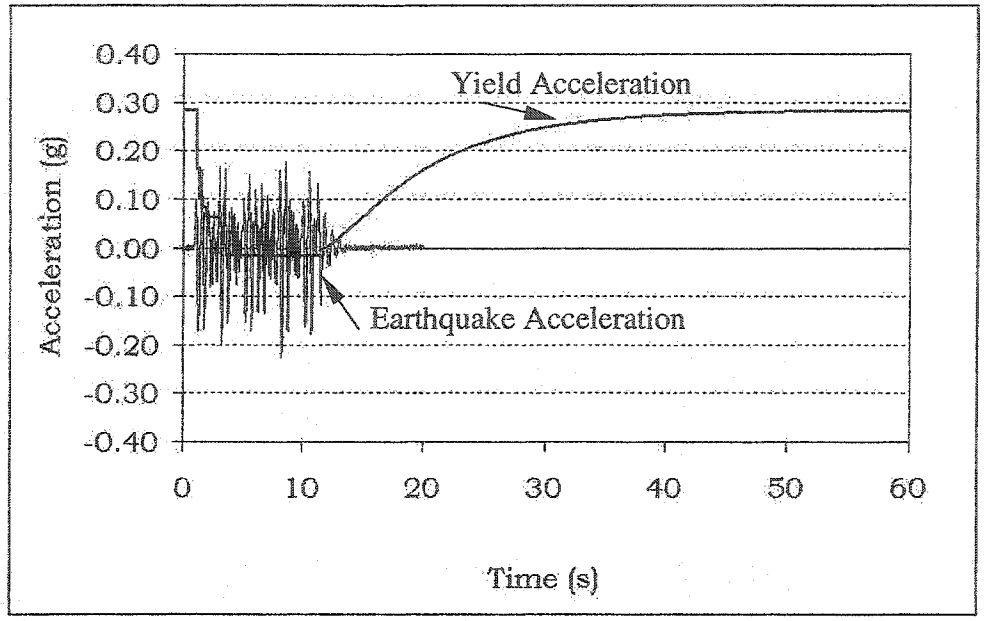

Figure 5-9. Yield Acceleration considering excess pore water pressure build-up and dissipation effects (for P6 – see Figure 3.7).

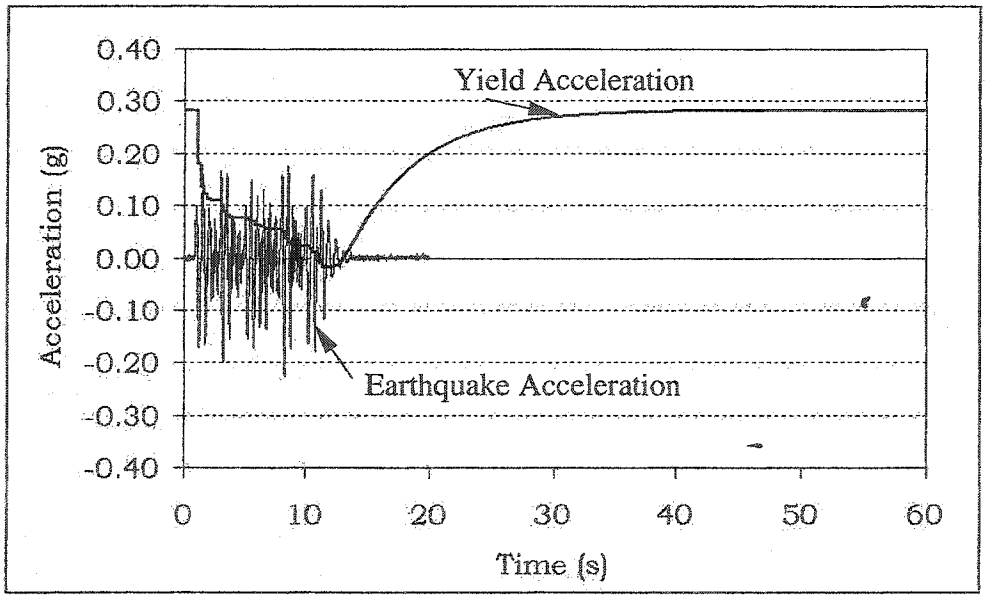

Figure 5-10. Yield Acceleration considering excess pore water pressure build-up and dissipation effects (for P7 – see Figure 3.7).

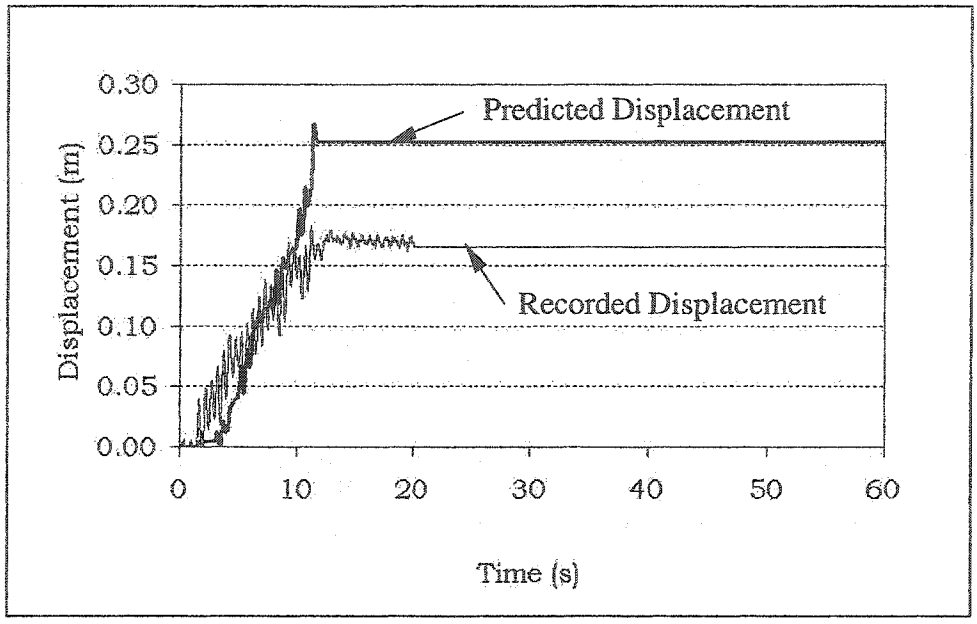

Figure 5-11. The predicted and measured permanent displacements considering excess pore water pressure build-up and dissipation effects (for P6– see Figure 3.7).

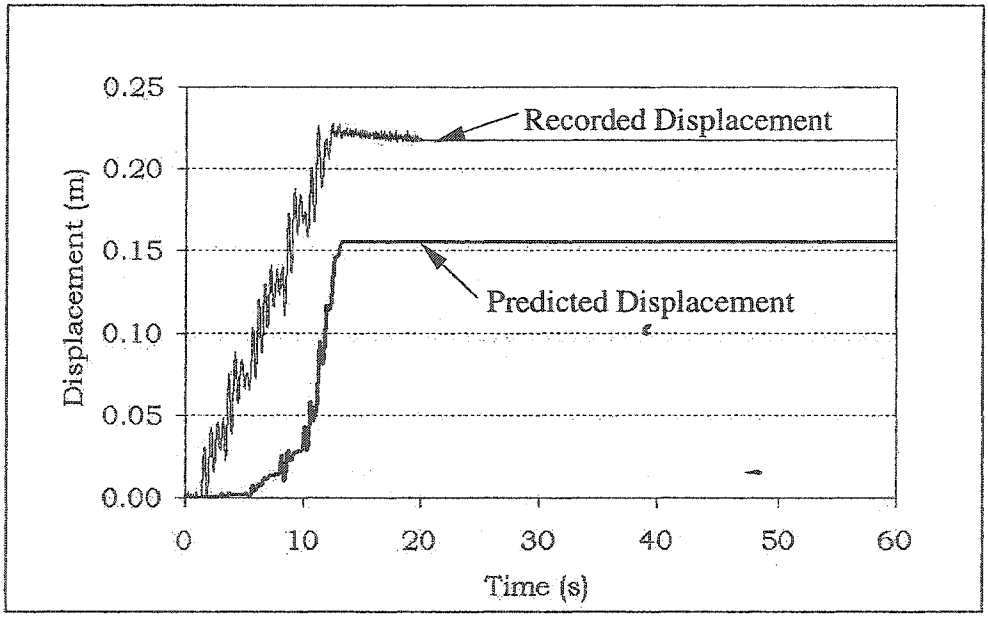

Figure 5-12. The predicted and measured permanent displacements considering excess pore water pressure build-up and dissipation effects (for P7 – see Figure 3.7).

5.5 Summary

The original Newmark model has been enhanced by applying state-of-practice methods of estimating the excess pore water pressure build-up during seismic events and dissipation after the earthquake to obtain more realistic predictions of permanent slope

displacements. The results have been calibrated, and validated based on centrifuge test results. The results show that the proposed procedure is promising, especially for risk assessment, involving a large number of analyses and requiring a reliable and time effective algorithm.

However, because of the fact that the recorded values in the centrifuge model show the gradual deformation in the soil (Figure 5.14.) and because by using a single rigid block, the model is not able to reproduce gradual soil deformation, it is important to account for more than one rigid block to achieve the distribution of displacement with depth.

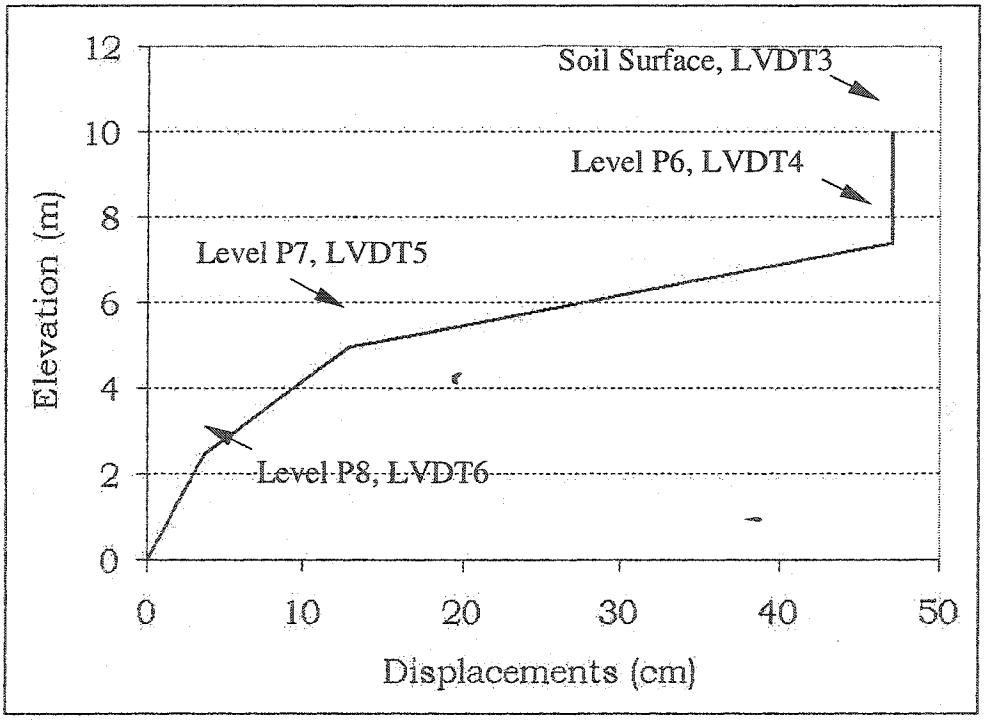

Figure 5-13. Recorded final displacements for centrifuge model # 2.

6 Accounting for more than one failure surface

6.1 Introduction

The Newmark model assumes that slope displacements are concentrated in a narrow band, i.e. below a moving block of soil. This is a good assumption for layered soils having a weaker layer between more resistant soils. In homogeneous soil deposits, the displacements are usually distributed with depth, with maximum values at the soil surface. For such situation, the rigid block assumption may induce significant differences between actual and predicted slope displacements. This limitation can be mitigated by considering a stack of rigid blocks (Figure 6.1). In this study, two moving blocks have been considered to investigate the importance of accounting for more than one block on the predicted slope displacements.

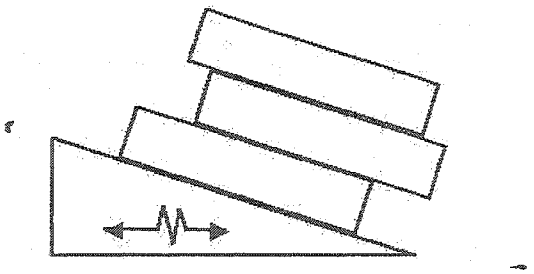

Figure 6-1. Model considering more than one rigid block.

6.2 Analysis Procedure

Two failure surfaces, parallel to the slope are considered in this study (Figure6.2). The factors of safety (FS) are expressed by the ratio of available soil shear strength (τ_f) to the shear stress developed on the failure plane (τ) for each failure surface separately as follows:

$$FS_1 = \frac{\tau_{f1}}{\tau_1} \tag{6.1}$$

$$FS_2 = \frac{\tau_{f2}}{\tau_2} \tag{6.2}$$

where, similar to one-failure surface case, soil shear strength at failure is expressed in terms of effective parameters according to the Mohr-Coulomb failure criterion:

$$\tau_{f1} = c_1' + (\sigma_1 - u_1)\tan\phi_1' \tag{6.3}$$

$$\tau_{f2} = c_2' + (\sigma_2 - u_2)\tan\phi_2' \tag{6.4}$$

where, c_1' and c_2' are the soil effective cohesions, for the bottom and the top layer, respectively, ϕ_1' and ϕ_2' are the effective internal friction angles at the base of the bottom layer and at the base of the top layer, respectively. σ_1 and σ_2 are the total stresses (normal to the failure surfaces), u_1 and u_2 are the total (hydrostatic + excess) pore water pressures, for the bottom and the top layer, respectively. It is assumed that the soil friction angle for the bottom layer is larger than that for the top layer.

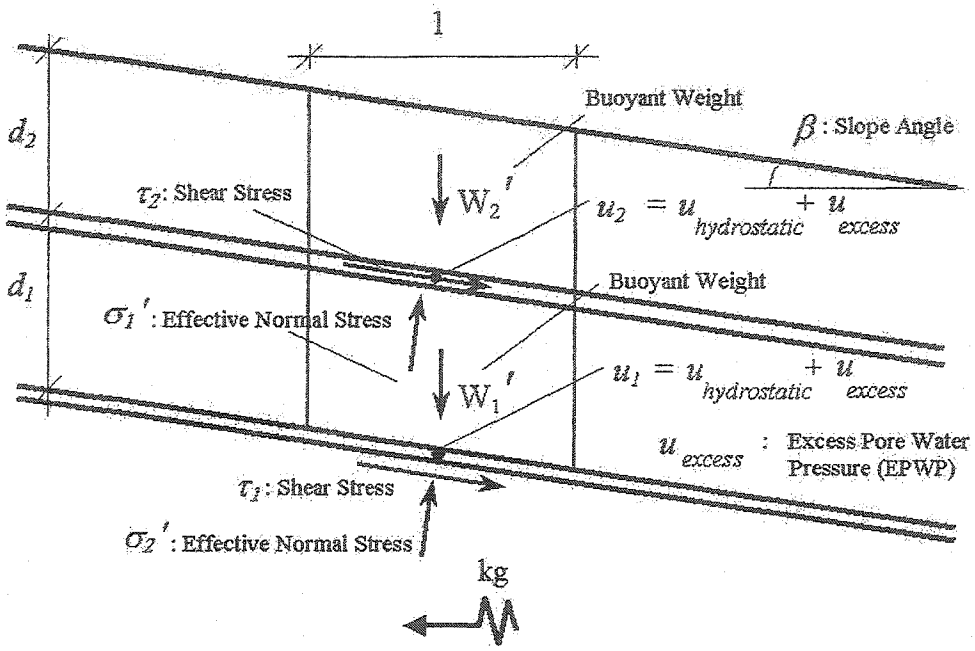

Figure 6-2. Pseudo-static analysis of an infinite submarine slope assuming two failure surfaces.

In the following, only the case where the top block moves first is considered.

From the beginning of the earthquake until the initiation of movement of the top block, the factor of safety for each layer can be written as follows:

$$FS_1 = \frac{c_1' + [\gamma'(d_1 + d_2)\cos^2\beta - u_{e1} - k\gamma(d_1 + d_2)\sin\beta\cos\beta]\tan\phi_1'}{\gamma'(d_1 + d_2)\sin\beta\cos\beta + k\gamma(d_1 + d_2)\cos^2\beta} \tag{6.5}$$

$$FS_2 = \frac{c_2' + (\gamma' d_2\cos^2\beta - u_{e2} - k\gamma d_2\sin\beta\cos\beta)\tan\phi_2'}{\gamma' d_2\sin\beta\cos\beta + k\gamma d_2\cos^2\beta} \tag{6.6}$$

where, with reference to Figure 6.2, γ' is the effective (or buoyant) unit weight of soil, d_1 and d_2 are the depths of failure plane for the bottom and the top layer, respectively, β is the slope angle, u_{e1} and u_{e2} are the excess pore water pressures (in excess of hydrostatic) generated due to earthquake for the bottom and the top layer, respectively, and k is the

seismic coefficient defined as the ratio between the horizontal earthquake acceleration and the gravitational acceleration (g).

When yield occurs at the top block while the bottom block is still moving with the ground, the situation is like one-block situation and the yield acceleration coefficient for the top block k_{y2} can be obtained by equating FS_2 with one in Equation (6.6).

If k increases further to trigger movement of the bottom block the factor of safety for bottom block can be written as follows:

$$FS_1 = \frac{c'_1 + [\gamma' d \cos^2\beta - u_{e1} - k_{y2}\gamma d_2 \sin\beta\cos\beta - k\gamma d_1 \sin\beta\cos\beta]\tan\phi'_1}{\gamma' d_1 \sin\beta\cos\beta + k\gamma d_1 \cos^2\beta + [c'_2 + (\gamma' d_2 \cos^2\beta - u_{e2} - k_{y2}\gamma d_2 \sin\beta\cos\beta)\tan\phi'_2]} \quad (6.7)$$

where $d = d_1 + d_2$.

6.2.1 Estimation of yield accelerations considering the effects of coupling

By setting both factors of safety equal to one, the yield acceleration coefficient at each time instant, t, from the beginning of the earthquake until the initiation of movement of top block (using equations 6.5 and 6.6) can be obtained as equations 6.8 and 6.9 for the bottom and the top blocks, respectively:

$$k_{y1}(t) = \frac{c'_1 + [\gamma'(d_1 + d_2)\cos^2\beta - u_{e1}(t)]\tan\phi'_1 - \gamma'(d_1 + d_2)\sin\beta\cos\beta}{\gamma(d_1 + d_2)\cos^2\beta + \gamma(d_1 + d_2)\sin\beta\cos\beta\tan\phi'_1} \quad (6.8)$$

$$k_{y2}(t) = \frac{c'_2 + [\gamma' d_2 \cos^2\beta - u_{e2}(t)]\tan\phi'_2 - \gamma' d_2 \sin\beta\cos\beta}{\gamma d_2 \cos^2\beta + \gamma d_2 \sin\beta\cos\beta\tan\phi'_2} \quad (6.9)$$

After yield of the top block, the yield acceleration coefficient for the bottom block at each time instant t can be obtained from Equations 6.7.

$$k_{y1}(t)=\frac{c'_1-c'_2+[\gamma' d\cos^2\beta-u_{e1}]\tan\phi'_1-(\gamma d_2\cos^2\beta-u_{e2})\tan\phi'_2-\gamma' d_2 k_{y2}\sin\beta\cos\beta(\tan\phi'_1-\tan\phi'_2)-\gamma' d_1\sin\beta\cos\beta}{\gamma' d_1(\cos^2\beta+\gamma' d_1\sin\beta\cos\beta\tan\phi'_1}$$

(6.10)

where $d = d_1+d_2$.

Under the assumption that the top block yields first its yield acceleration after the bottom block starts yielding is the same as before (Equation 6.9). Note that $r_u = u_e / \sigma'_{v0}$ is the excess pore water pressure ratio with respect to initial effective vertical stress, where σ'_{v0} for the bottom layer and the top layer are as follows, respectively:

$$\sigma'_{v01} = \gamma'(d_1 + d_2)\cos^2\beta \tag{6.11}$$

$$\sigma'_{v02} = \gamma' d_2 \cos^2\beta \tag{6.12}$$

The sliding block accelerations $a_{b1}(t)$, $a_{b2}(t)$ for the bottom layer and top layer, for each layer with respect to its lower layer, from the beginning of the earthquake until the initiation of movement of top block are as follows:

- before yielding of the top block:

$$a_{b1}(t) = \big(k(t) - k_{y1}(t)\big)g\,\frac{\cos(\phi'_1 - \beta)}{\cos\phi'_1} \tag{6.13}$$

$$a_{b2}(t) = \big(k(t) - k_{y2}(t)\big)g\,\frac{\cos(\phi'_2 - \beta)}{\cos\phi'_2} \tag{6.14}$$

- after yielding of the top block:

$$a_{b1}(t) = \big(k(t) - k_{y1}(t)\big)g[\frac{\cos(\phi'_1 - \beta)}{\cos\phi'_1} + \frac{d_2}{d_1}\sin\beta(\tan\phi'_1 - \tan\phi'_2)] \tag{6.15}$$

and $a_{b_2}(t)$ is given by Equation (6.14). $k(t) \cdot g$ represents the seismic acceleration time history. Finally, the displacement of each layer with respect to its lower layer can be computed by integrating twice each block's acceleration.

6.3 Slope displacements considering two blocks

By applying the described procedure, the yield acceleration for the top block and the bottom block are calculated as described before and shown in Figures 6.3 and 6.4, respectively. Also the displacement for the top block and the bottom block are calculated considering the effects of excess pore water pressure build-up and dissipation (as described in Chapter 3 and Chapter 5) and shown in Figures 6.5 and 6.6, respectively. All the parameters related to input acceleration and soil properties are described in Section 3.4.

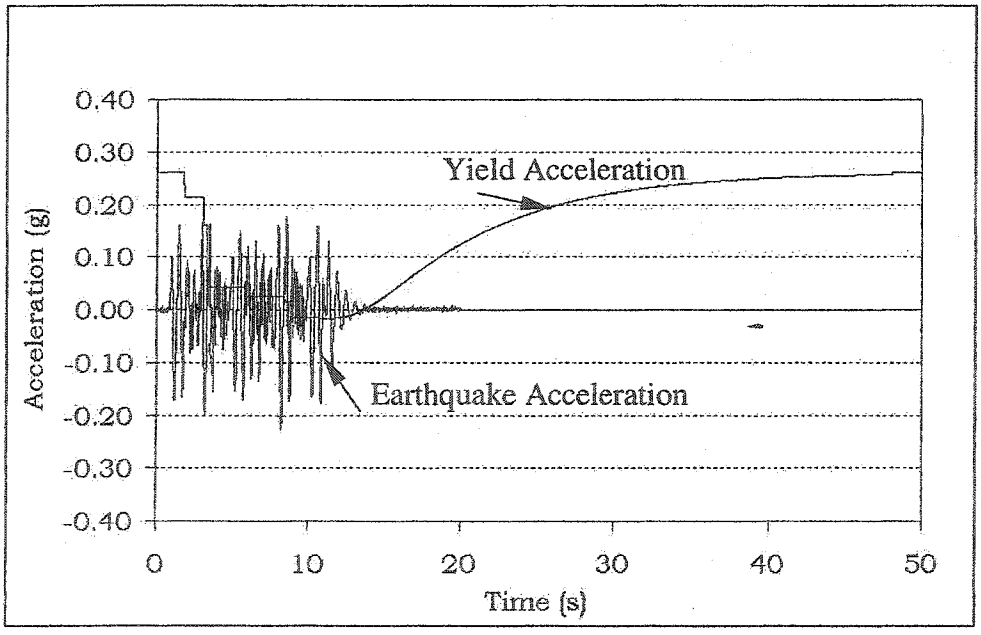

Figure 6-3. Yield Acceleration for the top block.

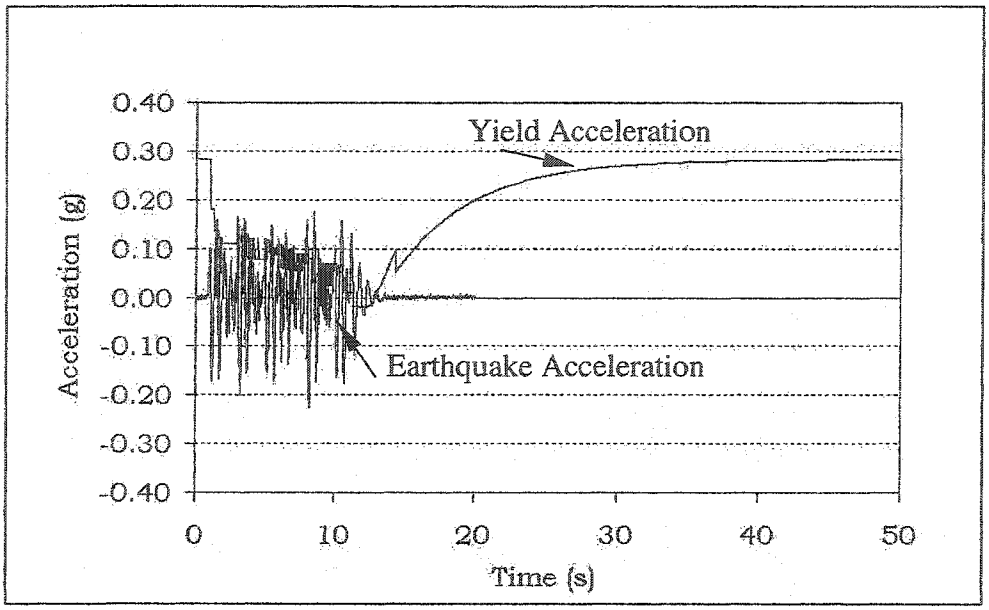

Figure 6-4. Yield Acceleration for the bottom block.

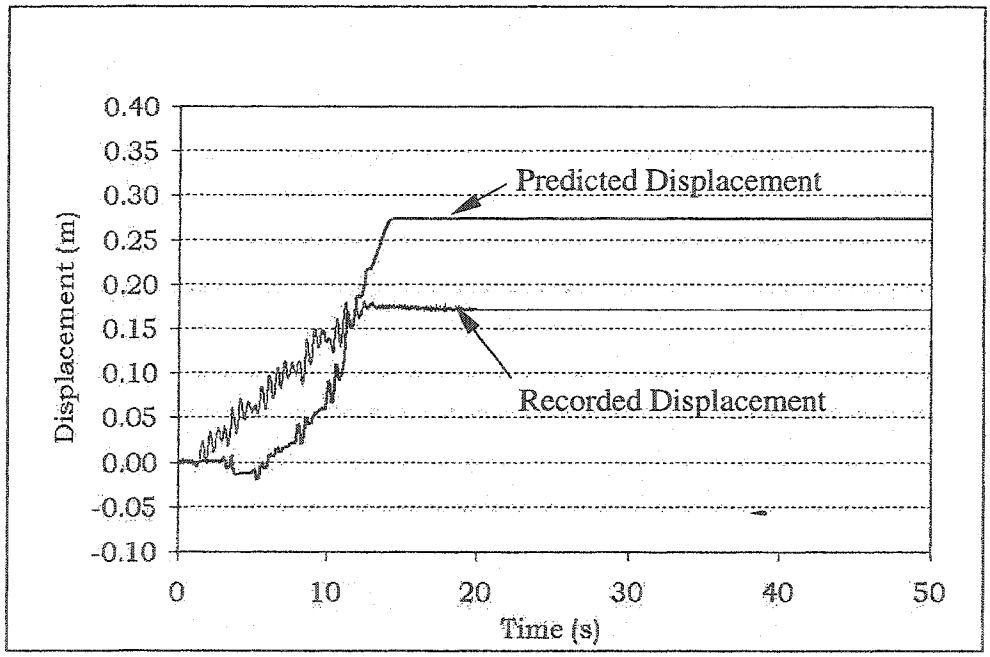

Figure 6-5. The predicted permanent displacements of the top layer.

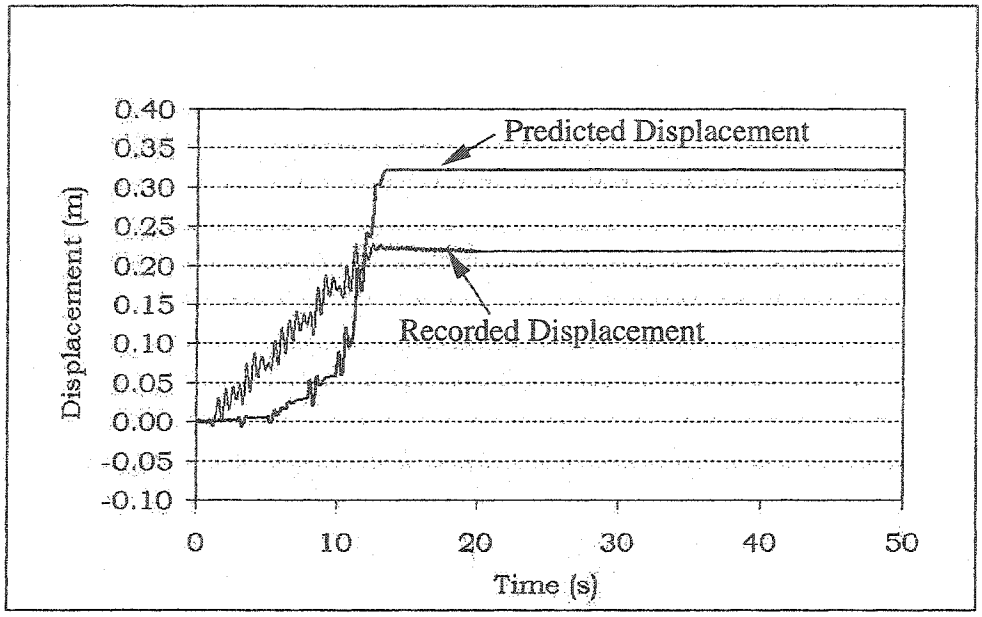

Figure 6-6. The predicted permanent displacements of the bottom layer.

To validate the described procedure, the results of centrifuge test for model 2 (described in section 3.3) have been used. The bottom block is considered from the level of P7 up to the level of P6 and the top block is considered from the level of P6 to the soil surface (Figure3.7.). The recorded displacement corresponds to the top block is considered (LVDT3-LVDT5)/2 and the recorded displacement corresponds to the bottom block is considered (LVDT4-LVDT6)/2. Comparing the predicted displacements with the centrifuge tests results (Figure 6.5 and 6.6) shows that the predicted permanent displacements of each block is satisfactorily close to the recorded values reported in the VELACS tests. The predicted permanent displacements of the two blocks are some what greater than the recorded values, owing to the assumption that liquefaction at the end of shaking extends to a depth of 10m. This assumption results in conservative results for predicted displacements.

6.4 Summary

The results presented in this chapter show that by considering more than one rigid block, the model is able to reproduce the gradual deformation of soil with depth and therefore provide more realistic prediction for uniform sand deposit.

7 Conclusions

In this work, the original Newmark method for analysis of seismically induced slope displacements is enhanced to obtain more realistic predictions for soil materials that experience pore water pressure build-up and dissipation, during and after earthquakes. The following aspects have been investigated:

- Effect of pore water pressure build-up:

In Chapter 3, an effective stress approach that accounts for the build-up of excess pore water pressure has been included in the Newmark method. The result of such a consideration is the decrease in the yield acceleration because of the build-up in pore pressure. The results have been verified based on centrifuge tests results. The results have shown that the predicted displacements at the end of earthquake are in fair agreement with the values recorded in the centrifuge experiment. As was recorded in the centrifuge experiments and predicted by the numerical model, the soil liquefied during the shaking. Therefore, the yield acceleration became negative, which leads to predicting infinite post-earthquake displacements whereas the recorded results showed limited displacements with no significant change after the end of shaking. Altogether, the analysis reported in Chapter 3 showed that although accounting for the build-up of excess pore pressure is necessary it is not enough, and therefore, the method should be further enhanced.

- Sensitivity analysis to find other important effects:

In Chapter 4, a sensitivity analysis has been performed to investigate and find other important factors that affect the results of the Newmark analysis. It has been found that

the Newmark displacement analysis is very sensitive to the maximum earthquake acceleration. This fact led us to the importance of accounting for the effects of excess pore water pressure dissipation because, especially in cases where soil liquefied, the yield acceleration at the end of earthquake was less than zero, which resulted in infinite displacement of slope. Recorded results, however, showed that after the earthquake, soil regains its shear strength and the yield acceleration should increase.

- Effect of pore water pressure dissipation:

In Chapter 5, the model developed in Chapter 3 has been further enhanced by applying the one-dimensional consolidation theory to account for the effect of excess pore pressure dissipation after the earthquake. The results showed that the predicted displacements at the end of earthquake are satisfactorily close to the values recorded in the centrifuge experiment.

- Effect of considering more than one failure surface:

In Chapter 6, the effects of accounting for more than one failure surface were investigated. For homogeneous soils, because the displacements are distributed with depth, the one rigid block assumption in Newmark method cannot reproduce the gradual soil deformation. To provide relatively more realistic predictions for a uniform sand deposit, two rigid blocks are considered to mitigate this limitation of Newmark method. The results were verified based on centrifuge tests results and it was shown that the predicted displacements at the end of earthquake were satisfactorily close to the recorded values with a better prediction of the gradual deformation with depth.

The proposed methodology has been implemented in a computer program.

8 References

Arulanandan, K. and Scott, R. F. (1994). "Verification of Numerical Procedures for the Analysis of Soil Liquefaction Problems.", Vol. 2.

Azizian, A. and Popescu, R. (2001). "Backanalysis of the 1929 Grand Banks submarine slope failure." *Proceedings, 54th Canadian Geotechnical Conference*, Calgary, Alberta, Canada, Vol. 2, pp. 808-815.

Baybutt, P., Cox, D.C., and Kurth, R.E. 1981. Methodology for uncertainty analysis of light water reactor meltdown accident consequences. Topical report from BCL to NRC.

Biondi, G., Cascone, E. (2000). "Seismic response of saturated cohesionless slopes." *Soil Dynamic and Earthquake Engineering*, 20, pp. 209-215.

Biot, M.A., 1962. "Mechanics of deformation and acoustic propagation in porous media." *Journal of Applied Physics*, 33(4), pp. 1482-1498.

Bishop, A.W., and Eldin, A.K.G. (1950). "Undrained triaxial tests on saturated sands and their significance in the general theory of shear strength." *Géotechnique*, 10, pp. 129-150.

Box, G.E.P., and Wilson, K.B. 1951. On the experimental attainment of optimum conditions. Journal of the Royal Statistical Society, B, 13, pp. 1-45.

Byrne, P.M. (1990). "A model for predicting liquefaction induced displacements." *2nd International Conference on Recent Advances in Geotechnical Earthquake Engineering and Soil Dynamics,* St. Louis, Paper 7.14.

Byrne, P.M., and Jitno, H., Garner, S., Lee, M. and Lou, J.K. (1991). "Analysis of earthquake induced displacements of the intake structures, John Hart Dam." *Proc. Canadian Dam Safety Conference Whistler*, B.C., pp. 97-116.

Byrne, P.M., and Hendra, J. (1992). "Earthquake induced displacements of soil-structures systems." *Earthquake Engineering, Tenth World Confernce*, pp. 1407-1412.

Chang, C.J., Chen, W.F., and Yao, J.T.P. 1984. Seismic displacement in slopes by limit analysis. Journal of Geotechnical Engineering, ASCE, 110(7), pp. 860-874.

Cox, D. C., and Baybutt, P. 1981. *Methods of uncertainty analysis*: A comparative survey. Risk Analysis, 1(4), pp. 251-258.

Cornell, J.A., 1990. *How to Apply Response Surface Methodology*. The ASQC Basic References in Quality Control: Statistical Techniques, Vol. 8, ASQC, Wisconsin.

COSTA-Canada, A Canadian Contribution to the Study of Continental Slope Stability: http://www.costa-canada.ggl.ulaval.ca/

Craig, R.F. (1992). *Soil Mechanics,* Chapman & Hall, London, p266.

Das, B.M. (1996). *Principles of Soil Dynamics*. PWS-KENT Publishing Company, Boston.

Kramer, S.L. (1996). *Geotechnical Earthquake Engineering*. Prentice Hall, New Jersey, p653.

Lee, H.J., Edwards, B.D. (1986). "Regional method to assess offshore slope stability." *Journal of Geotechnical Engineering*, ASCE, 112, pp. 489-509.

Lee, H., Locat, J., Dartnell, P., Israel, K., and Wong, F. (1999). "Regional variability of slope stability: application to the Eel margin, California." *Marine Geology*, 154, pp. 305-321.

Madabhushi, S.P.G., and Schofield, A.N. 1993. Centrifuge modeling of tower structures on saturated sand subjected to earthquake perturbations. *Géotechnique*, 43(4), pp. 555-565.

Makdisi, F.I., and Seed, H.B. (1978). "Simplified procedure for estimating dam and embankment earthquake-induced deformations." J. Geotechnical Engineering Divsion, ASCE, Vol. 104, No. GT7, 849-867.

Martin, P.P., and Seed, H.B. (1979). "Simplified procedure for effective stress analysis of ground response." *Journal of Geotechnical Engineering*, ASCE, 105(1), pp. 739-758.

Montgomery, D.C. (1997). *Design and Analysis of Experiments*. John Wiley & Sons, New York.

Montgomery, D.C., Peck, E.A., and Vining, G.G. 2000. *Introduction to Linear Regression Analysis*, 3rd ed. New York, John Wiley.

Morgenstern, N. M. (1967). "Submarine slumping and the initiation of turbidity currents." *Marine Geotechnique*, ed., A. F. Richards, Urbana: Illinois UP, pp. 189-220.

Myers, R.H. and Montgomery, D.C. 1995. *Response Surface Methodology*. John Wiley & Sons, New York.

Newmark, N.M., (1965). "Effects of earthquakes on dams and embankments." 5th. Rankine Lecture, *Géotechnique*, 15(2), 137-160.

Popescu, R. and Prevost, J.H. 1993. "Centrifuge validation of a numerical model for dynamic soil liquefaction." *Soil dynamics and Earthquake Engineering*, 12: 73-90.

Popescu, R., Prevost, J.H., and Deodatis, G. 1997. Effects of spatial variability of soil liquefaction: Some design recommendations. *Géotechnique*, 47(5), pp. 1019-1036.

Popescu, R. 2002. "Finite element assessment of the effects of seismic loading rate on soil liquefaction." *Canadian Geotechnical Journal*, 39(2), pp. 331-344.

Rathje, E. M., and Bray, J. D. (1999). "An examination of simplified earthquake-induced displacement procedures for earth structures." *Canadian Geotechnical Journal*, 36, pp. 72-87.

Rathje, E. M., and Bray, J. D. (2000a). "An examination of simplified earthquake-induced displacement procedures for earth structures: Reply." *Canadian Geotechnical Journal*, 37, pp. 731-732.

Rathje, E. M., and Bray, J. D. (2000b). "Nonlinear Coupled Seismic Sliding Analysis of Earth Structure." *Journal of Geotechnical and Geoenvironmental Engineering*, 126(11), pp. 1002-1014.

Seed, H.B. and Idriss, I.M. 1971. "Simplified procedure for evaluating soil liquefaction potential." *Journal of Geotechnical Engineering*, ASCE, 97(9), pp. 1249-1273.

Seed, H.B., Idriss, I.M., Makdisi, F. and Banerjee, N. (1975a). "Representation of irregular stress-time histories by equivalent stress series in liquefaction analyses." Report No. EERC 75-29, EERC, UC Berkeley, CA.

Seed, H.B., Martin, P.O., and Lysmer, J. (1975b). "The generation and dissipation of pore water pressure during soil liquefaction." Report No. EERC 75-26, EERC.

Seed, H.B., and Booker, J.R. (1977). "Stabilization of potential liquefaction sand deposits using gravel drains." *Journal of Geotechnical Engineering Div.*, ASCE, 103, GT7, pp. 757-768.

Seed, H.B. and Idriss, I.M. (1982). "On the importance of dissipation effects in evaluating pore pressure changes due to cyclic loading." *Soil Mechanics - Transient and Cyclic Loads*, eds., Pande, N., Zienkiewics, O.C., pp. 53-70.

Skempton, A.W. (1954). "The pore pressure coefficients A and B." *Géotechnique*, 4, pp. 143-147.

Taboada, V.M. and Dobry, R. (1993). Experimental results of Model No2 at RPI. In: "Verification of Numerical Procedures for the Analysis of Soil Liquefaction Problems.", Arulanandan, K. and Scott, R. F. editors. Vol. 1.

UBC, Uniform Building Code (1994). International Conference of Building Officials, ICBO, Whittier, CA, Vol. 2.

Urgeles, R., Locat, J., Lee, H., Martin, F., and Konrad, J.M. (2001). "The Saguenay Fjord: Integrating marine geotechnical and geophysical data for spatial slope stability hazard analysis." *Proceedings, 54th Canadian Geotechnical Conference*, Calgary, Alberta, Canada, Vol. 2, pp. 768-775.

VELACS, VErification of Liquefaction Analysis by Centrifuge Studies: http://geoinfo.usc.edu/gees/velacs/

Youd, T.L., and Idriss, I.M. (2001). "Liquefaction resistance of soils: summary report from the 1996 NCEER and 1998 NCEER/NSF workshops on evaluation of liquefaction resistance of soils." *Journal of Geotechnical and Geoenvironmental Engineering*, ASCE, 127(4), pp. 297-313.

Youd, T.L., Idriss, I.M., Andrus, R.D., Arango, I., Castro, G., Christian, J.T., Dobry, R., Finn, W.D.L., Harder , L.F., Hynes, M.E., Ishihara, K., Koester, J.P., Liao, S.S.C., Marcuson, W.F., Martin, G.R., Mitchell, J.K., Moriwaki, Y., Power, M.S., Robertson, P.K., Seed, R.B., and Stokoe, K.H. 2001, *Liquefaction Resistance of Soils: Summary report from the 1996 NCEER and 1998 NCEER/NSF workshops on Evaluation of liquefaction resistance of soils*, Journal of Geotechnical and Geoenvironmental Engineering, Vol. 127(10): 817-833.

Zangeneh, N., Azizian, A., Lye, L., and Popescu, R. (2002). "Application of Response Surface Methodology in numerical geotechnical analysis." *Proceedings, 55th Canadian Geotechnical Conference*, Niagara Falls, Ontario, Canada, 321-329.

Zangeneh, N. and Popescu, R. (2003). "Displacement analysis of submarine slopes using enhanced Newmark method." *Proceedings, First International Symposium on Submarine Mass Movements and Their Consequences*, eds., Locat, J., and Mienert, J., Nice, France, 193-202.

Zeng, X. (1998). "Seismic Response of Gravity Quay Walls. I: Centrifuge Modeling." *Journal of Geotechnical and Geoenvironmental Engineering*, 124(5), pp. 406-417.

Appendix A: Determination of Equivalent Number of Uniform Cycles (N_{eq})

According to Seed et al. (1975) the equivalent number of uniform cycles at $0.65\tau_{max}$ is determined by the following steps. These steps are also shown in Table A.1 (positive acceleration) and Table A.2 (negative acceleration) for a sample earthquake acceleration time history (Figure A.1).

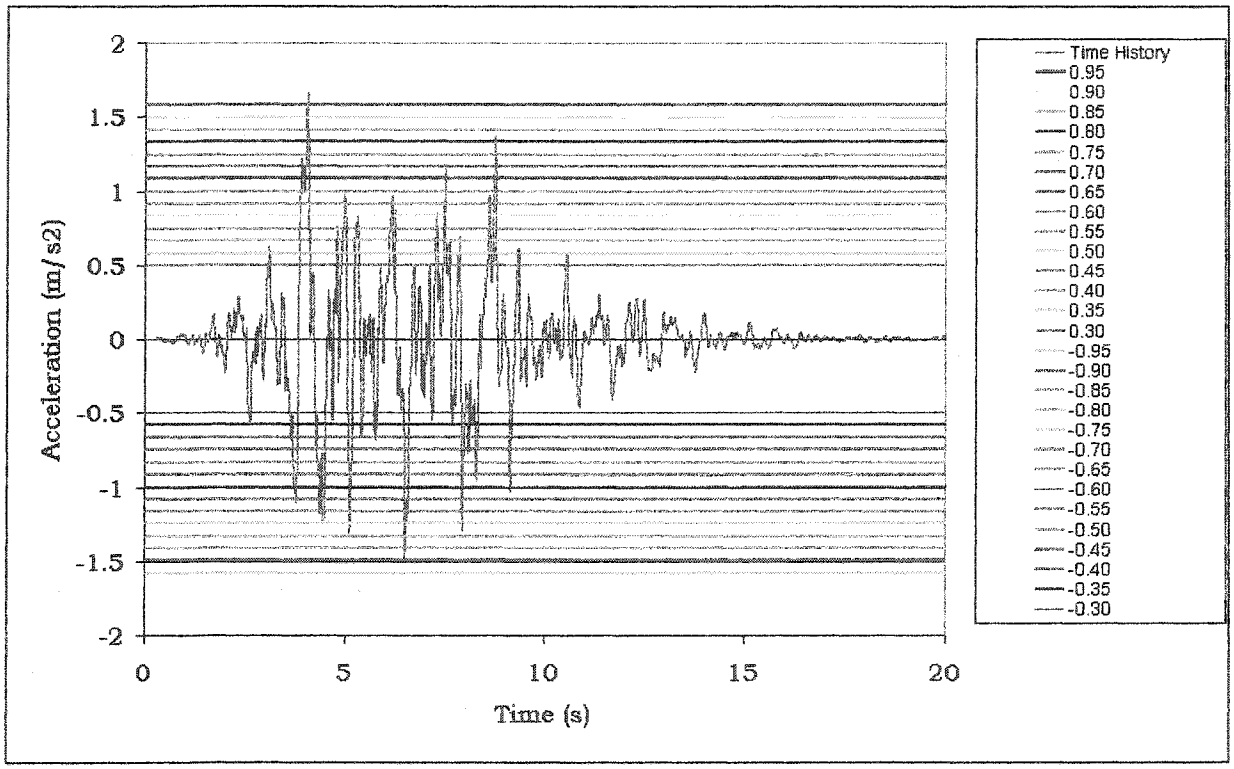

Figure A-1. A sample acceleration time history and various stress levels above and below the horizontal.

- For the acceleration-time history determine the number of stress cycles at various stress levels such as τ_{max}, $0.95\tau_{max}$, $0.9\tau_{max}$, ... above the horizontal axis (positive acceleration) and bellow the horizontal axis (positive acceleration). (it is assumed that

the shear stress applied by the earthquake is proportional to the horizontal seismic acceleration)

- Using the conversion factors from Figure A.2 calculate the equivalent number of cycles for each peak in the acceleration time history and then sum them up

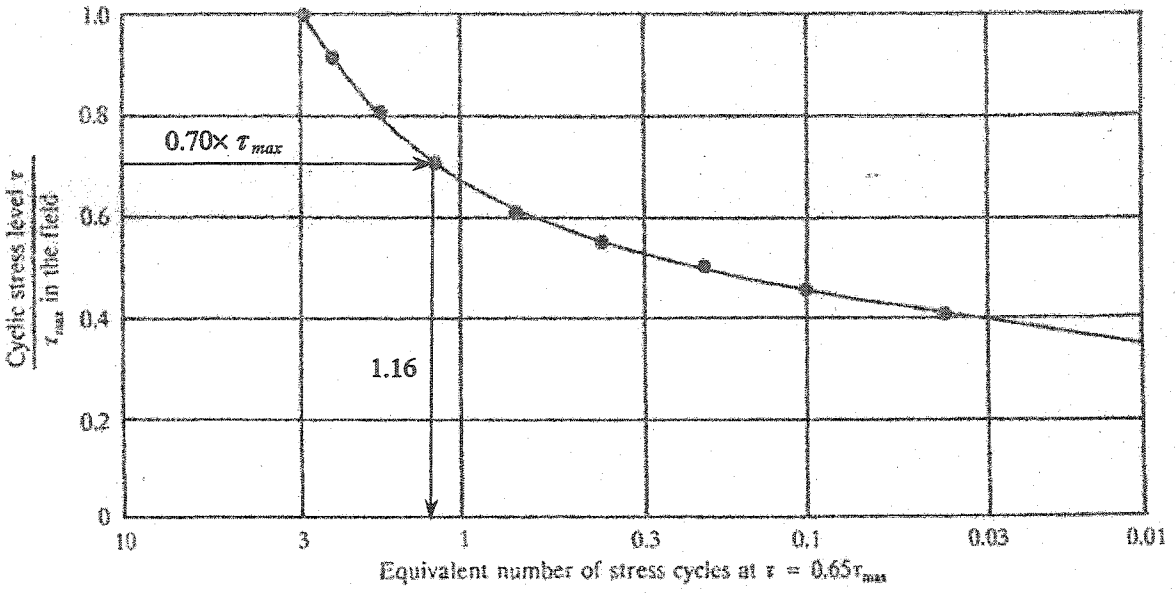

Figure A-2. Plot of t/t max versus Neq at t=0.65 t max (after Seed et al. 1975) (example: line 7 in Table A.1).

- Determining the total number of equivalent stress cycles at $0.65\tau_{max}$ (sum of Column 4 in Table A.1 and Table A.2)

- N_{eq}= ½ (equivalent number of cycles for positive acceleration + equivalent number of cycles negative acceleration)

Table A-1. Calculation of Neq for positive acceleration.

	Above Horizontal		
Stress Level ($\times \tau_{max}$) (C1)	Number of Stress cycles (C2)	Conversion Factor (C3)	Equivalent Number of cycles at $0.65\tau_{max}$ (C4) = (C2) * (C3)
1.00	1	3.00	3.00
0.95	0	2.8	0
0.90	0	2.6	0
0.85	0	2.05	0
0.80	0	1.6	0
0.75	0	1.42	0
0.70	1	1.16	1.16
0.65	1	0.91	0.91
0.60	0	0.7	0
0.55	3	0.3	0.9
0.50	2	0.24	0.48
0.45	3	0.09	0.27
0.40	2	0.04	0.08
0.35	2	0.02	0.04
Total	-	-	6.84

Table A-2. Calculation of Neq for negative acceleration.

	Below Horizontal		
Stress Level ($\times \tau_{max}$)	Number of Stress cycles (C2)	Conversion Factor (C3)	Equivalent Number of cycles at $0.65\tau_{max}$ (C4) = (C2) * (C3)
1.00	0	3.00	0
0.95	0	2.8	0
0.90	0	2.6	0
0.85	1	2.05	2.05
0.80	0	1.6	0
0.75	2	1.42	2.84
0.70	2	1.16	2.32
0.65	1	0.91	0.91
0.60	1	0.7	0.7
0.55	1	0.3	0.3
0.50	0	0.24	0
0.45	1	0.09	0.09
0.40	3	0.04	0.12
0.35	2	0.02	0.04
Total	-	-	9.37

Average number of cycles at $0.65\tau_{max} \cong 1/2\ (6.84+9.37) = 8.105$

Appendix B: Determination of Number of Cycles to Liquefaction (N_L)

The number of cycles to liquefaction for a given soil can be calculated as follows:

- Using the soil properties (namely standard penetration or cone penetration resistance), the cyclic resistance ratio (CRR) can be found from charts such as that shown in Figure 8.3. This corresponds to liquefaction occurring in 15 equivalent cycles (or less) and to an earthquake magnitude $M = 7.5$.

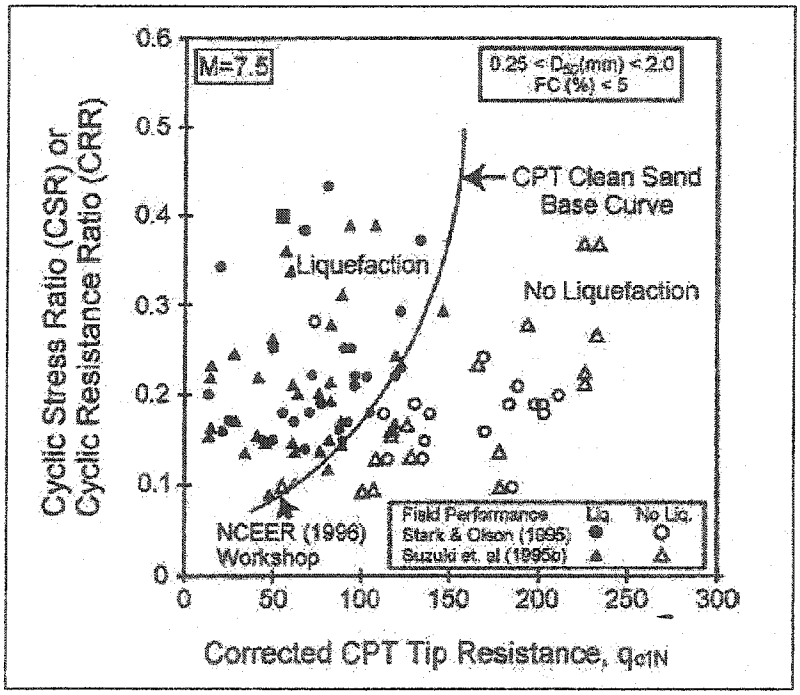

Figure B-1. Chart recommended for calculation of CRR from CPT data (Youd et al. 2001).

- Using the acceleration time-history, the equivalent cyclic stress ratio (CSR) applied by the earthquake at a given depth can be obtained using Equation 4.10 in Section 4.3.2.

- Using the above obtained cyclic resistance ratio (CRR) and cyclic stress ratio (CSR) the magnitude scaling factor *MSF* corresponds to a factor of safety for liquefaction *FS=1* can be calculated as follows (Youd et. al. 2001):

$$MSF = \frac{CSR}{CRR_{7.5}} \tag{8.1}$$

The earthquake magnitude can be back calculated from *MSF* using the following relationship from Youd et al. (2001):

$$M = 10^{[(2.24 - \log MSF)/2.56]} \tag{8.3}$$

- The equivalent number of cycles for liquefaction, N_L, can be obtained as function of earthquake magnitude using a relation such as that presented in Figure B.2 (after Seed and Idriss 1982).

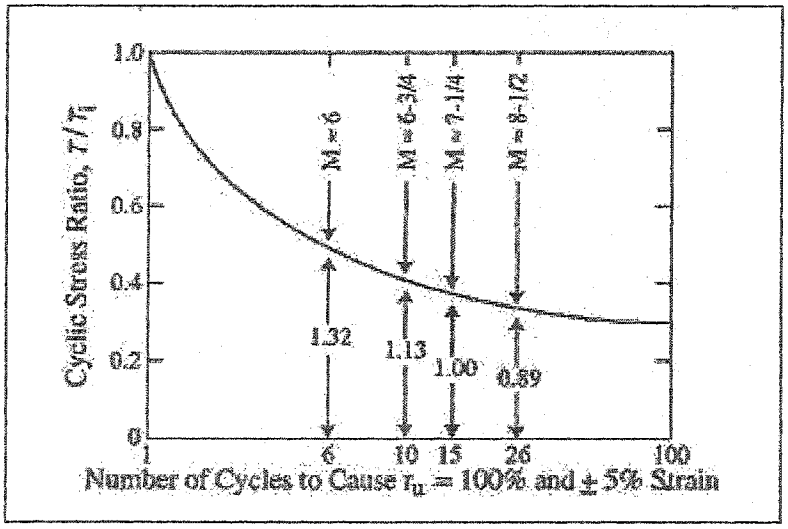

Figure B-2. Representative relationship between CSR and number of cycles to cause liquefaction (Seed and Idriss 1982).

Appendix C: Program ENEDAS User's Manual

The algorithm presented in this work has been implemented in an Excel spreadsheet – Program ENEDAS.

The general procedure for using ENEDAS is outlined and explained in this section. Six spreadsheets have been designed to perform the calculations and present the results. Spreadsheets contain Visual Basic for Application (VBA) Macros for some of the calculations that cannot be done by ordinary Excel cell commands.

The user can easily enter the input parameters (see step 1 bellow) and input acceleration time-history (see step 2 bellow), obtain the results by pressing **Ctrl+a,** and view the results as charts automatically presented in the 'Charts' worksheet; however, individual worksheets are also described in the following sections.

C.1 Step 1: Entering input parameters in 'Input' worksheet

The input parameters, except the earthquake acceleration time-history (see Step 2), should be entered in the **'Input'** worksheet. These parameters are shown in Table 8.3.

Table C-1. Input data: symbols, description, and the values used in this example.

Symbol	Description	Value
g	Gravitational acceleration (m/s^2)	9.81
ρ_w	Density of water (kg/m^3)	1000
n^w	Porosity of soil	0.4
G_s	Specific gravity of soil	2.67
k	Hydraulic conductivity (m/s)	0.0033
B_0	Low-strain bulk modulus at reference mean stress (Pa)	5.42E+07
P_0	Reference mean effective confining stress (Pa)	1.00E+05
β	Slope angle (°)	2
c_1'	Soil cohesion for bottom block (Pa)	0
ϕ_1'	Soil friction angle for bottom block (°)	35
d_1	Height of bottom block (m)	5
c_2'	Soil cohesion for top block (Pa)	0
ϕ_2'	Soil friction angle for top block (°)	33
d_2	Height of top block (m)	3
$d_{drainage}$	Length of longest drainage path (m)	10
No-Time-Steps	Number of time steps for time history	5000
PGA	Peak Ground Acceleration (g)	0.170
N_L	Number of cycles to induce initial liquefaction (*)	7.5
α_{ave}	A parameter defining the rate of excess pore pressure generation (**)	4

(*) N_L corresponds to an uniform equivalent cyclic stress ratio $\frac{\tau_{av}}{\sigma'_{v0}}$ (see Equation 4.10) estimated as described in Appendix B.

(**) See section 3.2.2.

In case of using the program for one block, the values of d_2 and ϕ_2' should be entered as zero. There will be some cells showing #NUM! warning, which should be disregarded.

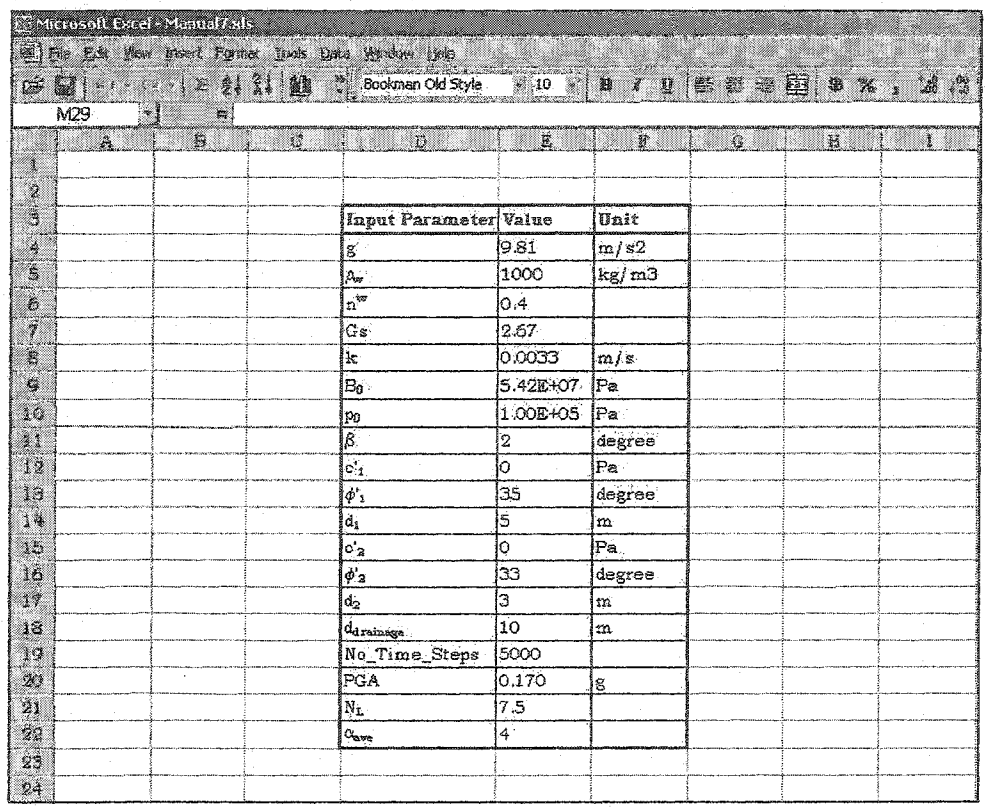

Input Parameter	Value	Unit
g	9.81	m/s2
ρ_w	1000	kg/m3
n^w	0.4	
Gs	2.67	
k	0.0033	m/s
B_0	5.42E+07	Pa
p_0	1.00E+05	Pa
β	2	degree
c'_1	0	Pa
ϕ'_1	35	degree
d_1	5	m
c'_2	0	Pa
ϕ'_2	33	degree
d_2	3	m
$d_{drainage}$	10	m
No_Time_Steps	5000	
PGA	0.170	g
N_L	7.5	
α_{ave}	4	

Figure C-1. 'Input' Excel Worksheet Snapshot.

C.2 Step 2: Calculating the Equivalent Number of Cycles Using 'N_eq' worksheet

The 'N_eq' worksheet converts the earthquake acceleration time-history to a time-history of the equivalent number of cycles. A VBA Macro program calculates the equivalent number of uniform cycles at 0.65τmax based on the procedure proposed by Seed et al. (1975) (refer to Chapter 2.3.4 and Appendix A).

The input data consists of step number and acceleration time-history (in g's), which should be entered in columns D, E and F, respectively. Keys Ctrl+a should be pressed for running the program. The output data is the equivalent number of cycles up to each time step calculated and shown in column G. The equivalent number of cycles at the end of the earthquake will be calculated and shown in cell J2 (Figure 8.6).

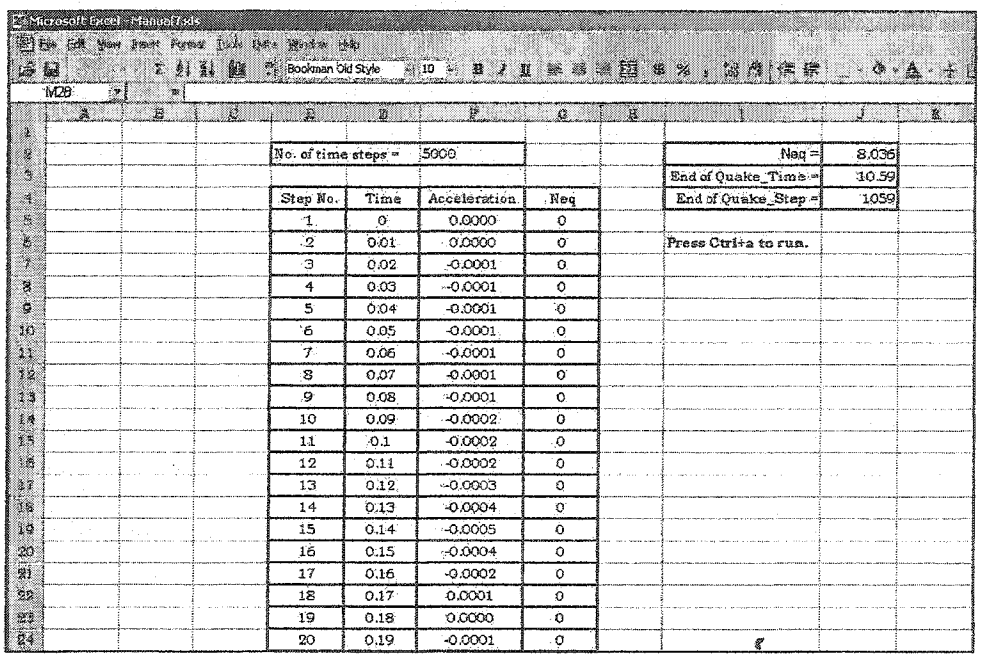

				No. of time steps =	5000				Neq =	8.036	
									End of Quake_Time =	10.59	
				Step No.	Time	Acceleration	Neq		End of Quake_Step =	1059	
				1	0	0.0000	0				
				2	0.01	0.0000	0		Press Ctrl+a to run.		
				3	0.02	-0.0001	0				
				4	0.03	-0.0001	0				
				5	0.04	-0.0001	0				
				6	0.05	-0.0001	0				
				7	0.06	-0.0001	0				
				8	0.07	-0.0001	0				
				9	0.08	-0.0001	0				
				10	0.09	-0.0002	0				
				11	0.1	-0.0002	0				
				12	0.11	-0.0002	0				
				13	0.12	-0.0003	0				
				14	0.13	-0.0004	0				
				15	0.14	-0.0005	0				
				16	0.15	-0.0004	0				
				17	0.16	-0.0002	0				
				18	0.17	0.0001	0				
				19	0.18	0.0000	0				
				20	0.19	-0.0001	0				

Figure C-2. 'N_eq' Excel Worksheet Snapshot.

C.3 Step 3: Calculating the Excess Pore Water Pressure Dissipation Using 'RuDissip' worksheet

The worksheets **'RuDissip1'** and **'RuDissip2'** calculate the excess pore water pressure ratio during the dissipation phase for the bottom block and the top block, respectively. The results are shown in column D (Figure 8.7 and Figure 8.8).

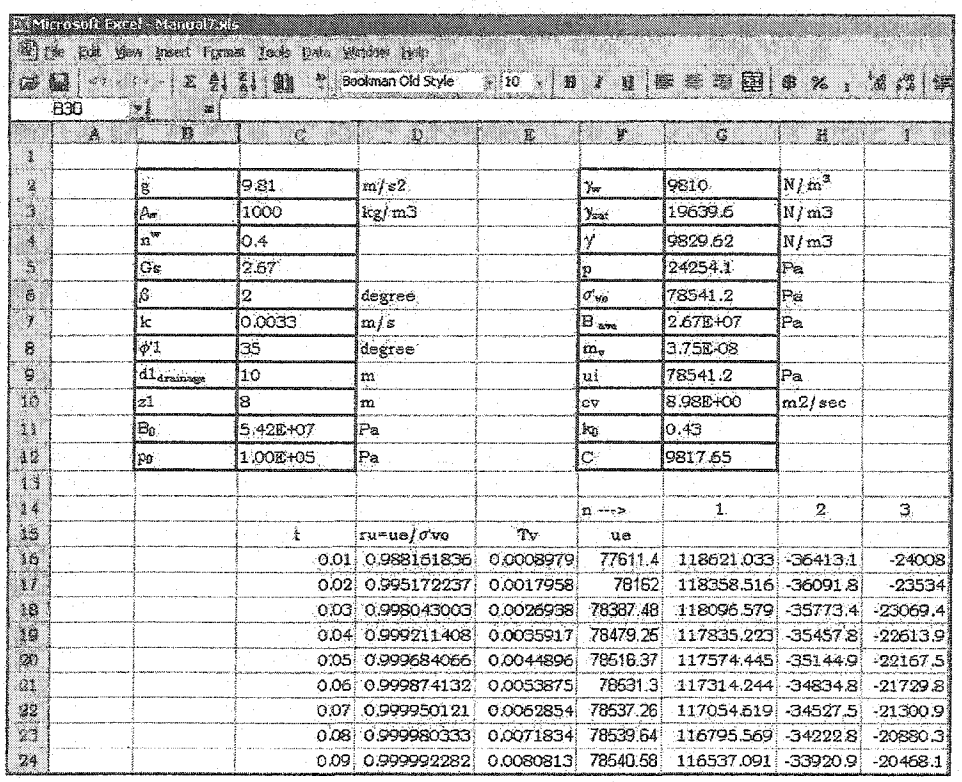

g	9.81	m/s2		γ_w	9810	N/m^3	
ρ_w	1000	kg/m3		γ_{sat}	19639.6	N/m3	
n^w	0.4			γ'	9829.62	N/m3	
Gs	2.67			p	24254.1	Pa	
β	2	degree		σ'_{vo}	78541.2	Pa	
k	0.0033	m/s		B_{ave}	2.67E+07	Pa	
ϕ'1	35	degree		m_v	3.75E-08		
$d1_{drainage}$	10	m		ui	78541.2	Pa	
z1	8	m		cv	8.98E+00	m2/sec	
B_0	5.42E+07	Pa		k_0	0.43		
p_0	1.00E+05	Pa		C	9817.65		

				n --->	1	2	3
t	ru=ue/σ'vo	Tv	ue				
0.01	0.988161836	0.0008979	77611.4	118621.033	-36413.1	-24008	
0.02	0.995172237	0.0017958	78162	118358.516	-36091.8	-23534	
0.03	0.998043003	0.0026938	78387.48	118096.579	-35773.4	-23069.4	
0.04	0.999211408	0.0035917	78479.25	117835.223	-35457.8	-22613.9	
0.05	0.999684066	0.0044896	78516.37	117574.445	-35144.9	-22167.5	
0.06	0.999874132	0.0053875	78531.3	117314.244	-34834.8	-21729.8	
0.07	0.999950121	0.0062854	78537.26	117054.619	-34527.5	-21300.9	
0.08	0.999980333	0.0071834	78539.64	116795.569	-34222.8	-20880.3	
0.09	0.999992282	0.0080813	78540.58	116537.091	-33920.9	-20468.1	

Figure C-3. 'RuDissip1' Excel Worksheet Snapshot.

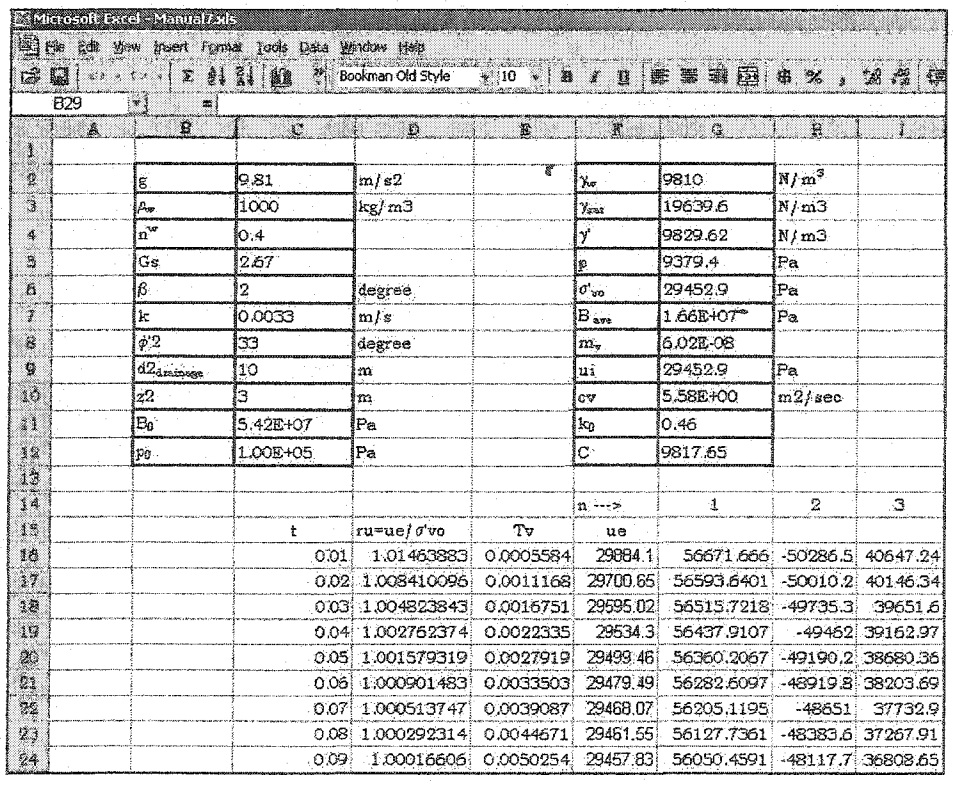

g	9.81	m/s2		γ_w	9810	N/m^3	
ρ_w	1000	kg/m3		γ_{sat}	19639.6	N/m3	
n^w	0.4			γ'	9829.62	N/m3	
Gs	2.67			p	9379.4	Pa	
β	2	degree		σ'_{vo}	29452.9	Pa	
k	0.0033	m/s		B_{ave}	1.66E+07	Pa	
ϕ'2	33	degree		m_v	6.02E-08		
$d2_{drainage}$	10	m		ui	29452.9	Pa	
z2	3	m		cv	5.58E+00	m2/sec	
B_0	5.42E+07	Pa		k_0	0.46		
p_0	1.00E+05	Pa		C	9817.65		

			n --->	1	2	3
t	ru=ue/σ'vo	Tv	ue			
0.01	1.01463883	0.0005584	29884.1	56671.666	-50286.5	40647.24	
0.02	1.008410096	0.0011168	29700.65	56593.6401	-50010.2	40146.34	
0.03	1.004823843	0.0016751	29595.02	56515.7218	-49735.3	39651.6	
0.04	1.002762374	0.0022335	29534.3	56437.9107	-49462	39162.97	
0.05	1.001579319	0.0027919	29499.46	56360.2067	-49190.2	38680.36	
0.06	1.000901483	0.0033503	29479.49	56282.6097	-48919.8	38203.69	
0.07	1.000513747	0.0039087	29468.07	56205.1195	-48651	37732.9	
0.08	1.000292314	0.0044671	29461.55	56127.7361	-48383.6	37267.91	
0.09	1.00016606	0.0050254	29457.83	56050.4591	-48117.7	36808.65	

Figure C-4. 'RuDissip2.' Excel Worksheet Snapshot.

Column G to Z contain partial results for solving Equation 5.4.

C.4 Step 4: Calculating the Permanent Displacements Using 'Newmark' Worksheet

The main worksheet **'Newmark'** calculates the permanent displacements of the bottom and the top block. The numerical results are in terms of block displacements as follow:

- For the bottom block, with respect to the ground.
- For the top block, with respect to the bottom block.

Those numerical results are given in columns K and L for the bottom and the top blocks, respectively (Figure 8.9).

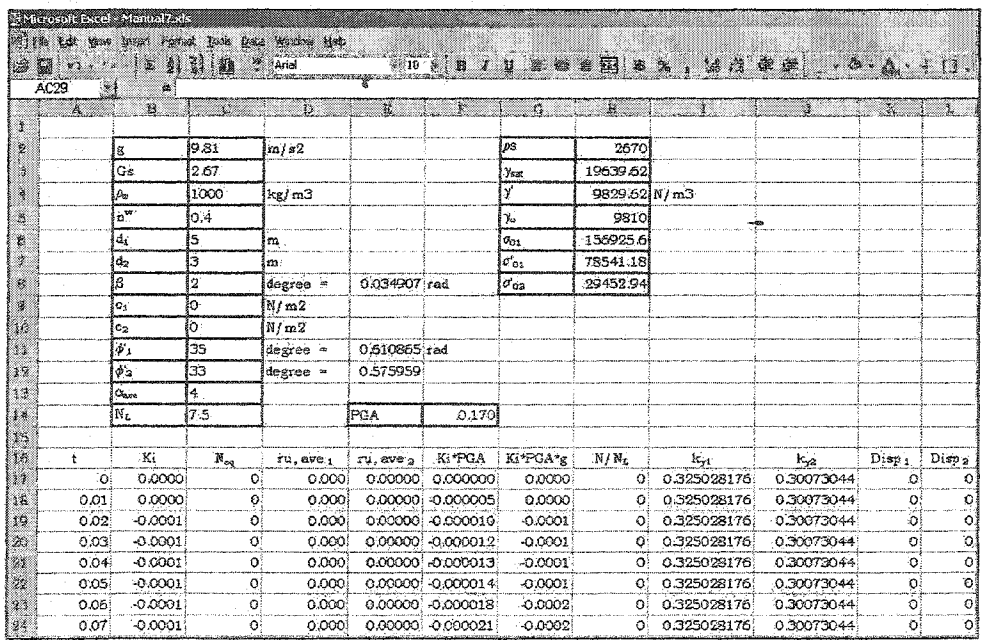

	g	9.81	m/s2			ρs	2670					
	Gs	2.67				γsat	19639.62					
	ρw	1000	kg/m3			γ'	9829.62	N/m3				
	n''	0.4				γw	9810					
	d1	5	m			σ01	156925.6					
	d2	3	m			σ'01	78541.18					
	β	2	degree =	0.034907	rad	σ'02	29452.94					
	c1	0	N/m2									
	c2	0	N/m2									
	φ'1	35	degree =	0.610865	rad							
	φ'2	33	degree =	0.575959								
	αave	4										
	Nc	7.5		PGA	0.170							
t	Ki	Neq	ru, ave 1	ru, ave 2	Ki*PGA	Ki*PGA*g	N/Nc	ky1	ky2	Disp 1	Disp 2	
0	0.0000	0	0.000	0.00000	0.000000	0.0000	0	0.325028176	0.30073044	0	0	
0.01	0.0000	0	0.000	0.00000	-0.000005	0.0000	0	0.325028176	0.30073044	0	0	
0.02	-0.0001	0	0.000	0.00000	-0.000010	-0.0001	0	0.325028176	0.30073044	0	0	
0.03	-0.0001	0	0.000	0.00000	-0.000012	-0.0001	0	0.325028176	0.30073044	0	0	
0.04	-0.0001	0	0.000	0.00000	-0.000013	-0.0001	0	0.325028176	0.30073044	0	0	
0.05	-0.0001	0	0.000	0.00000	-0.000014	-0.0001	0	0.325028176	0.30073044	0	0	
0.06	-0.0001	0	0.000	0.00000	-0.000018	-0.0002	0	0.325028176	0.30073044	0	0	
0.07	-0.0001	0	0.000	0.00000	-0.000021	-0.0002	0	0.325028176	0.30073044	0	0	

Figure C-5. 'Newmark' Excel Worksheet Snapshot.

C.5 Step 5: Viewing the results in 'Charts'

The worksheet '**Charts**' shows the earthquake acceleration, the yield accelerations, and displacements of the bottom and the top blocks (Figure 8.9).

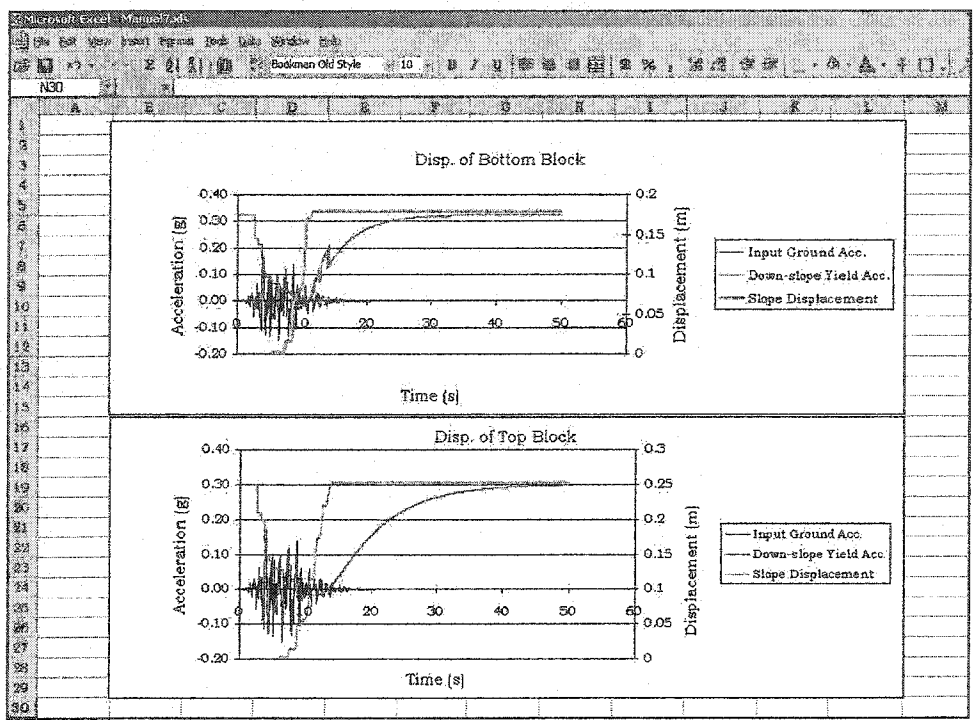

Figure C-6. 'Charts' Excel Worksheet Snapshot.